


Fall 12-2008

## Synthesis, Propagation Kinetics, and Characterization of D,L-Lactide-Based Polyols and Polyurethanes Therefrom

Scott Joseph Moravek  
*University of Southern Mississippi*

Follow this and additional works at: <https://aquila.usm.edu/dissertations>

 Part of the [Materials Chemistry Commons](#), and the [Polymer Chemistry Commons](#)

---

### Recommended Citation

Moravek, Scott Joseph, "Synthesis, Propagation Kinetics, and Characterization of D,L-Lactide-Based Polyols and Polyurethanes Therefrom" (2008). *Dissertations*. 1156.  
<https://aquila.usm.edu/dissertations/1156>

This Dissertation is brought to you for free and open access by The Aquila Digital Community. It has been accepted for inclusion in Dissertations by an authorized administrator of The Aquila Digital Community. For more information, please contact [aquilastaff@usm.edu](mailto:aquilastaff@usm.edu).

The University of Southern Mississippi

SYNTHESIS, PROPAGATION KINETICS, AND CHARACTERIZATION OF  
D,L-LACTIDE-BASED POLYOLS AND POLYURETHANES THEREFROM

by

Scott Joseph Moravek

Abstract of a Dissertation  
Submitted to the Graduate Studies Office  
of The University of Southern Mississippi  
in Partial Fulfillment of the Requirements  
for the Degree of Doctor of Philosophy

December 2008

COPYRIGHT BY  
SCOTT JOSEPH MORAVEK  
2008

The University of Southern Mississippi

SYNTHESIS, PROPAGATION KINETICS, AND CHARACTERIZATION OF  
D,L-LACTIDE-BASED POLYOLS AND POLYURETHANES THEREFROM

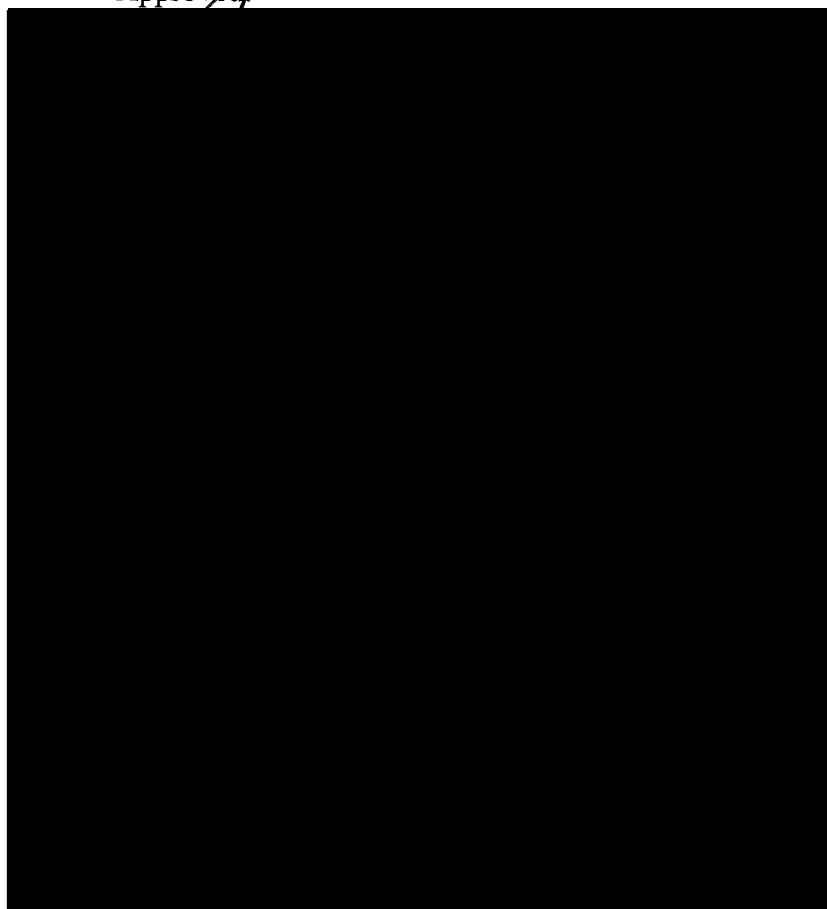
by

Scott Joseph Moravek

A Dissertation

Submitted to the Graduate Studies Office  
of The University of Southern Mississippi  
in Partial Fulfillment of the Requirements  
for the Degree of Doctor of Philosophy

Approved:



December 2008

## ABSTRACT

### SYNTHESIS, PROPAGATION KINETICS, AND CHARACTERIZATION OF D,L-LACTIDE-BASED POLYOLS AND POLYURETHANES THEREFROM

by Scott Joseph Moravek

December 2008

In order to expand the usefulness of degradable polyesters, degradable polyurethanes were synthesized using a mixed polyol system including poly(D,L-lactide-*co*-glycolide) (PLGA), a well-known degradable polyester. Two isocyanate systems, methyl 2,6-diisocyanatocaproate (LDI) and dicyclohexylmethane-4,4'-diisocyanate(H<sub>12</sub>MDI), were studied in order to achieve optimal physical and thermal properties of the thermoplastic polyurethane (TPU) while maintaining degradability. The LDI based systems had excellent physical properties as well as thermal properties that may make them suitable for biomedical devices. The H<sub>12</sub>MDI based TPUs also had excellent physical properties as well as a higher melting temperature.

The aforementioned TPUs were synthesized in small batches. Another method of TPU polymerization was also developed. A reactive extrusion method was developed using a co-rotating twin screw extruder. This system was designed to emulate commercial processes, but on a smaller scale. This method proved to be very successful for synthesizing high molecular weight TPUs.

In order to better understand the urethane forming isocyanate/alcohol reaction, a model system was design based on the polymerization conditions of the TPU synthesis. 1-Butanol and 2-butanol served as the representative primary and secondary alcohol

respectively. Three different catalysts were investigated to determine the effect on the rate of the reaction; dibutyl tin dilaurate, tin (II) 2-ethylhexanoate (SnOct), and triethylamine. The reaction of each alcohol with H<sub>12</sub>MDI was monitored by real-time transmission FTIR, utilizing a temperature controlled flow cell connected to an external reactor. The isocyanate peak at 2256 cm<sup>-1</sup> was monitored and second order kinetic plots were generated. The rate constant of each urethane-forming reaction was determined.

Ring-opening polymerization kinetics of D,L-lactide in refluxing tetrahydrofuran were investigated using a number alcohol/SnOct initiating systems. The alcohols used to initiate polymerization were of varying architecture, with functionalities of one to four, to study the effects of that architecture on the rate of polymerization. The polymerization reaction was monitored by following the 1240 cm<sup>-1</sup> C-O-C asymmetric stretch and 933 cm<sup>-1</sup> ring breathing mode of D,L-lactide in real-time using ATR-FTIR spectroscopy. First order kinetic plots were generated and apparent rate constants,  $k_{app}$ , were determined for each system.

The kinetics of D,L-lactide/ $\epsilon$ -caprolactone copolymerization were also investigated, using two different methods of copolymerization. First, a conventional copolymerization was conducted where both monomers were polymerized in one reactor such that the monomer sequencing was controlled only by monomer reactivities. The second method was a two-pot synthesis where  $\epsilon$ -caprolactone was polymerized and used as a macroinitiator for D,L-lactide. The goal of this alternate copolymerization method is to reduce the overall time required to achieve high conversion of both monomers.

## DEDICATION

*To my wife, Michelle Moravek,  
who always pushed me to do my best while providing endless love and support.*

*To my parents, John and Karen Moravek,  
whose loving upbringing and constant support made me who I am today.*

*And to my father- and mother-in-law, Ray and Nora Drexler,  
who treated me as their own son, making numerous trips to Mississippi from  
Pennsylvania, giving their love and support.*

## ACKNOWLEDGEMENTS

I would like to thank all those at the University of Southern Mississippi who helped make USM an excellent university. Particularly, I would like to thank the staff and faculty of the School of Polymers and High Performance Materials for providing world class facilities and exceptional educational opportunities. I also thank all those that have participated on my committee: Dr. Stephen Boyes, Dr. Lon Mathias, Dr. Kenneth Mauritz, Dr. Robert Moore, Dr. Douglas Wicks, and Dr. Jeffrey Wiggins for their teaching, advice, and guidance. I give special thanks to my advisor, Dr. Robson Storey, for always pushing me to provide the best possible science and for growing my skills as a scientific writer. I thank Dr. Charles Hoyle and Dr. Sarah Morgan who were always willing to lend a helping hand. I thank Dr. Jarrett for maintaining NMR spectrometers and teaching us how to “drive.” I also thank all the staff for keeping the building and department running everyday, especially Laura Fosselman and Steve Selph.

Next, I want to thank all of my Polymer Science colleagues, these are the people that added to my learning experiences and also helped make my time USM fun and exciting. I want to thank all the members of the Storey Research Group, past and present, who have been the hardest working scientists I know and the best labmates you can imagine. There are a number of my colleagues and friends that I want to specifically thank for making my time at USM a pleasure: Dr. Adam Scheuer, Dr. Jamie Messman, Kelby Simison, Dr. Tim Cooper, Dr. Lisa Kemp, David Morgan, Andy Magenau, Megan Powell, Irene Gorman, Yaling Zhu, David Drake, Justin Poelma, Brooks Abel, Misty Rowe, Jay Hotchkiss, Shawn Osborn, and Matt Kellum.



A special thanks goes to Dr. Paul Koch of Penn State Erie – The Behrend College, for providing me a number of opportunities and encouraging me to consider graduate school.

I would like to thank all sources of funding that made my time at USM financially possible: the Office of Naval Research grant no. N00014-04-1-0703, the Naval Research Laboratory/NAVSEA grant N00173-06-2-C008, and the Robert M. Hearin Foundation for providing my fellowship.

Finally, I want to thank all of my family; my parents John and Karen; my grandparents, John, Josephine and Carol; my parents-in-law, Ray and Nora; and my siblings, Jennifer, Neil, and Steve, for encouraging me along the way. Especially to my wife, Michelle, thank you for sharing this entire experience with me.

## TABLE OF CONTENTS

ABSTRACT.....	i
DEDICATION.....	iv
ACKNOWLEDGEMENTS.....	v
LIST OF TABLES.....	xiii
LIST OF FIGURES.....	x
CHAPTER	
I.    INTRODUCTION.....	1
II.   BACKGROUND AND REVIEW.....	5
Degradable Polyesters and Degradation.....	5
Ring-Opening Polymerization of Cyclic Lactones Using Stannous Octoate.....	8
Degradable Thermoplastic Polyurethanes.....	12
Real-time Reaction Monitoring Using FTIR Spectroscopy.....	14
Copolymers of D,L-lactide.....	18
III.  EXPERIMENTAL.....	21
Materials.....	21
Instrumentation.....	23
<i>Size Exclusion Chromatography (SEC)</i> .....	23
<i>Proton Nuclear Magnetic Resonance (<sup>1</sup>H NMR) Spectroscopy</i> ....	24
<i>Carbon Nuclear Magnetic Resonance (<sup>13</sup>C NMR) Spectroscopy</i> ..	25
<i>Differential Scanning Calorimetry (DSC)</i> .....	25
<i>Dynamic Mechanical Analysis (DMA)</i> .....	25
<i>Tensile Testing</i> .....	26
<i>pH Determination of Aqueous Solutions</i> .....	27
General Procedures.....	27
<i>Synthesis of Hydroxy-Terminated Telechelic Poly(D,L-lactide)</i> ...	27
<i>Synthesis of Poly(D,L-lactide) with Primary Hydroxyl Endgroups</i> .....	29
<i>Synthesis of Hydroxy-Terminated Poly(D,L-lactide) from 2,2-</i> <i>Bis(hydroxymethyl) butyric acid (BHMBA-PDLLA)</i> .....	30
<i>Synthesis of Hydroxy-Terminated Telechelic Poly(D,L-lactide-co-</i> <i>Glycolide) (BD-PLGA)</i> .....	30
<i>Synthesis of Hydroxy-Terminated Poly(D,L-lactide-co-Glycolide)</i> <i>from 2,2-Bis(hydroxymethyl) butyric acid (BHMBA-PLGA)</i> .....	31

	<i>Monomer Conversion and Kinetic Measurements of D,L-Lactide Polymerization in Tetrahydrofuran by Real-time ATR-FTIR</i> .....	36
	<i>Degradation Analysis of Polymers</i> .....	40
IV.	DEGRADABLE THERMOPLASTIC POLYURETHANES.....	42
	Introduction.....	42
	Results and Discussion.....	42
	Conclusions.....	53
V.	PRIMARY VS. SECONDARY POLY(D,L-LACTIDE) POLYOLS IN THERMOPLASTIC POLYURETHANES .....	54
	Introduction.....	54
	Results and Discussion.....	54
	Conclusions.....	59
VI.	REACTIVE EXTRUSION OF THERMOPLASTIC POLYURETHANES.....	60
	Introduction.....	60
	Optimization of Reactive Extrusion (REX) Synthesis Parameters.....	61
	<i>LDI-based Thermoplastic Polyurethane</i> .....	61
	<i>H<sub>12</sub>MDI-based Thermoplastic Polyurethane</i> .....	63
	Results and Discussion.....	64
	Conclusions.....	70
VII.	REACTION KINETICS OF DICYCLOHEXYLMETHANE-4,4'- DIISOCYANATE WITH 1- AND 2-BUTANOL: A MODEL STUDY FOR POLYURETHANE FORMATION.....	71
	Introduction.....	71
	Results and Discussion.....	72
	Conclusions.....	79
VIII.	POLYMERIZATION KINETICS OF <i>RAC</i> -LACTIDE INITIATED WITH ALCOHOL/STANNOUS OCTOATE COMPLEXES USING <i>IN SITU</i> ATTENUATED TOTAL REFLECTANCE-FOURIER TRANSFORM INFRARED SPECTROSCOPY: AN INITIATOR STUDY .....	81
	Introduction.....	81
	Results and Discussion.....	83
	Conclusions.....	93
IX.	CONVENTIONAL AND MACROINITIATOR COPOLYMERIZATION .....	94

Introduction.....	94
Results and Discussion.....	94
Conclusions.....	105

APPENDIX

A. HYDROLYTIC DEGRADATION OF POLY(D,L-LACTIDE) AND RESPIROMETRY DEGRADATION OF D,L-LACTIDE-BASED POLYOLS AND POLYURETHANES .....	107
--	-----

Introduction.....	107
Results and Discussion.....	107
Conclusions.....	124

REFERENCES .....	125
------------------	-----

## LIST OF FIGURES

### Figure

II-1. Mechanism of the SnOct catalyzed ROP, including formation of the tin(II) alkoxide initiating species (A-C) and the coordination-insertion ring opening mechanism.....	11
II-2. Glass transition temperature of (L-lactic acid-co- $\epsilon$ -caprolactone) and Fox equation plotted against the amount of L-lactic acid. <sup>154</sup> .....	19
III-1. Schematic representation of reactive extrusion process. ....	33
III-2. Schematic representation of FTIR flow cell system utilized for data collection. (A) Temperature controlled flow cell, (B) flow cell window setup, (C) temperature controlled oil bath, (D) pump.....	35
IV-1. Carbonyl region of <sup>13</sup> C NMR of H <sub>12</sub> MDI and 12% HS 50BA/50BHMBA-PLGA TPU.....	44
IV-2. HFIP GPC chromatogram of BA and 8% HS 100% BA polyol TPU (Entry 1, Table IV-1).....	45
IV-3. DMA plots of storage modulus vs. temperature (A) and tan $\delta$ vs. temperature (B) for 8% HS TPUs. The number in parenthesis corresponds to the entry number of Table IV-1. ....	47
IV-4. DMA plots of storage modulus vs. temperature (A) and tan $\delta$ vs. temperature (B) for 12% HS TPUs. The number in parenthesis corresponds to the entry number of Table IV-1. ....	48
IV-5. Stress vs. strain tensile test of 8%HS TPUs. The number in parenthesis corresponds to the entry number of Table IV-1. ....	50
IV-6. Stress vs. strain tensile test of 12%HS TPUs. The number in parenthesis corresponds to the entry number of Table IV-1. ....	51
IV-7. Remaining mass of 8%HS TPUs vs. immersion time in seawater at 37°C. The number in parenthesis corresponds to the entry number of Table IV-1. ....	52
IV-8. Remaining mass of 12%HS TPUs vs. immersion time in seawater at 37°C. The number in parenthesis corresponds to the entry number of Table IV-1. ....	53
V-1. <sup>1</sup> H NMR of BD initiated PDLLA.....	55
V-2. <sup>1</sup> H NMR of BD initiated PDLLA-COOH (DCE = dichloroethane). ....	56
V-3. <sup>1</sup> H NMR of BD initiated PDLLA-COCl (DCE = dichloroethane). ....	56
V-4. <sup>1</sup> H NMR of BD initiated PDLLA-1OH. ....	57
V-5. GPC of primary and secondary PDLLA.....	57
V-6. Second order kinetic plot of 1/[NCO] vs. time of the reaction of modified PDLLA (PDLLA-1°OH) and unmodified PDLLA (PDLLA-2°OH) with H <sub>12</sub> MDI and 300 ppm Sn of DBTDL.....	58
VI-1. Pareto chart showing the importance of each variable from the LDI-TPU DOE...	67
VI-2. Pareto chart showing the importance of each variable from the H <sub>12</sub> MDI-TPU DOE. ....	69
VI-3. DMA of row 3, 2 <sup>nd</sup> run. ....	70
VII-1. Partial FTIR spectrum for the reaction of H <sub>12</sub> MDI with 2-BuOH using DBTDL (300 ppm Sn) catalyst showing the progression of isocyanate consumption (Table VII-1, Exp. 4). ....	72

Figure

VII-2. Isocyanate peak height at 2266 $\text{cm}^{-1}$ vs. isocyanate concentration for $\text{H}_{12}\text{MDI}$ in DMF at 40°C.....	74
VII-3. Normalized isocyanate concentration ( $[\text{NCO}]/[\text{NCO}]_0$ ) vs. time for the experiments listed in Table VII-1.....	75
VII-4. Second-order rate plot of $\text{H}_{12}\text{MDI}$ and BuOH in DMF with DBTDL catalyst (300 ppm Sn; Table VII-1, Exp. 3 and 4).....	76
VII-5. Second-order rate plot of $\text{H}_{12}\text{MDI}$ and 1-BuOH in DMF with varying concentrations of DBTDL catalyst at 40°C.....	78
VII-6. Second-order rate constant vs. [DBTDL], for reaction of $\text{H}_{12}\text{MDI}$ with 1-BuOH in DMF at 40°C.....	79
VIII-1. ATR-FTIR calibration curve and equation for the <i>rac</i> -LA concentration at reflux (72°C) in THF.....	84
VIII-2. Partial ATR-FTIR spectra demonstrating the progression of for <i>rac</i> -LA polymerization initiated with PrOH/Sn(Oct) <sub>2</sub> (Table VIII-2, Experiment 1).....	85
VIII-3. Reduction of the 1240 $\text{cm}^{-1}$ peak height with time for <i>rac</i> -LA polymerization initiated with PrOH/Sn(Oct) <sub>2</sub> (Table VIII-2, Experiment 1).....	86
VIII-4. First-order kinetic plots of <i>rac</i> -LA polymerizations initiated with PrOH/Sn(Oct) <sub>2</sub> , demonstrating the effect of the initial Sn(Oct) <sub>2</sub> concentration ( $[\text{rac-LA}]_0=1.0$ M, $[\text{PrOH}]_0=0.05$ M; Table VIII-2, Entries 1, 5, 9, 11, and 12).....	89
VIII-5. $R_p$ of <i>rac</i> -LA as a function of $[\text{Sn}(\text{Oct})_2]_0/[\text{PrOH}]_0$ ( $[\text{PrOH}]_0 = 0.050$ M, $[\text{rac-LA}]_0 = 1.0$ M).....	90
VIII-6. First-order kinetic plots of <i>rac</i> -LA polymerizations initiated with various alcohols/Sn(Oct) <sub>2</sub> , demonstrating the effect of the initiator architecture.....	91
IX-1. Refractive Index calibration plot of D,L-lactide.....	95
IX-2. Refractive Index calibration plot of $\epsilon$ -caprolactone.....	96
IX-3. GPC chromatogram (refractive index trace) of 50/50 mol% DLLA/CL conventional copolymerization at 6 minutes.....	97
IX-4. Conversion vs. time for conventional copolymerization of 90/10 mol% DLLA/CL.....	98
IX-5. Conversion vs. time for macroinitiator copolymerization of 90/10 mol% DLLA/CL.....	98
IX-6. Conversion vs. time for conventional copolymerization of 50/50 mol% DLLA/CL.....	99
IX-7. Conversion vs. time for macroinitiator copolymerization of 50/50 mol% DLLA/CL.....	99
IX-8. DSC of 90/10 mol% DLLA/CL copolymers.....	100
IX-9. DSC of 50/50 mol% DLLA/CL copolymers.....	101
IX-10. Carbonyl region of the <sup>13</sup> C NMR of conventional (A) and macroinitiator (B) 90/10 mol% DLLA/CL.....	103
IX-11. Carbonyl region of the <sup>13</sup> C NMR of conventional (A) and macroinitiator (B) 50/50 mol% DLLA/CL.....	103
IX-12. Conversion of macroinitiator copolymerization of 50/50 mol% DLLA/CL synthesized at 150°C.....	104

## Figure

IX-13. DSC of 50/50 mol% DLLA/CL macroinitiator copolymer synthesized at 150°C, 24 h reaction time. ....	104
IX-14. Carbonyl region of the <sup>13</sup> C NMR of macroinitiator 50/50 mol% DLLA/CL synthesized at 150°C; reaction time: 24 h (A), 48 h (B), 72 h (C), and 97 h (D). ....	105
IX-15. <sup>13</sup> C NMR of PDLLA-OH and PDLLA-COOH. ....	109
IX-16. Remaining mass of dried samples vs. immersion time in phosphate-buffered saline at 37°C. ....	110
IX-17. Buffer solution pH vs. time for degradation of PDLLA-OH, PDLLA-COOH, and PDLLA-BHMBA. ....	111
IX-18. Remaining mass of dried samples vs. immersion time in sewerage at 37°C. ....	112
IX-19. pH vs. time for degradation of 5,000 g/mol PDLLA-COOH, and PDLLA-BHMBA. ....	112
IX-20. Biodegradation Results for Sample 847-1A 2000 BHMBA-PLGA. ....	116
IX-21. Biodegradation Results for Sample 847-1B 2000 BD-PLGA. ....	117
IX-22. Biodegradation Results for Sample 847-4B 5000 BHMBA-PDLLA. ....	118
IX-23. Biodegradation Results for Sample 847-5B 5000 PDLLA-COOH. ....	119
IX-24. Biodegradation Results for Sample 531-40A-1 HMDI TPU 12% HB. ....	120
IX-25. Biodegradation Results for Sample 531-40B-1 HMDI TPU 12% HB. ....	121
IX-26. Biodegradation Results for Sample 531-48A-1, the scaled up TPU. ....	122
IX-27. Carbon Dioxide Evolution of Negative Control Samples (Baseline). ....	123
IX-28. Carbon Dioxide Evolution of Positive Control Sample (Glucose). ....	123

## LIST OF TABLES

### Table

II-1. Comparison of polymerizability factors (from ref <sup>62</sup> ). .....	20
IV-1. TPU polyol compositions, HFIP GPC results relative to PMMA standards and tensile data. ....	46
V-1. Design of experiments used for reactive extrusion of LDI-TPUs.....	62
V-2. Reagent flow rates. ....	62
V-3. Extruder temperature profiles. ....	62
V-4. Design of experiments used for reactive extrusion of H <sub>12</sub> MDI-TPUs. ....	63
V-5. Reagent flow rates for H <sub>12</sub> MDI TPU DOE.....	63
V-6. ANOVA table of LDI-TPU DOE.....	66
V-7. Molecular weight of LDI-TPU DOE runs. ....	66
V-8. Molecular weight of H <sub>12</sub> MDI-TPU DOE runs.....	68
V-9. ANOVA table of H <sub>12</sub> MDI-TPU DOE. ....	68
VI-1. Reaction Formulations and Second -Order Rate Constants for Isocyanate/Alcohol Reactions in <i>N,N</i> -Dimethylformamide <sup>a</sup> at 40°C with [NCO]/[OH]=1.00.....	74
VI-2. Reaction Formulations and Second-Order Rate Constants for Isocyanate/Alcohol Reactions in <i>N,N</i> -Dimethylforamide at 40°C with [NCO]/[OH]=1.00 with varying [DBTDL].....	78
VII-1. Testing of refractive index (RI) response of <i>rac</i> -LA and poly( <i>rac</i> -LA). ....	88
VII-2. Reaction Formulations and <i>k</i> <sub>app</sub> Values for <i>rac</i> -LA Polymerizations.....	92
A-1. Tin level of PDLLA with various post-polymerization preparations.....	108
A-2. Experimental Conditions for Polymerizations of D,L-Lactide <sup>a</sup> .....	109
A-3. Carbon Content Analysis Results of Samples. <sup>163</sup> .....	115



## CHAPTER I

### INTRODUCTION

As the use of polymers becomes increasingly prevalent so does the presence of polymers in the waste stream. In 2006, 14 million tons of plastic containers and packaging were part of the municipal waste stream according to the Environmental Protection Agency.<sup>1</sup> The majority of plastic waste ends up in landfills, but some other methods of handling plastic waste include incineration and recycling. This continuous growth in plastic waste is one main motivation for continued research toward degradable polymers, defined as polymers that undergo bond scission through biotic or abiotic mechanisms, leading to eventual fragmentation or disintegration. A biotic mechanism would include the activity of an organism that breaks down the covalent bonds of the polymer backbone. Abiotic degradation is controlled by environmental factors such as temperature, UV exposure, moisture, and others.

Aliphatic polyesters are the most well-known and popular type of degradable polymer. They are susceptible to hydrolysis as well as mineralization<sup>2</sup> and oxidation,<sup>3-6</sup> and their degradation rate can be controlled by manipulation of structure of the polymer including initial molecular weight, hydrophilic-hydrophobic balance, side groups, crystallinity, and glass transition temperature.<sup>7</sup> The growing popularity of degradable polyesters can also be measured by the growing number of commercial degradable polyesters including Ecoflex® (BASF), Eastar® Bio (Developed by Eastman), Bionelle® (Showa Polymers), Biomax® (Dupont) and NatureWorks™ PLA (Cargill-Dow).<sup>8-25</sup>

Poly(lactide) (PLA) is prevalent in degradable polymer research because of its physical and degradation properties, which make it suitable for a number of applications. It is available commercially from Cargill-Dow under the tradename NatureWorks®. The process used to make NatureWorks® involves the fermentation of corn to obtain L-lactic acid. The L-lactic acid is then converted into the cyclic dimer, or can be converted into a mixture of the three stereoisomers using tin catalysis. This process of monomer synthesis from corn is attractive because it is a renewable resource and does not depend on oil as a raw material. High molecular weight polymers are synthesized from lactide by ring-opening polymerization (ROP). There are a number of applications that utilize PLA including medical devices, clothing fibers, packaging applications, coatings, and blow-molded bottles, to name a few. There are two primary types of poly(lactide), poly(L-lactide) (PLLA) and poly(D,L-lactide) (PDLLA), synthesized from the racemic mixture of L- and D- lactide. Poly(L-lactide) is particularly favorable for the production of fibers since it is a semi-crystalline polymer. Poly(lactide)s are excellent packaging materials because they have high gloss and clarity (depending on the amount of crystallinity for PLLA), excellent printability, resistance to aliphatic molecules such as oils, good barrier properties including flavor and aroma barrier characteristics, heat-sealable at low temperatures, and high tensile modulus.<sup>18</sup> However PLA does have limitations related to its physical and thermal properties. Poly(L-lactide) has a  $T_g$  of 50-59°C and a  $T_m$  of 130-196°C and tends to be brittle.<sup>26</sup> There is a large body of research aimed at improving the degradation, physical, and/or thermal properties of PLA through copolymerization or chemical modification.<sup>27-31</sup>

In addition to polyesters, another area of increasing research activity is that of degradable polyurethanes.<sup>32-39</sup> Thermoplastic polyurethanes (TPUs) are versatile polymers created through the reaction of a diisocyanate with a mixture of a chain-extending diol and/or diamine and a polymeric polyol. TPUs are characterized by a phase separated morphology that exists between the so-called hard segment (HS) and soft segment (SS). The HS is the product of the reaction of the diisocyanate and chain extender, and the SS is the polyol.<sup>40</sup> The properties of TPUs are readily tunable to span a range of physical properties from elastomeric, to plastic, to high-strength fiber, by varying the amount and composition of each segment. The polyol is usually either a polyether or polyester; thus polyurethanes offer the possibility of incorporating biodegradable polyester chain elements into a family of polymers whose properties can be readily tuned for a variety of applications, including soft plastic and elastomeric applications for which traditional biodegradable polymers are ill-suited. Typically, these systems utilize aliphatic isocyanates that are less toxic than their aromatic counterparts, both in terms of initial polyurethane synthesis and potential amine degradation products. Polyurethanes offer a broader range of physical and thermal properties compared to polyesters. The use of polyurethanes that incorporate degradable polyesters is a promising method to develop degradable materials that can potentially replace a wide range of traditional thermoplastics such as poly(styrene) and poly(propylene) as well as elastomers such as poly(isobutene) and poly(butadiene).

The goal of the research presented herein was to develop degradable materials with potential applications such as stretch wrap and other non-fiber applications. Also, the understanding of the polymerization reactions to synthesize these materials was a key

component of the work carried out. This manuscript describes the synthesis and characterization of homo- and copolymers of D,L-lactide as well as degradable polyurethanes that incorporate lactide-containing degradable polyesters. Additionally, investigations into the reaction kinetics of homo- and copolymerizations of D,L-lactide and urethane forming reactions with isocyanates are described.

## CHAPTER II

### BACKGROUND AND REVIEW

#### Degradable Polyesters and Degradation

The need for degradable materials is of growing importance as non-degradable consumer waste is continually increasing. This not only an issue on land, but also at sea, where million of tons of plastic waste are accumulating and disrupting the stability of marine life.<sup>41</sup> Current solutions to control plastic waste include recycling, incineration for energy production, and alternative degradable plastics with benign degradation products.<sup>42</sup> The latter solution is made even more attractive by the fact that degradable plastics are often produced from a renewable, bio-based raw material. Hence, research and development of degradable materials has been increasing over the last several decades, resulting in a growing number of publications every year on this topic. There is also a growing number of commercially available degradable polymers on the global market. This growing interest in degradable materials is an indication of the awareness of the benefits offered by environmentally friendly polymers.

In the development of degradable materials a key polymer type has been aliphatic polyesters. Early studies by Carothers and coworkers at DuPont in the 1920s and 30s established the relationship between molar mass and extent of reaction, including the effect of stoichiometric imbalance of functional groups, for condensation and step growth polymerizations, and they developed the first fundamental approach to lactone polymerization.<sup>43</sup> Early aliphatic polyesters were plagued with poor mechanical properties as a result of low molecular weights. These materials were used as soft segments in the production of polyurethanes<sup>44</sup> and plasticizers in poly(vinylchloride)

(PVC).<sup>45</sup> Poly(lactides) were considered for use as a biocompatible, biodegradable, and bioresorbable material as early as the 1960s and have received significant attention ever since. Homo- and copolymers of lactide and glycolide have been developed for use as surgical sutures, drug delivery devices, and other body implants by a number of research groups.<sup>46-49</sup> Vert and coworkers have contributed significantly to the research of implantable materials over the years and have been instrumental in the pursuit to use biodegradable polyesters as an alternative to commodity plastics in this area.<sup>50</sup>

Another indication that degradable polymers are growing in popularity is the number of commercial materials available. Presently, Eastman, BASF, Showa Highpolymer (Japan), SK Chemicals (South Korea), DuPont, Mitsubishi Gas Chemical (Japan), and Cargill-Dow have developed and marketed degradable polyesters with the target of replacing commodity plastics. Two examples are poly(butylene adipate-co-terephthalate) produced by Showa Highpolymer and SK Chemicals and for sale in the U.S, and poly(L-lactide) sold by Cargill-Dow under the trade name NatureWorks® with applications as fiber, film, and sheet.

These materials are being developed primarily for their degradation characteristics, which are influenced by many factors. Environmental factors that can affect degradation of polymers include temperature, moisture, trace minerals and salts, nutrients and co-metabolites, oxygen, pH, redox potential, pressure, and light.<sup>3</sup> Also, the nature of the polymer itself governs degradation behavior. Properties such as molecular weight, hydrophilicity, branching, surface area, and crystallinity play a role in polymer degradation.<sup>3</sup> Enzymes can also trigger degradation, which is termed biodegradation.

Biodegradation is governed by the type and level of enzyme, the location of the enzyme (intracellular vs. extracellular), and the presence of inhibitors or enzyme inducers.<sup>3</sup>

Susceptibility to hydrolysis is an inherent characteristic of ester linkages.

Accordingly, the polyester's affinity for water is a pivotal factor in controlling hydrolytic degradation. Generally, an increase in the polymer's polarity enhances degradability and vice versa. For instance, Guiding and Reed showed that increasing the glycolide content in amorphous copolymers derived from glycolide and L-lactide results in an increase in both water uptake and rate of hydrolytic degradation due to increased hydrophilicity of the copolymers.<sup>51</sup>

Another important factor that controls the rate of degradation is crystallinity.<sup>26,52-</sup>

<sup>57</sup> Degradation by hydrolysis can occur no faster than the rate at which water enters the polymer. In a semi-crystalline polymer, the degradation of the crystalline regions is hindered by the very low permeability of water into the crystalline domain. Also, polymers with a higher degree of crystallinity have lower degrees of freedom of motion, lessening the probability of attaining the proper orientation to induce chain cleavage. Both of these factors make ester linkages within a crystallite more resistant to simple hydrolysis. In contrast, the permeability toward water of the amorphous regions of the polyester is relatively high. This behavior was demonstrated by Fukuzaki and coworkers by using low molecular weight copolymers of D- and L-lactide, whereby highly crystalline copolymers containing high feed ratios of one stereoisomer degraded more slowly in comparison to the totally amorphous racemic mixture.<sup>58</sup> The different rates of hydrolysis of amorphous and crystalline regions, results in a characteristic degradation mechanism in semi-crystalline polyesters. Hydrolysis begins first in the amorphous

regions. Random cleavage of ester bonds forms hydroxyl and carboxylic acid end group (Scheme II-1), upon which degradation accelerates due to increased hydrophilicity due to the formation of these polar groups and the acid catalytic effect.



**Scheme II-1.** Hydrolysis of ester linkage contained in a polyester.

Once sufficient tie molecules between crystallites have broken, the polymer loses physical properties and begins to fragment. In a slower process, crystalline regions undergo surface erosion leading to eventual disintegration of the polymer.

Molecular weight and chain flexibility, which are related to glass transition temperature ( $T_g$ ), also affect hydrolytic degradation. A polymer below its  $T_g$  will resist the entry of water due to reduced chain mobility. Negligible degradation is observed at temperatures below the glass transition of PET as determined by Hosseini and coworkers.<sup>59</sup> Hydrolytic degradation of the PET increased as temperatures increased above  $T_g$  due to increased chain flexibility and diffusion of water.

#### Ring-Opening Polymerization of Cyclic Lactones Using Stannous Octoate

Ring-opening polymerization (ROP) is a convenient method to synthesize polymers that typically would be synthesized by condensation polymerization.<sup>60,61</sup> In contrast to the step growth mechanism of condensation reactions, ROP proceeds through a chain growth mechanism comprising the steps, initiation, propagation, chain-transfer, and termination. ROP can typically deliver higher molecular weight compared to step-growth polymerization because the strict requirements of the Carothers equation



regarding reaction stoichiometry and conversion do not apply. However, ROP does not involve any small molecule by-product, typical of a condensation reaction, whose removal could be used to drive the reaction to high conversion. Thus, the ability of a given lactone (or cyclic carbonate) to undergo ROP to high conversion is a function not only of reactions kinetics, but also of the thermodynamics of the reaction. Factors that effect the thermodynamics of ROP are ring size; the presence, number, and type of substituents; and ring strain.<sup>62</sup> Conversion of medium-sized rings (5-7 atoms) rarely reaches 100% due to a thermodynamically controlled equilibrium between polymerization and depolymerization.<sup>63</sup> This equilibrium behavior is indicative of systems that have a ceiling temperature.<sup>64</sup>

The first reported ROP of the cyclic dimer of glycolic acid using ZnCl was reported in 1893 by Bischoff and Walden.<sup>65,66</sup> In 1903, room temperature oligomerization of  $\delta$ -valerolactone was reported by Fichter and Beisswenger.<sup>67</sup> Later, Carothers and coworkers reported polymerizations of glycolide, trimethylene carbonate, ethylene oxalate, p-dioxan-2-one,  $\delta$ -valerolactone as well as the synthesis of  $\epsilon$ -caprolactone monomer and polymer.<sup>43</sup> Scientific interest in lactones and polymerization of lactones has grown steadily since this early work. However, it was in the 1960's, with the introduction of commercially available lactone monomers, that rapid growth in this area was realized.

The first reports of tin(II) 2-ethylhexanoate (SnOct) catalyzed ROP appeared in the late 1960s.<sup>68,69</sup> SnOct has become one of the most popular catalysts because of its low cost, low toxicity, and high efficiency<sup>70</sup> as well as certain FDA approvals for food and medical products.<sup>71</sup> The mechanism of SnOct catalyzed polymerization has been a

disputed topic over the last thirty years; cationic,<sup>72,73</sup> activated monomer,<sup>74,75</sup> direct SnOct activation,<sup>75</sup> and SnOct/alcohol cointiation<sup>70,76-85</sup> mechanisms have all been proposed. Kowalski and coworkers recently provided evidence that SnOct is converted into a tin(II) alkoxide that is the initiating species of the polymerization, supporting the cointiation-type mechanism.<sup>86,87</sup> Figure II-1 illustrates the formation of the tin(II) alkoxide initiating species and the coordination-insertion ring opening mechanism for the polymerization of lactide. The alcohol initiator initially complexes and subsequently reacts with SnOct producing a stannous alkoxide species (**1**) and liberating 2-ethylhexanoic acid (**3**) before polymerization commences (reaction **D**). The stannous dialkoxide initiator (**2**) is formed upon further reaction with a second equivalent of alcohol, simultaneously releasing a second equivalent of 2-ethylhexanoic acid (reaction **B**). Competing reactions of adventitious water with (**1**) or (**2**) serve mainly to deactivate the catalyst *via* a reversible reaction (reaction **C**), effectively decreasing the concentration of active stannous alkoxide and producing a stannous alcohol derivative (**4**), which is more thermodynamically stable than the stannous dialkoxide, but less efficient as an initiator.<sup>81</sup> The first actively propagating chain end (**5**), which consists of both the initiating alcohol fragment and the active propagating center derived from the first monomer unit and stannous alkoxide, is generated by reaction of (**2**) with monomer *via* coordination-insertion (reaction **D**). Subsequently, (**5**) either propagates or undergoes rapid intermolecular exchange of the stannous alkoxide moiety for a proton from either hydroxyl groups of initiator (if remaining) or another hydroxy chain end, which can also be polymeric in nature. Ultimately these processes establish a dynamic equilibrium between activated and deactivated chain ends such that R represents unreacted alcohol initiator or hydroxy chain

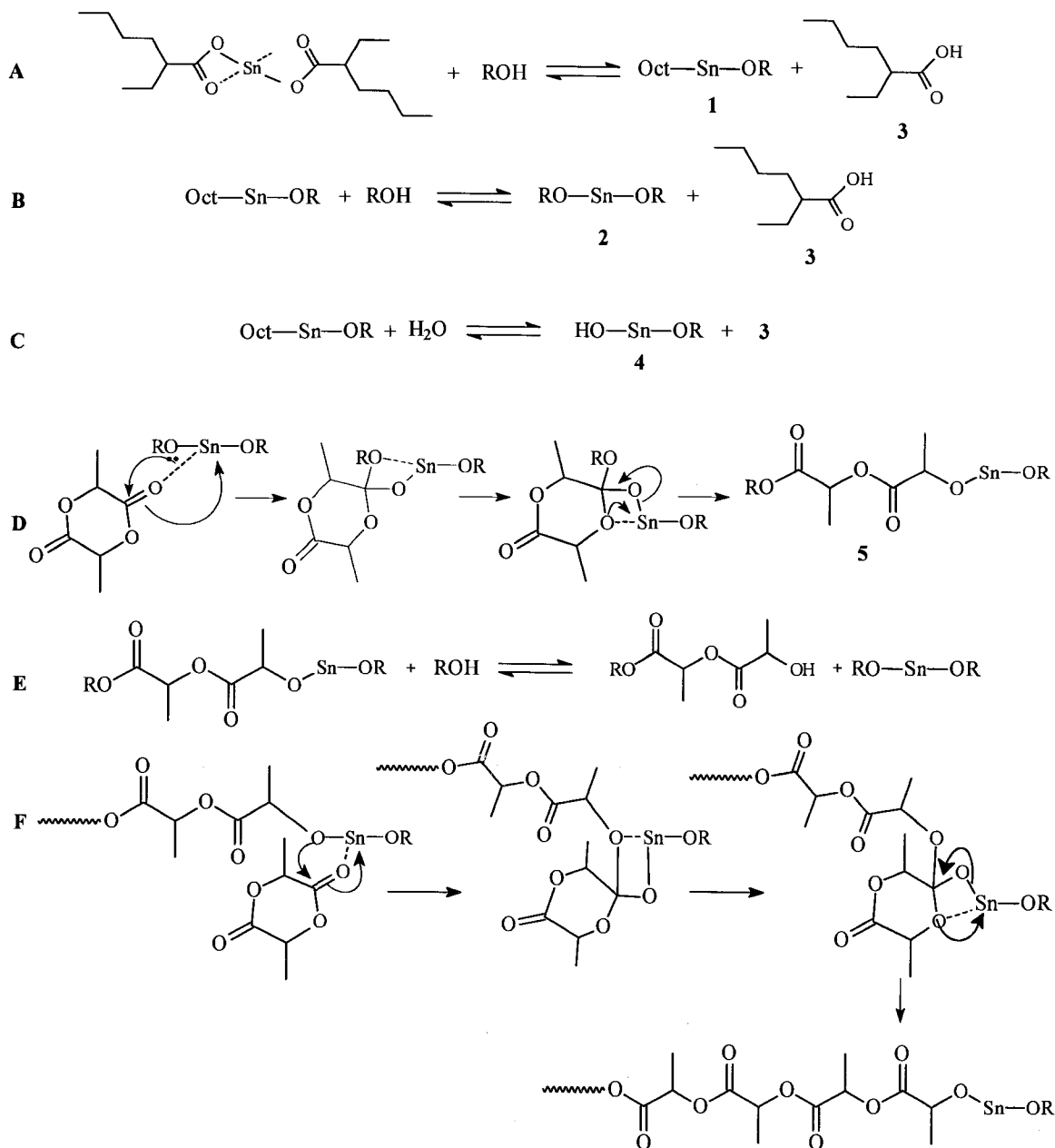


**Figure II-1.** Mechanism of the SnOct catalyzed ROP, including formation of the tin(II) alkoxide initiating species (A-C) and the coordination-insertion ring opening mechanism.

ends generated *in-situ* (reaction E). Propagation proceeds through acyl oxygen cleavage of the cyclic monomer (reaction F).

SnOct is perhaps the most commonly used catalyst for ROP of lactones and cyclic carbonates in both industry and academia, however there are a number of other catalysts

that have also been investigated. Alkoxy complexes based on other metals such as Al(III),<sup>76,88-91</sup> Fe(II),<sup>92</sup> Sn(IV),<sup>80,93-101</sup> Ti(IV),<sup>102</sup> scandium,<sup>103</sup> zinc,<sup>104</sup> and germanium<sup>105</sup> have also been used for ROP of lactones. Also, totally organic catalysts, such as guanidine and amidine have been investigated.<sup>106</sup>

### Degradable Thermoplastic Polyurethanes

Polyurethanes (PUs) are an important and versatile class of polymeric materials, with many uses within the fields of coatings, foams, sealants, adhesives, elastomers, and biomaterials.<sup>107,108</sup> They are conveniently divided into two classes depending upon whether having been derived from aromatic or aliphatic isocyanates. Recently, a number of reports have issued concerning biodegradable polyurethanes containing hydrolytically unstable polyester soft segments, for example, poly( $\epsilon$ -caprolactone), poly(D,L-lactide), poly(glycolide), and/or copolymers therefrom.<sup>32-39,109-114</sup> For these materials, aliphatic isocyanates are overwhelmingly preferred due to the toxicity of aromatic amines, which are potential degradation products of an aromatic PU.<sup>115,116</sup>

Thermoplastic polyurethanes (TPUs) are versatile polymers created through the reaction of a diisocyanate with a mixture of a chain-extending diol and/or diamine and a polymeric polyol. They are thermoplastic because they can be cycled between the solid and molten state such that they will flow when heated.<sup>64</sup> TPUs are characterized by a phase separated morphology that exists between the so-called hard segment (HS) and soft segment (SS). The HS is the product of the reaction of the diisocyanate and chain extender, and the SS is the polyol.<sup>40</sup> The properties of TPUs are readily tunable to span a range of physical properties from elastomeric, to plastic, to high-strength fiber, by

varying the amount and composition of each segment. The polyol is usually either a polyether or polyester; thus PUs offer the possibility of incorporating biodegradable polyester chain elements into a family of polymers whose properties can be readily tuned for a variety of applications, including soft plastic and elastomeric applications for which traditional biodegradable polymers are ill-suited. The elastomeric properties are developed because the phase-separated morphology allows HSs of adjacent polymer chains to crystallize acting as physical crosslinks.<sup>64,107</sup> This physical crosslink is in contrast to conventional elastomers that utilize chemical crosslinking.<sup>64</sup>

There has been scientific interest in polylactone-containing degradable polyurethanes for the past few decades largely because of their potential applicability as biomedical materials and more recently for environmental concerns. In particular, a significant amount of research has been conducted on degradable polyurethane materials for the application of tissue engineering.<sup>33,109-114</sup> Pennings and coworkers have examined a number of poly(ester-urethanes) for use as artificial dermal layers, including polymers produced from poly(lactide-co- $\epsilon$ -caprolactone) or poly(gycolide-co- $\epsilon$ -caprolactone) prepolymers and aliphatic isocyanates such as lysine diisocyanate and lysine diisocyanate methyl ester.<sup>109,110</sup> *In vitro* and *in vivo* degradation of these materials was examined and *in vivo* degradation was found to be more rapid because of enzymatic degradation that takes place in addition to hydrolytic degradation; the latter was the only mode of degradation studied *in vitro*. Guan and coworkers used poly( $\epsilon$ -caprolactone) and poly( $\epsilon$ -caprolactone-*b*-polyethylene glycol-*b*- $\epsilon$ -polycaprolactone) in the preparation of poly(ether-ester-urethane-urea) biodegradable polymer cell scaffolds.<sup>33</sup> De Groot and coworkers investigated poly( $\epsilon$ -caprolactone) based PUs for reconstructing menisci.<sup>111</sup>

Foams were made by the freeze-drying/salt-leeching technique and implanted in dogs. Long-term (up to three years) *in vivo* degradation of D,L-lactide / $\epsilon$ -caprolactone containing poly(urethanes) was studied by van Minnen and coworkers.<sup>114</sup> It was shown that after three years of implantation the PUs had resorbed almost completely, indicating safe biodegradability. Guelcher provides a detailed discussion about the developments of degradable poly(urethanes) for use in regenerative medicine applications.<sup>113</sup>

Research that is not directly focused on medical applications largely deals with TPU elastomers because of the excellent physical properties that can be achieved over a wide temperature range. Tatai and coworkers investigated TPUs with a degradable HS based on a chain extender composed of D,L-lactic acid and ethylene glycol and a poly( $\epsilon$ -caprolactone) SS. Some of the materials synthesized had elongations at break in excess of 1000% and sub-zero  $T_g$ s, typical of an elastomer. Wiggins and coworkers described degradable TPU elastomers based on L-lysine diisocyanate and poly( $\epsilon$ -caprolactone) with excellent physical properties and which might serve as high strength materials.<sup>34</sup> Moravek and coworkers also described TPU elastomers, but based on dicyclohexylmethane-4,4'-diisocyanate ( $H_{12}$ MDI) and a mixed polyol system consisting of poly(butylene adipate) and poly(D,L-lactide-*co*-glycolide) (PLGA).<sup>35,36</sup> These materials also demonstrated excellent physical properties, and they exhibited enhanced degradation because of the incorporation of PLGA.

#### Real-time Reaction Monitoring Using FTIR Spectroscopy

The FTIR monitoring of reactions in real-time was popularized after Milosevic and coworkers at ASI Applied Systems described the development of a new ATR-FTIR

sampling technology based on a small multi-reflection diamond crystal, such that a probe could be inserted directly into a reactor for *in-situ* reaction monitoring.<sup>117</sup> Shortly thereafter, a number of publications followed pertaining to *in-situ* monitoring of surface polymerizations<sup>118-121</sup> as well as the synthesis of mesoporous silicate.<sup>122</sup> However, Storey and coworkers provided the first detailed report of *in-situ* reaction monitoring of a solution polymerization.<sup>30</sup> The authors accurately described the methods of data collection and processing, the system capabilities, and the kinetic analysis of the carbocationic polymerization of isobutylene. Since then, a number of polymerization systems have been studied including carbocationic polymerization of isobutylene<sup>30,123,124</sup> and styrene (carbocationic<sup>125,126</sup> and also free radical<sup>127</sup>), metathesis polymerization,<sup>128</sup> urethane reactions,<sup>129-133</sup> and solution ROP of D,L-lactide.<sup>134-136</sup> Recently, Long and coworkers demonstrated the use of *in situ* FTIR spectroscopy to determine reactivity ratios for maleic anhydride/norbornene-free radical copolymerization,<sup>137</sup> and the influence of hydroxyl-containing monomers and additives on the kinetics of alkyl acrylate monomers using *in situ* FTIR spectroscopy.<sup>138</sup>

Prior to the development of *in-situ* FTIR spectroscopy, instantaneous isocyanate concentration of urethane-forming reactions was determined by quenching the aliquot with a known excess of amine, and then back-titrating unreacted amine with an acid to determine the concentration of isocyanate within the aliquot.<sup>139-145</sup> In at least one case, isocyanate concentration was determined through FTIR spectroscopic analysis of the reaction aliquots.<sup>129</sup> In all cases, collection, titration, and analysis of the reaction aliquots was very laborious and time-consuming. For lactone polymerizations, common techniques employed to monitor monomer conversion include <sup>1</sup>H NMR, size exclusion

chromatography (SEC), polarimetry, and calorimetry. For example, Gross and coworkers<sup>146</sup> examined the enzyme-catalyzed polymerization of  $\epsilon$ -caprolactone (CL) by in-situ  $^1\text{H}$  NMR. However, the NMR tube had to be removed periodically and shaken because of poor mixing, making evaluation of the kinetics and polymerization mechanism an arduous process. Another method used to determine conversion of CL was size exclusion chromatography (SEC) using a variety of  $\text{Sn}(\text{Oct})_2/\text{ROH}$  co-initiating systems.<sup>70</sup> However, time-consuming and laborious removal of aliquots and subsequent sample preparation followed by chromatographic separation are significant limitations of this method. Penczek and coworkers<sup>87</sup> monitored L-lactide conversion using polarimetry and SEC, where they found good correlation between the two techniques. However, the polarimetric cells were attached to a custom glass reactor, which was built especially for the kinetic measurements, and polymerizations were carried out using high vacuum techniques. Soum and coworkers<sup>147</sup> studied monomer conversion of various lactones using adiabatic calorimetry within an adiabatic vessel connected to a temperature recorder. Temperature measurements were correlated to monomer conversion; however, no comparison with conversion data determined separately by NMR or gas chromatography was discussed.

The progression of ROP of lactides may be followed by measuring the decrease in absorbance of the  $933\text{ cm}^{-1}$  ( $-\text{CO}-\text{O}-$  ring breathing mode) or the  $1240\text{ cm}^{-1}$  (C-O-C stretch) peak of D-, L-, or D,L-lactide.<sup>148,149</sup> The first research group to report a kinetic investigation of the ROP of lactide by monitoring the  $1240\text{ cm}^{-1}$  peak using *in-situ* spectroscopy was Hillmyer and coworkers in 2002.<sup>134</sup> Monomer conversion and rate constants of propagation were determined for bis(amidinate) Sn(II) alkoxide-catalyzed



polymerizations of D,L-lactide but, little information was given about how the data were processed. Messman and Storey investigated the solution ROP of D,L-lactide utilizing *in-situ* spectroscopy to follow the  $1240\text{ cm}^{-1}$  peak.<sup>135,150</sup> These authors describe a method whereby peak height was measured and correlated to actual monomer concentration by way of a calibration curve that was generated using known concentrations of monomer and polymer. The peak height vs. time data were subsequently used to construct kinetic plots whereby the rate constants were calculated for reactions of varying concentrations of alcohol and catalyst. Also, the reported data were in good agreement with SEC measurements, indicating that the FTIR method using  $1240\text{ cm}^{-1}$  peak height was an accurate and convenient method to study the effect of different experimental variables on the rate of polymerization.

To monitor urethane reactions, the isocyanate peak ( $2260\text{-}2290\text{ cm}^{-1}$ ) is easily identified and monitored in the IR spectrum allowing for straightforward calculation of reaction progress.<sup>130</sup> The formed urethane carbonyl peak at  $\sim 1700\text{ cm}^{-1}$  has also been observed and is of significant intensity for kinetic calculations.<sup>132,133,151</sup> Xu and coworkers<sup>132</sup> determined reaction kinetics and activation energies of phenylisocyanate with short chain alcohols. They monitored the isocyanate double band at  $2284\text{ cm}^{-1}$  and the urethane carbonyl at  $\sim 1700\text{ cm}^{-1}$  stating that there was good agreement in the kinetic data calculated from each band. Two reports by Yilgor and coworkers<sup>133,151</sup> investigated urea copolymers synthesized with  $\text{H}_{12}$ MDI using *in-situ* FTIR favoring the urethane carbonyl band at  $\sim 1700\text{ cm}^{-1}$  for kinetic calculations. Moravek and Storey recently described an *in-situ* method of transmission FTIR data collection using a flow-through transmission cell. This communication described the reaction kinetics of  $\text{H}_{12}$ MDI with

primary and secondary alcohols as a model for different polyols that could be used in PU synthesis. The isocyanate peak height at  $2266\text{ cm}^{-1}$  was monitored and correlated to a calibration of known concentrations of  $\text{H}_{12}\text{MDI}$ . The effects of different catalyst and catalyst concentrations were determined by calculating reaction rate constants from the real-time data.

### Copolymers of D,L-lactide

Copolymerization of two monomers is an effective way to customize the properties of a material. Generally, the physical and thermal properties of the resultant copolymer will be intermediate between those of either homopolymer.<sup>64</sup> One of the most researched lactide containing copolymers is poly(D,L-lactide-*co*-glycolide) (PLGA) because of its numerous uses in biomedical applications. PLGA has long been used as degradable sutures, bone fixatives, artificial skins and cartilages, dental materials, materials for bone regeneration, drug delivery<sup>152</sup> and many others partly because the degradation products are metabolised in the Krebs cycle.<sup>153</sup> More recently there has been a large number of publications concerning PLGA microspheres, usually used as a drug carrier for therapeutic applications via encapsulated antigens.<sup>153</sup> A good review of PLGA and other polyhydroxyalkanoates used as biomedical materials is provided by Ueda and Tabata.<sup>152</sup> For most biomedical applications, poly(glycolide) degrades too quickly and is difficult to process because of its high crystallinity and low solubility.<sup>152</sup> The incorporation of a comonomer such as D,L-lactide,  $\epsilon$ -caprolactone, and trimethylene carbonate allows the properties to be tuned for specific applications or processes.

The ability to control the properties of the copolymer is the primary benefit of copolymers. For example, the glass transition temperature ( $T_g$ ) can be controlled such that it can be deliberately made to fall between the  $T_g$ s of the respective homopolymers. This behavior of copolymers with respect to  $T_g$  is predicted by the Fox equation (Equation II-1):

$$\frac{1}{T_{gco}} = \frac{w_1}{T_{g1}} + \frac{w_2}{T_{g2}} \quad \text{Equation II-1}$$

where  $w_1$  and  $w_2$  are the weight fractions of the two monomers whose homopolymers have glass transition temperatures of  $T_{g1}$  and  $T_{g2}$ . Kylma and Seppala demonstrated this behavior with L-lactide and  $\epsilon$ -caprolactone as displayed in Figure II-2.<sup>154</sup>

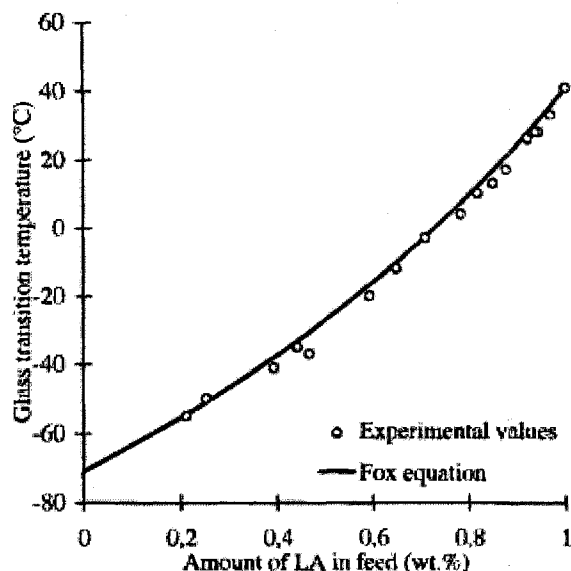


**Figure II-2.** Glass transition temperature of (L-lactic acid-co-  $\epsilon$ -caprolactone) and Fox equation plotted against the amount of L-lactic acid.<sup>154</sup>

The synthesis of copolymers is typically performed by initiation of a comonomer mixture where the final copolymer composition will approximately equal the initial monomer feed. However, variations in copolymer composition can arise, largely because of reactivity (or polymerizability) differences of the monomers. For lactones, as monomer ring size increases from 5 to 7 (e.g.  $\gamma$ -

butyrolactone→ $\delta$ -valerolactone→ $\epsilon$ -caprolactone), the ring strain and polymerizability increases.<sup>62</sup> The bond angle, strain energy, and  $\Delta H_p$  as listed in Table II-1, are indicators of this trend.

**Table II-1.** Comparison of polymerizability factors (from ref<sup>62</sup>).

Monomer	C-C-C Bond Angle (calc.) (deg.)	Strain energy (kJ/mol)	$\Delta H_p$ (calc.) (kJ/mol)	$\Delta H_p$ (obs.) (kJ/mol)
$\gamma$ -butyrolactone	102.1	32.2	-15.4	-6.8
$\delta$ -valerolactone	113.9	39.7	-26.8	-27.4
$\epsilon$ -caprolactone	114.4		-35.9	-28.8

In the case of cyclic dimer monomers of glycolic and lactic acid, where the ring size is constant, increasing substitution on the  $\alpha$ -carbon decreases polymerizability, mainly because of a decrease in  $\Delta H_p$ . Though ring strain is an important factor, this shows that ring substitution also has a significant influence. An increase in the number or size of pendant groups will decrease polymerizability due to increased steric repulsions in the chain relative to the ring.<sup>62</sup> For instance, a copolymerization of lactide and glycolide can result in irregular unit distributions because of differences in reactivity.<sup>155</sup>

CHAPTER III  
EXPERIMENTAL

Materials

Acetone-*d* (99.8% D, Aldrich Chemical Company) was used as received.

Argon (99.9%, Nordan Smith) was used as received.

Buffer Solutions, pH 4.00, 7.00, 7.40, 10.00 (Fisher Scientific) was used as received.

1,4-Butanediol (99.5%, anhydrous, Aldrich Chemical Company) was used as received.

1-Butanol (99.8%, anhydrous, Aldrich Chemical Company) was used as received.

2-Butanol (99.8%, anhydrous, Aldrich Chemical Company) was used as received.

Calcium hydride (Aldrich Chemical Company) was used as received.

$\epsilon$ -Caprolactone (99+%, Dow Chemical Company) was freshly distilled from CaH<sub>2</sub> under reduced pressure and stored under Argon prior to use.

Chloroform (anhydrous, 99+%, Fisher Scientific) was used as received.

Chloroform-*d* (99.8% D 0.03% v/v TMS, Aldrich Chemical Company) was used as received.

Dibutyltin dilaurate (98%, Aldrich Chemical Company) was used as received.

1,2-Dichloroethane (99%, Aldrich Chemical Company) was distilled from CaH<sub>2</sub> prior to use.

Dicyclohexylmethane-4,4'-diisocyanate (Desmodur W, Bayer) was fractionally vacuum distilled and stored under N<sub>2</sub> prior to use.

4-(Dimethylamino)pyridine (99%, Aldrich Chemical Company) was used as received.

Dimethyl sulfoxide-*d*<sub>6</sub> (99+%, Aldrich Chemical Company) was used as received.

Ethyl acetate (anhydrous, HPLC grade, Fisher Scientific) was used as received.

Ethylene glycol (99.8%, anhydrous, Aldrich Chemical Company) was used as received.

Glycolide (Ortec; Easley, SC) was used as received.

1,1,1,3,3,3-Hexafluoro-2-propanol (99%, Oakwood Products Inc.) was distilled from 3 Å molecular sieves prior to use.

5-Hexyn-1-ol (96%, Aldrich Chemical Company) was used as received.

Hydrochloric acid (12.1 N, Fisher Scientific) was used as received.

2,2-Bis-(hydroxymethyl)butyric acid (98%, Aldrich Chemical Company) was used as received.

D,L-lactide or *rac*-Lactide (Ortec; Easley, SC), which is 50:50 mixture of D- and L-lactide isomers, was used as received.

L-lactide (Ortec; Easley, SC) was used as received.

Magnesium sulfate (anhydrous, certified A.C.S., Fisher Scientific Company) was used as received.

Methyl alcohol (Fisher Scientific Company) was used as received.

Methylene chloride (99+%, J.T. Baker Chemical Company) was stored over 4A molecular sieves prior to use.

Methyl 2,6-diisocyanatocaproate or L-Lysine diisocyanate, methyl ester (Kyowa Hakko) was distilled under reduced pressure and stored under N<sub>2</sub> prior to use.

1-Methylimidazole (99+%, redistilled, Aldrich Chemical Company) was used as received.

Oxalyl chloride (98%, Aldrich Chemical Company) was used as received.

Poly(butylene adipate) (Desmophen 2502, Bayer) was used as received.

Poly( $\epsilon$ -caprolactone) (TONE 5249, Dow) was used as received.

Potassium hydroxide (Fisher Scientific) was used as received.

1,2-Propanediol (99.5%, Aldrich Chemical Company) was used as received.

Pyridine (anhydrous, 99.8%, Aldrich Chemical Company) was used as received.

Seawater (Aldrich Chemical Company) was used as received.

Sodium (20% suspension in toluene, Aldrich Chemical Company) was used as received.

Succinic anhydride (97%, Aldrich Chemical Company) was used as received.

Tetrahydrofuran (HPLC grade, Fisher Scientific) was distilled from CaH<sub>2</sub> prior to use.

Tin (II) 2-ethylhexanoate (95%, Aldrich Chemical Company) was used as received.

Toluene (anhydrous, 99.8%, Aldrich Chemical Company) was used as received.

Water was filtered and deionized to a resistance value of > 10 MΩ-cm prior to use.

## Instrumentation

### *Size Exclusion Chromatography (SEC)*

Molecular weights (number average and weight average) and molecular weight distributions (MWD) of THF-soluble polymeric materials were determined using a SEC system consisting of a Waters Alliance 2695 Separations Module, an on-line multi-angle laser light scattering (MALLS) detector (MiniDAWN™ or MiniDAWN™ TREOS, Wyatt Technology Inc.), an interferometric refractometer (Optilab DSP™, Wyatt Technology Inc.) and one of two sets of PLgel™ (Polymer Laboratories Inc.) SEC columns. Each set, consisting of two 3 μm mixed E or two 5 μm mixed D PLgel™ columns connected in series, was attached in a separate switchable loop (Waters EV700-100-WA switching valve) with only one of the two sets active during data acquisition. The 3 μm particle-size columns were used for samples that did not contain molecules

larger than ca. 10,000 g/mol; the 5  $\mu\text{m}$  particle-size columns were used in separating molecules between ca. 10,000-2,000,000 g/mol. Freshly distilled THF served as the mobile phase and was delivered at a flow rate of 1.0 mL/min. Sample concentrations were ca. 7-40 mg of polymer/mL of THF, and the injection volume was 100  $\mu\text{L}$ . The detector signals were simultaneously recorded using ASTRA™ 4.9 or 5.3 software (Wyatt Technology Inc.), and absolute molecular weights were determined by MALLS using a  $dn/dc$  value calculated from the signal response of the Optilab DSP and assuming 100% mass recovery from the columns.

Relative molecular weights and molecular weight distributions (MWD) of polymers not soluble in THF were determined using a SEC system consisting of a Waters Alliance 2695 Separations Module, two PL HFIPgel columns connected in series, and a Waters 2410 refractive index detector. Freshly distilled 1,1,1,3,3,3-hexafluoro-2-propanol (HFIP) served as the mobile phase and was delivered at a flow rate of 1.0 mL/min. The sample molecular weights and MWDs were calculated using a calibration curve derived from PMMA standards in the range of 1,300 to 910,500 g/mol. Sample concentrations were 5-30 mg/mL in freshly distilled HFIP, and the injection volume was 50  $\mu\text{L}$ . The detector signal was recorded and analyzed using Empower Pro software (Waters).

#### *Proton Nuclear Magnetic Resonance ( $^1\text{H}$ NMR) Spectroscopy*

$^1\text{H}$  NMR spectra were obtained using two different NMR spectrometers: a 200 or 300 MHz Varian Mercury<sup>VX</sup> spectrometer. The samples were prepared in 5-mm (o.d.) glass tubes, and the concentration was approximately 5-25% (w/w) in *d*-chloroform, *d*-



acetone or *d*-DMSO. Proton signals were reported against the published solvent lock resonance or an internal reference, tetramethylsilane (TMS) at 0 ppm.  $^1\text{H}$  spin-lattice relaxation times ( $T_1$ ) were determined using an inversion-recovery pulse sequence ( $180^\circ$ - $\tau$ - $90^\circ$ ) with a delay of  $\sim 20$ - $30$  s between scans.

#### *Carbon Nuclear Magnetic Resonance ( $^{13}\text{C}$ NMR) Spectroscopy*

$^{13}\text{C}$  NMR spectra were obtained using two different NMR spectrometers: a 200 or 300 MHz Varian Mercury <sup>VX</sup> spectrometer. The samples were prepared in 5-mm (o.d.) glass tubes and the concentration was approximately 10-25% (w/w) in *d*-chloroform or *d*-acetone. Carbon signals were reported against the published solvent lock resonance or an internal reference, tetramethylsilane (TMS) at 0 ppm.

#### *Differential Scanning Calorimetry (DSC)*

Glass transition temperatures ( $T_g$ ) and the crystalline melting temperature ( $T_m$ ) of the polymer samples were measured using a TA Instruments DSC Q100. Samples (6-15 mg) were heated from  $25^\circ\text{C}$  to  $90$ - $180^\circ\text{C}$  at a heating rate of  $10^\circ\text{C}/\text{min}$ , quenched, and heated again from  $-50^\circ\text{C}$  to  $90$ - $180^\circ\text{C}$  at the same rate. The reported  $T_g$  values represent the mid-point temperature for the glass-transition of the second heating cycle.

#### *Dynamic Mechanical Analysis (DMA)*

Dynamic mechanical analysis (DMA) was utilized to determine the viscoelastic transition temperatures. A TA instruments DMA Q800 was operated in film tension geometry mode with sample thickness between 0.8 and 1.1 mm. The films were tested at

a frequency of 1 Hz and an oscillation amplitude of 5  $\mu\text{m}$  at a heating rate of 2° C/min from -80-180°C.

#### *Fourier Transform Infrared (FTIR) Spectroscopy*

A Bruker Equinox™ 55 FTIR (Bruker Optics, Inc., Billerica, MA), equipped with OPUS 4.2 software, an Axiom Analytical Diamond Attenuated Total Reflectance (ATR) Probe DMD-270 (Axiom Analytical, Irvine, CA), and external mercury-cadmium-telluride (MCT) mid-band detector, and a silicone oil bath controlled using a DigiSense® 68900-01 temperature controller was used to collect real-time infrared spectra of the polymerization reaction. Spectra were acquired in the double-sided, forward-backward mode, with a phase resolution of 128  $\text{cm}^{-1}$  using a Mertz phase correction mode. Interferograms were truncated using the Norton-Beer medium apodization function with a zero-filling factor of 2.

Routine infrared analysis was performed by collecting transmission spectra of thin polymer films cast onto polished NaCl plates from ca. 25% (w/v) solution of the polymer dissolved in chloroform or THF. Solvent was removed by a gentle flow of dry  $\text{N}_2$  gas at room temperature.

#### *Tensile Testing*

Tensile measurements were made using a Material Testing System Alliance RT/10 and analyzed using an MTS Testworks 4 software package. Stress vs. strain measurements were made under ambient conditions using test specimens (Type M-II) prepared according to ASTM D882-02. Specimens were clamped using AL 2000N

pneumatic grips set at 40 p.s.i. and the tests were conducted using a 2250 lbf load cell operating at 10% range. The draw rate for the experiments was 10 mm/min.

#### *pH Determination of Aqueous Solutions*

pH values were acquired using an Accumet AR20 pH meter equipped with a accuTupH probe (Ag/AgCl double junction) and a variable temperature reference. The pH meter was calibrated before each use by a 3 point calibration curve method including buffer solutions 4.00, 7.00 and 10.00.

#### General Procedures

##### *Synthesis of Hydroxy-Terminated Telechelic Poly(D,L-lactide)*

Reactions were formulated within a Vacuum Atmospheres Company Dri-Lab glove box under an inert N<sub>2</sub> atmosphere. A representative procedure was as follows: 155.152 g (1.076 mol) of D,L-lactide, 2.848 g (0.032 mol) of 1,4-butanediol, and 0.162 g (0.40 mmol, 300 ppm Sn) of Sn(Oct)<sub>2</sub> were added to a 250 mL, 1-neck round bottom flask. The flask was then equipped with an overhead stirrer, and the polymerization was carried out by immersion of the flask in a 130° C thermostated oil bath contained within a dry N<sub>2</sub> glove box, for a predetermined time (3-5 h), after which the molten reactor contents were poured into a Teflon dish to cool. Catalyst was removed by dissolving the crude polymer in chloroform (20%, w (g),v (mL)) and washing the solution one time with 300 mL of a 1.0 M HCl (aq) solution. The polymer solution was then washed with 300-mL portions of de-ionized water until a constant pH was obtained. The pH of the polymer solution was tested using Hydrion pH test paper (pH range of 0-13), and a constant pH reading was assumed to indicate complete removal of residual HCl.

Typically, five water washes were sufficient to achieve complete removal of HCl. The organic layer was collected and subsequently dried over  $\text{MgSO}_4$  and filtered, and the excess solvent was removed by vacuum at ambient temperature.

*Synthesis of (Carboxylic-Acid)-Terminated Telechelic Poly(D,L-lactide)*

Hydroxy-terminated telechelic PDLLA was reacted with succinic anhydride catalyzed by 1-methylimidazole (NMI) to generate (carboxylic-acid)-terminated telechelic PDLLA. A representative procedure was as follows: hydroxy-terminated PDLLA (30.0 g, 6.0 mmol) was dissolved in 100 mL dichloroethane at 60°C, followed by the addition of succinic anhydride (1.700 g, 0.017 mol). After complete dissolution of the succinic anhydride, NMI catalyst (0.987 g, 0.012 mmol) was added and the mixture was allowed to react for ~48 h. The polymer solution was then allowed to cool to room temperature. Excess, unreacted succinic anhydride was removed by washing the polymer solution twice with 100 mL portions of 1 M aqueous HCl solution, followed by a wash with 100 mL saturated NaCl solution, and finishing with 100-mL portions of de-ionized water until a constant pH was obtained. The pH of the polymer solution was roughly tested using Hydrion pH test paper (pH range of 0-13), and a constant pH, indicating complete removal of residual HCl and/or succinic acid was typically achieved after five water washes. The organic layer was collected and subsequently dried over  $\text{MgSO}_4$  and filtered. The dried polymer solution was then precipitated once into cold MeOH and once into hexanes. The precipitated polymer was collected and excess solvent was removed by vacuum at ambient temperature.

*Synthesis of Poly(D,L-lactide) with Primary Hydroxyl Endgroups*

Carboxylic acid-terminated PDLA was reacted with excess oxalyl chloride to generate acid chloride-terminated PDLA. The acid-chloride terminated polymer was then reacted with 1,4-butanediol (BD) to yield a primary hydroxyl-terminated PDLA. A representative procedure was as follows: carboxylic acid-terminated PDLA (56.5 g, 11.1 mmol) was dissolved in 200 mL chloroform at room temperature in a 500 ml round bottom flask. After dissolution of the polymer, oxalyl chloride (4.303 g, 33.9 mmol, 3 eq of carboxylic acid) was added to the flask. The polymer solution was then allowed to react overnight to ensure complete conversion of the acids. Excess, unreacted oxalyl chloride was removed along with the solvent by rotary evaporation. Then, acid chloride-terminated polymer (54.0 g, 10.6 mmol) was again dissolved in chloroform. After complete dissolution of the polymer, BD (18.958 g, 0.210 mol, 10 eq per acid chloride) and 4-(dimethylamino)pyridine (DMAP) (1.295 g, 10.6 mmol) were added to the flask. The reaction was allowed to stir overnight. Excess, unreacted BD and DMAP were removed by washing the polymer three times with deionized water. The organic layer was subsequently collected and dried with  $\text{MgSO}_4$  and filtered. The dried polymer solution was then precipitated once into cold MeOH and once into hexanes. The precipitated polymer was collected and excess solvent was removed by vacuum at ambient temperature.

*Synthesis of Hydroxy-Terminated Poly(D,L-lactide) from 2,2-Bis(hydroxymethyl) butyric acid (BHMBA-PDLLA)*

Reactions were formulated within a Vacuum Atmospheres Company Dri-Lab glove box under an inert N<sub>2</sub> atmosphere. A representative procedure was as follows: 38.815 g (0.270 mol) of D,L-lactide, 1.185 g (8.00 mmol) of BHMBA, and 0.041 g (0.101 mmol, 300 ppm Sn) of Sn(Oct)<sub>2</sub> were added to a 100 mL, 1-neck round bottom flask. The flask was then equipped with an overhead stirrer, and the polymerization was carried out by immersion of the flask in a 130° C thermostated oil bath contained within a dry N<sub>2</sub> glove box, for 3-5 h, after which the molten reactor contents were poured into a Teflon dish to cool. The polymer was then stored under vacuum or in a desiccator.

*Synthesis of Hydroxy-Terminated Telechelic Poly(D,L-lactide-co-Glycolide) (BD-PLGA)*

Reactions were formulated within a Vacuum Atmospheres Company Dri-Lab glove box under an inert N<sub>2</sub> atmosphere. A representative procedure was as follows: 54.394 g (0.377 mol) of D,L-lactide and 43.804 g (0.377 mol) of glycolide were added to a 250 mL, 1-neck round bottom flask. The flask was then equipped with an overhead stirrer, and immersed into a 150° C thermostated oil bath, contained within a dry N<sub>2</sub> glove box, for ~20 min to fully melt the monomers. Then, 1.802 g (0.0200 mol) of BD and 0.102 g (0.253 mmol, 300 ppm Sn) of Sn(Oct)<sub>2</sub> were injected into the flask and the polymerization was carried out for 3-5 h. Upon removal from the oil bath the molten reactor contents were poured into a Teflon dish to cool. The polymer was then stored under vacuum or in a desiccator.

*Synthesis of Hydroxy-Terminated Poly(D,L-lactide-co-Glycolide) from 2,2-Bis(hydroxymethyl) butyric acid (BHMBA-PLGA)*

Reactions were formulated within a Vacuum Atmospheres Company Dri-Lab glove box under an inert N<sub>2</sub> atmosphere. A representative procedure was as follows: 53.751 g (0.373 mol) of D,L-lactide, 43.286 g (0.373 mol) of glycolide, and 2.963 g (0.0200 mol) of BHMBA, were added to a 250 mL, 1-neck round bottom. The flask was then equipped with an overhead stirrer, and immersed into a 150° C thermostated oil bath, contained within a dry N<sub>2</sub> glove box, for ~20 min to fully melt the monomers and BHMBA. Then, 0.102 g (0.25 mmol, 300 ppm Sn) of SnOct was injected into the flask and the polymerization was carried out for 3-5 h. Upon removal from the oil bath the molten reactor contents were poured into a Teflon dish to cool. The polymer was then stored under vacuum or in a desiccator.

*Synthesis of Degradable Thermoplastic Polyurethanes*

The following is a representative procedure for the synthesis of an H<sub>12</sub>MDI-based TPU carried out in a Vacuum Atmospheres Company Dri-Lab glove-box under an inert N<sub>2</sub> atmosphere. A 250 mL beaker was charged with 6.24 g (3.12 mmol) of BA, 6.23 g (3.12 mmol) of BD-PLGA or BHMBA-PLGA and 100 mL of DMF. This was set aside to allow the polyols to dissolve. A two-neck 250 mL round-bottom flask was charged with 100 mL of DMF, 6.162 g (23.5 mmol) of H<sub>12</sub>MDI, 1.494 g (16.6 mmol) of BD, and 0.032 g (0.051 mmol, 300 ppm Sn) of DBTDL. The flask was then submerged into a 40°C silicone oil bath and fitted with a mechanical stirrer. The solution was allowed to react with stirring for 30 min after which the previously weighed polyol solution was

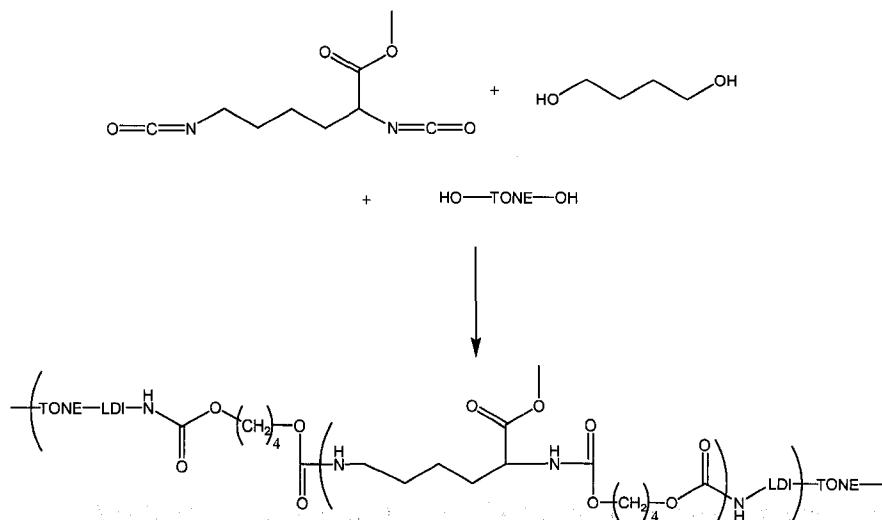
added and the reaction was continued for an additional 22 h. Upon completion of the reaction, the DMF was removed by rotary evaporation. The resultant polymer was then dissolved in chloroform and poured into a 300 mL PTFE dish. The dish was then placed in a room temperature vacuum oven to remove chloroform. Films of each sample (1 mm thick) were made using a hot press at 90-150° C. Mini dog bone specimens were cut out of the films using a stamping tool and these pieces were used for mechanical testing.

#### *Synthesis of TPUs via Reactive Extrusion*

TPUs were synthesized with a Prism TSE 16TC co-rotating twin-screw extruder. LDI, BD, and TONE 5249 were metered into the extruder using a Cole Parmer Gear Pump Drive Console (C-75211-50) coupled with a Cole Parmer MICROPUMP® Suction Shoe Pump Head (07002-25) for each reagent. Tygon Fuel and Lubricant Tubing was used for LDI and BD. Tone was pumped from a 1L round-bottom flask maintained at 65-70°C with a heating mantle. Viton tubing wrapped with heat tape was connected to the gear pump head that was also wrapped with heat tape to ensure that the polyol remained molten, allowing for proper dosing of the polyol. DBTDL was metered into the extruder using a RAZEL A-99 syringe pump. The reagents were fed into the feed throat of the extruder using a feed throat adapter. The adapter was designed such that the HS reagents, LDI, BD, and DBTDL, were injected into the extruder 2 cm upstream from where the polyol entered the extruder. TPUs were formulated using  $[NCO]/[OH] = 1.05$ . The amount of BD used was calculated as 12 wt.% of the polyol used, referred to as 12% HS. Formulations are listed in Table 2. The reaction scheme is illustrated in Scheme



III-1. A schematic representation of the reactive extrusion process is shown in Figure III-1.



**Scheme III-1.** TPU synthesis via reactive extrusion.

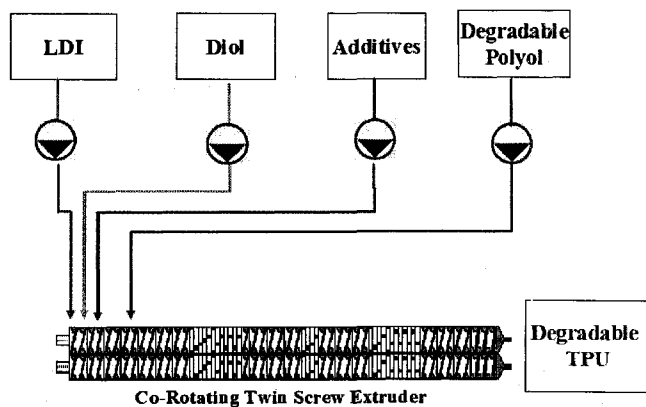


**Figure III-1.** Schematic representation of reactive extrusion process.

Similar TPUs were synthesized via reactive extrusion using the same procedure as above using H<sub>12</sub>MDI instead of LDI and poly(butylene adipate) instead of poly( $\epsilon$ -caprolactone).

### *H<sub>12</sub>MDI Kinetics Monitoring*

Isocyanate reactions were monitored using a Bruker Equinox 55 FTIR spectrometer set at a spectral resolution of 4 cm<sup>-1</sup>. A schematic representation of the reaction vessel and flow cell set up is displayed in Figure III-2. The flow cell assembly (A) (64401-2, New Era Enterprises, Vineland, NJ) possessed a 20 mm diameter aperture equipped with ZnSe windows and 0.20 mm Teflon spacers (see detail B). The intensity of the IR signal was controlled by spacer thickness between windows (path length) and IR beam intensity (controlled with adjustable iris aperture). The flow cell temperature was controlled using an Ace Glass temperature controller (12111-15, Vineland, NJ). The reaction vessel temperature was controlled with a silicone oil bath (C) and a Therm-O-Watch L6-1000SS temperature controller. The reaction vessel consisted of a 100 mL 3-neck round bottom flask, equipped with a magnetic stir bar and suction and discharge tubes (6 mm O.D. PTFE) passing through rubber septa fitted to the necks of the flask. The suction tube was submerged below the liquid level in the flask. The reaction vessel contents were continuously pumped through the flow cell using a Cole Parmer Master Flex PTFE Tubing Pump Head (D) connected to a digital Cole Parmer Master Flex Drive, using 6 mm O.D. PTFE tubing and a pump head speed of 75 RPM. The system was designed with materials, such as PTFE, that would not interfere with the reactions being monitored and were easily cleaned after each reaction. To prevent contamination from one reaction to the next, the flow cell was completely disassembled, cleaned, and reassembled between reactions.

A representative procedure for the reaction was as follows: within a Vacuum Atmospheres Co. Dri-Lab glovebox under inert N<sub>2</sub> atmosphere, a 3-neck 100 mL round

bottom flask equipped with a magnetic stir bar was charged with 74.440 g (~80 mL) of anhydrous DMF. The flask was capped with rubber septa, taken out of the glovebox, and connected to a dry N<sub>2</sub> purge. After connecting the flask to the PTFE tubing, the N<sub>2</sub> purge was removed, the pump was turned on, and air was removed from the tubing by first elevating the pump and then the flow cell until all air had been displaced from the tubing. The flask was then lowered into the 40°C oil bath and the flow cell temperature controller was also set to 40°C. The system was then allowed to equilibrate for approximately 20 min, after which a 32 scan solvent background was collected using OPUS 4.2 software. Then, 1.053 g (4.0 mmol) H<sub>12</sub>MDI was added to the flask via syringe, and spectra (average of 8 scans) were collected every 5 min. Once the isocyanate peak at 2266 cm<sup>-1</sup> had equilibrated (~20 min), 0.595 g (8.0 mmol) 1- or 2- BuOH (1:1 OH:NCO) was added along with the desired amount of catalyst. The reaction was allowed to continue until 30-

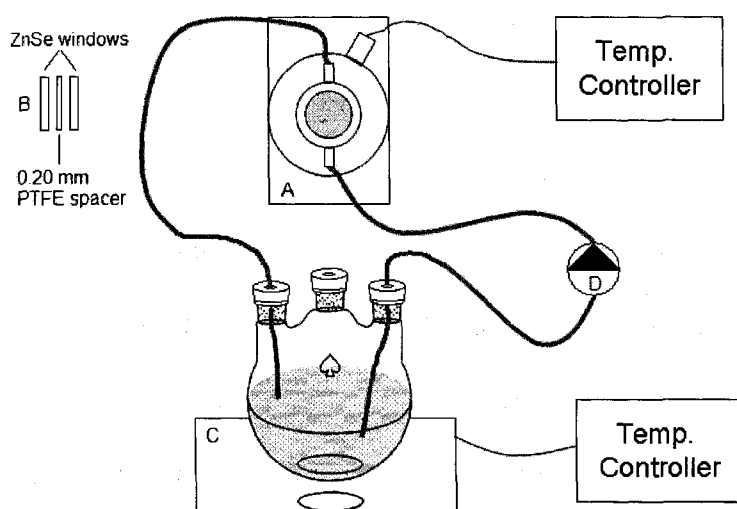


**Figure III-2.** Schematic representation of FTIR flow cell system utilized for data collection. (A) Temperature controlled flow cell, (B) flow cell window setup, (C) temperature controlled oil bath, (D) pump.

50% conversion of isocyanate was observed as shown by a reduction in the 2266  $\text{cm}^{-1}$  peak.

*Peak Integration and Regression Analysis.* Spectral analysis was performed on the calibration and real-time FTIR data with respect to the 2266  $\text{cm}^{-1}$  peak. Upon completion of the reaction, the data set collected was converted into a GC (3D) file using OPUS 4.2. The peak height was measured between 2330 and 2180  $\text{cm}^{-1}$  with a straight baseline from 2450 to 2175  $\text{cm}^{-1}$  (OPUS method L). Linear regressions were calculated with Origin 7.0 graphing software.

*Monomer Conversion and Kinetic Measurements of D,L-Lactide Polymerization in Tetrahydrofuran by Real-time ATR-FTIR*

Reactions were formulated within a Vacuum Atmospheres Company Dri-Lab glove box under an inert  $\text{N}_2$  atmosphere. In a typical experiment, 5.009 g of *rac*-LA (35 mmol), 0.105 g PrOH (1.7 mmol), and 29.956 g THF were charged into a 100-mL, three-necked, round bottom flask. The flask was capped with rubber septa, taken out of the glovebox, and subsequently connected to a dry Ar purge. After the collection of a THF background, the round-bottom flask was carefully connected to the ATR probe (24/40 joint) under a continuous Ar purge to exclude atmosphere components (moisture and air). A Liebig condenser was quickly fitted into one of the remaining 24/40 joints, and the continuous Ar purge was immediately connected to the top of the condenser. In all instances, a thermocouple was inserted into the reaction vessel through another rubber septum while maintaining a dry Ar purge. An oil bath, thermostated to 85°C was raised to entirely submerge the flask and its contents. The reaction mixture reached a maximum

temperature of 72 °C at which point the THF maintained a steady reflux. After approximately 10 min., the system was considered stable and data collection began. The reaction was stirred with a magnetic stirrer, and spectra (average of eight scans) were collected every 180 s to high monomer conversions over the spectral range of 5000-2300 and 1800-600  $\text{cm}^{-1}$  with 4  $\text{cm}^{-1}$  resolution. Before the collection of the 5<sup>th</sup> spectrum (15 min), 0.070 g  $\text{Sn}(\text{Oct})_2$  (0.17 mmol) catalyst solution (in THF) was prepared within a glove box and subsequently transferred via syringe to the reactor. Typically, catalyst solutions were made by weighing 0.700 g  $\text{Sn}(\text{Oct})_2$  catalyst directly into a 10 mL volumetric flask and diluting accordingly with THF. Thus, 1 mL of  $\text{Sn}(\text{Oct})_2$  catalyst solution was added to the reaction flask in all instances. The ROP was monitored by measuring the diminution of the 1240  $\text{cm}^{-1}$  peak. ATR-FTIR data files were selected and assembled into a GC or 3-D file using OPUS 4.2 software. Peak height was measured between the limits of 1247 and 1236  $\text{cm}^{-1}$ , relative to a straight baseline from 1276 to 1034  $\text{cm}^{-1}$  (OPUS method L). These reference points were chosen to obtain a baseline that was unchanging throughout the course of the polymerization reaction. The relationship between D,L-lactide (DLLA) concentration and peak height of the 1240  $\text{cm}^{-1}$  absorbance was established by calibration using peak height measurements made of refluxing THF solutions (72°C) containing known proportions of monomer and polymer. The calibration data were fitted to a second order polynomial. A representative calibration was as follows:

$$[\textit{rac-LA}] = -0.07246 + 4.20336 H_{1240} - 1.04493 H_{1240}^2 \quad \text{Equation III-1}$$

where  $H_{1240}$  is the  $1240\text{ cm}^{-1}$  peak height. The coefficients of the calibration equation varied over time due to changes in instrument configuration, etc.

Peak height values were copied into a Microsoft Excel spreadsheet and converted to concentration values based on the above calibration curve. The initial monomer concentration ( $[M]_0$ ) was correlated to the average  $1240\text{ cm}^{-1}$  peak height of the first few spectra taken before addition of the catalyst. Kinetic rate constants were determined from a plot of  $\ln ([M]_0 - [M]_{eq}) / ([M] - [M]_{eq})$  vs. time where  $[M]_{eq}$  is equilibrium monomer concentration as measured by integrating the area of the RI signal of monomer and polymer using SEC. These plots yielded a slope equal to the first-order (apparent) rate constants for propagation,  $k_{app}$ , where  $k_{app} = k_p[M^*]$ ;  $k_p$  is the rate constant for propagation and  $[M^*]$  is the concentration of actively growing chains.

#### *Conventional Copolymerization of D,L-Lactide and $\epsilon$ -Caprolactone*

Reactions were formulated within a Vacuum Atmospheres Company Dri-Lab glove box under an inert  $N_2$  atmosphere. A representative procedure was as follows: 66.847 g (0.464 mol) of D,L-lactide and 5.882 g (0.0516 mol) of  $\epsilon$ -caprolactone were added to a 100 mL, 2-neck round bottom flask. The flask was then equipped with an overhead stirrer, and immersed into a  $130^\circ\text{C}$  thermostated oil bath, contained within a dry  $N_2$  glove box, for  $\sim 20$  min to fully melt the monomers. Then, 1.335 g (0.0148 mol) of BD was injected and the mixture was stirred briefly. Then 0.025 g (0.062 mmol, 100 ppm Sn) of SnOct was injected into the flask and the polymerization was carried out for 24 h. Aliquots of the reactor contents were collected at the following time intervals: 30 s, 2, 4, 6, 8, 10, 15, 20, and 40 min, 1, 1.5, and 2 h, and then hourly up to at least 8 h and

lastly sometime between 22-24 h. Aliquots were collected in scintillation vials and cooled to room temperature in the antechamber of the glove box.

#### *Macroinitiator Copolymerization of D,L-Lactide and $\epsilon$ -Caprolactone*

Reactions were formulated within a Vacuum Atmospheres Company Dri-Lab glove box under an inert N<sub>2</sub> atmosphere. A representative procedure was as follows: 23.530 g (0.206 mol) of  $\epsilon$ -caprolactone and 5.341 g (0.0593 mol) BD were added to a 100 mL, 2-neck round bottom flask. Then, 66.868 g (0.464 mol) of D,L-lactide was added to a second 100 mL, 2-neck round bottom flask. The first flask, containing the  $\epsilon$ -caprolactone, was then equipped with an overhead stirrer, and immersed into a 130° C thermostated oil bath, contained within a dry N<sub>2</sub> glove box, for ~5 min to heat the monomer. Then, 0.102 g (0.20 mmol, 100 ppm Sn in final polymer) of SnOct was injected into the flask and the polymerization was carried out for 1 h. Aliquots were collected at 1, 5, 10, 20, 30, 45, and 60 min. Aliquots were collected in scintillation vials and cooled to room temperature in the antechamber of the glove box. At an elapsed time of 40 min the second flask, containing D,L-lactide, was immersed into a 130° C thermostated oil bath, contained within a dry N<sub>2</sub> glove box, to melt the lactide monomer. After the 60 min aliquot had been collected from the first flask, 7.246 g of the reaction mixture was added to the second flask. During the reaction in the second flask, aliquots were collected at the following time intervals: 30 sec, 2, 4, 6, 8, 10, 15, 20, and 40 min, 1, 1.5, and 2 h, then hourly up to at least 8 h, and lastly sometime between 22-24 h. Aliquots were collected in scintillation vials and cooled to room temperature in the antechamber.

### *Degradation Analysis of Polymers*

Select polymers were hydrolytically degraded by immersion into a phosphate buffered solution at a pH of 7.4 (0.05M) or seawater held at a constant temperature of 37°C. Sample disks of the polyesters were prepared by portioning an arbitrary amount of the polyester onto a mylar film, which was then placed into a vacuum oven. The polymer was then heated to 150 to 170° C, higher temperatures (170° C) were needed for the higher molecular weight materials, until a molten state was achieved, after which a vacuum was applied. The application of the vacuum removed all air pockets contained in the sample and the molten polymer was formed into disks using a circular die with a diameter of 2.54 cm. Disks with a mass of 0.5 to 1.1 gm were used for the study; this mass range corresponds to a disk thickness of ~2 to 3 mm.

Disks of polyurethanes were cut from a 1 mm thick melt pressed film using a 19 mm diameter circular punch. The polyurethanes were melt pressed at 140-150°C using 5000 psi clamping force for 5 minutes in a mold with a 1 mm cavity depth.

A representative procedure for polymer degradation was as follows: A polymer disk was placed into a glass jar (125mL) filled with 100mL of buffered solution. The jar and its contents were then placed into an incubator held at a constant temperature of 37° C. The discs were removed for analysis at predetermined time periods based on preliminary degradation rate studies.

At a predetermined time a sample disk was removed from the buffered solution and placed into a pre-weighed polystyrene weighing dish. The disk was brought to



constant mass in a vacuum oven, after which percent remaining mass ( $m_r$ ) was calculated using Equation III-2:

$$m_r = \left( \frac{m_{dry}}{m_0} \right) \times 100 \quad \text{Equation III-2}$$

where  $m_{dry}$  is the mass of the sample after drying and  $m_0$  is the initial mass before immersion.

## CHAPTER IV

### DEGRADABLE THERMOPLASTIC POLYURETHANES

#### Introduction

The goal of the work reported in this chapter was to develop a degradable material that could replace common non-degradable materials in specific applications. The targeted application was that of pallet stretch wrap. The funding of this research was provided by the Navy with the idea of developing materials that could be used onboard a ship and then be safely discarded into the ocean. Currently, any plastic materials brought onto a ship must remain on the ship until port is made. This creates storage and sanitary issues. If a plastic could be simply discarded into the ocean where it would break down into non-toxic byproducts, that would be a tremendous improvement over the current methods of handling plastic waste onboard any sea faring vessel. Such materials would also have a large number of applications for degradable products for consumer goods and even biomedical applications.

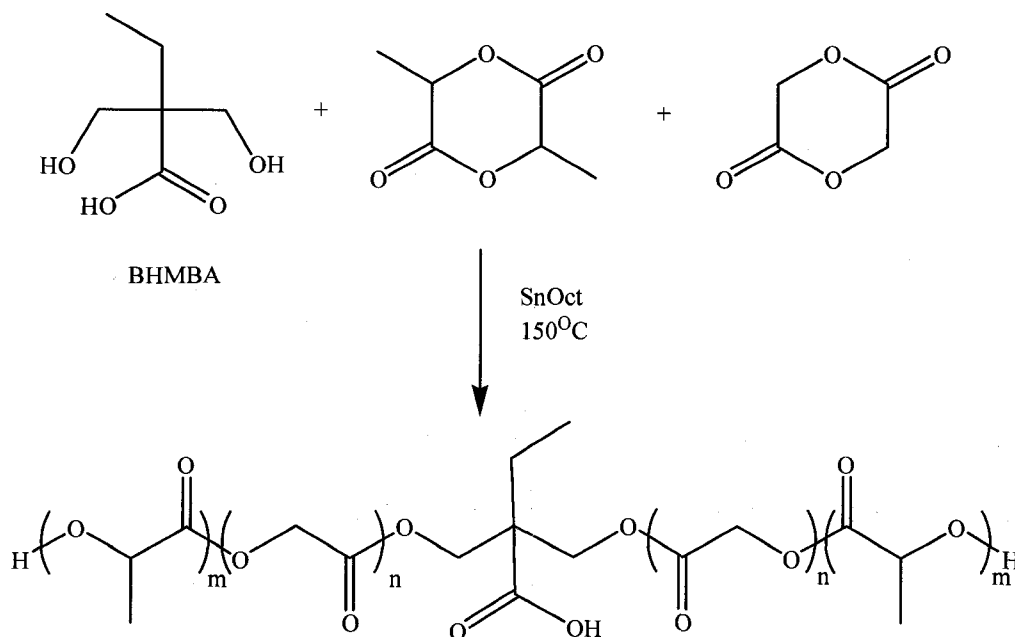
#### Results and Discussion

##### *Synthesis*

When engineering a degradable polymer, consideration must be given to the anticipated degradation products. For this reason, the less toxic aliphatic diisocyanate, H<sub>12</sub>MDI, was favored over the aromatic diisocyanates such as 4,4'-methylenebis(phenylisocyanate) (MDI).

The rate of degradation of a TPU will be affected by the type and amount of HS and polyol. The reported work initiates PLGA with BD and BHMBA as shown in

Scheme IV-1. The use of BHMBA places a pendant carboxylic acid group along the backbone of the polyol, leading to an increased rate of water uptake and increased overall rate of degradation of the polyol.<sup>156</sup>



**Scheme IV-1.** Synthesis of BHMBA initiated PLGA (alternatively BD could be used instead of BHMBA).

An important aspect of TPU formulation is the relative HS content. This parameter is controlled by the relative amounts of chain extender and polyol and can be quantified in a number of ways; herein it is expressed as percent HS where the weight of chain extender (BD) times 100% divided by the weight of polyol. Two HS concentrations were studied, 8% and 12%. The amount of H<sub>12</sub>MDI was calculated with  $[NCO]/[OH] = 1.03$ , where the total  $[OH]$  was the sum of polyol and chain extender. Typically, this ratio should be close to 1.0, but is generally between 1.0-1.1<sup>40</sup> to account for side reactions that may occur.

Mixed polyols were utilized to achieve a balance of good physical and thermal properties with enhanced rates of degradation. The polyol compositions used are listed in Table 1.

### Characterization

$^{13}\text{C}$  NMR was used to monitor the isocyanate to urethane conversion as well as to verify the incorporation of both polyol components. Figure IV-1 shows a representative partial spectrum of  $\text{H}_{12}\text{MDI}$  and 12% HS 50BA/50BHMBA-PLGA TPU (where 12% HS refers to the amount of chain extender and 50BA/50BHMBA-PLGA refers to the mol% and type of polyols). The isocyanate carbon peak of  $\text{H}_{12}\text{MDI}$  appears at 122.3 ppm as shown in spectrum A. The TPU spectrum (B) shows complete disappearance of the isocyanate carbon peak, as well as the formation of a urethane carbon peak at 156.0 ppm. Also, the carbonyl carbons of the two polyols are present, butylene adipate at 173.2 ppm, and the PLGA lactoyl units at 169.2 ppm and the glycol units at 166.5 ppm.

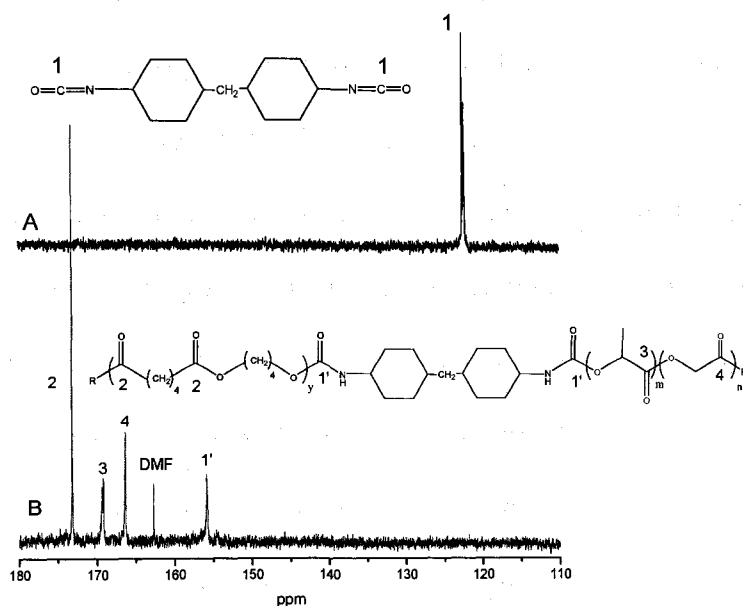


**Figure IV-1.** Carbonyl region of  $^{13}\text{C}$  NMR of  $\text{H}_{12}\text{MDI}$  and 12% HS 50BA/50BHMBA-PLGA TPU.

The relative molecular weight and MWD of the synthesized polymers were evaluated using HFIP GPC because more common solvents, such as THF, did not dissolve the polymers. The results of the GPC analyses are listed in Table IV-1, and a representative chromatogram is displayed in Figure IV-2. The chromatogram of the TPU synthesized with BA as the polyol is compared to the BA polyol to show the increase in molecular weight.

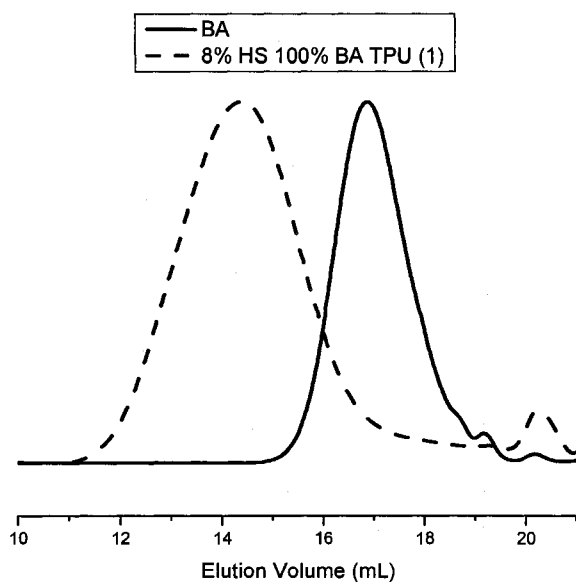


**Figure IV-2.** HFIP GPC chromatogram of BA and 8% HS 100% BA polyol TPU (Entry 1, Table IV-1).

**Table IV-1.** TPU polyol compositions, HFIP GPC results relative to PMMA standards and tensile data.

Entry	Polyol Composition	HFIP GPC			Modulus (MPa)	Energy to Break (N*mm)	Peak Stress (MPa)	Ultimate Strain (%)
		Mn (g/mol)	Mw (g/mol)	PDI				
1	8%HS 100%BA	33,855	104,085	3.07	20.1	8792	23.3	750
2	8%HS 75%BA 25%BHMBA-PLGA(847-1A)	12,870	24,104	1.87	15.2	3317	10.4	553
3	8%HS 75%BA 25%BD-PLGA(847-1B)	18,393	36,411	1.98	9.3	3338	9.9	612
4	8%HS 50%BA 50%BHMBA-PLGA(847-1A)	8,740	20,522	2.35	130.9	530	6.8	105
5	8%HS 50%BA 50%BD-PLGA(847-1B)	16,245	36,047	2.22	37.3	1879	6.2	395
6	12%HS 100%BA	71,339	145,913	2.05	13.1	6893 <sup>a</sup>	20.3 <sup>a</sup>	608 <sup>a</sup>
7	12%HS 75%BA 25%BHMBA-PLGA(847-1A)	12,257	29,619	2.42	30.4	4760	18.9	517
8	12%HS 75%BA 25%BD-PLGA(847-1B)	11,888	42,577	3.58	26.6	6849	21.7	598
9	12%HS 50%BA 50%BHMBA-PLGA(847-1A)	8,147	17,294	2.12	94.3	2889	12.1	344
10	12%HS 50%BA 50%BD-PLGA(847-1B)	11,453	35,369	3.09	49.4	2828	12.7	345

<sup>a</sup> Sample pulled out of grips prior to failure

Dynamic mechanical analysis (DMA) was used to probe the thermomechanical properties of the TPUs, showing thermal transitions and indicating useful temperature ranges. Figure IV-3 and Figure IV-4 show the plots of  $\tan \delta$  vs. temperature for the 8% and 12% HS TPUs respectively.

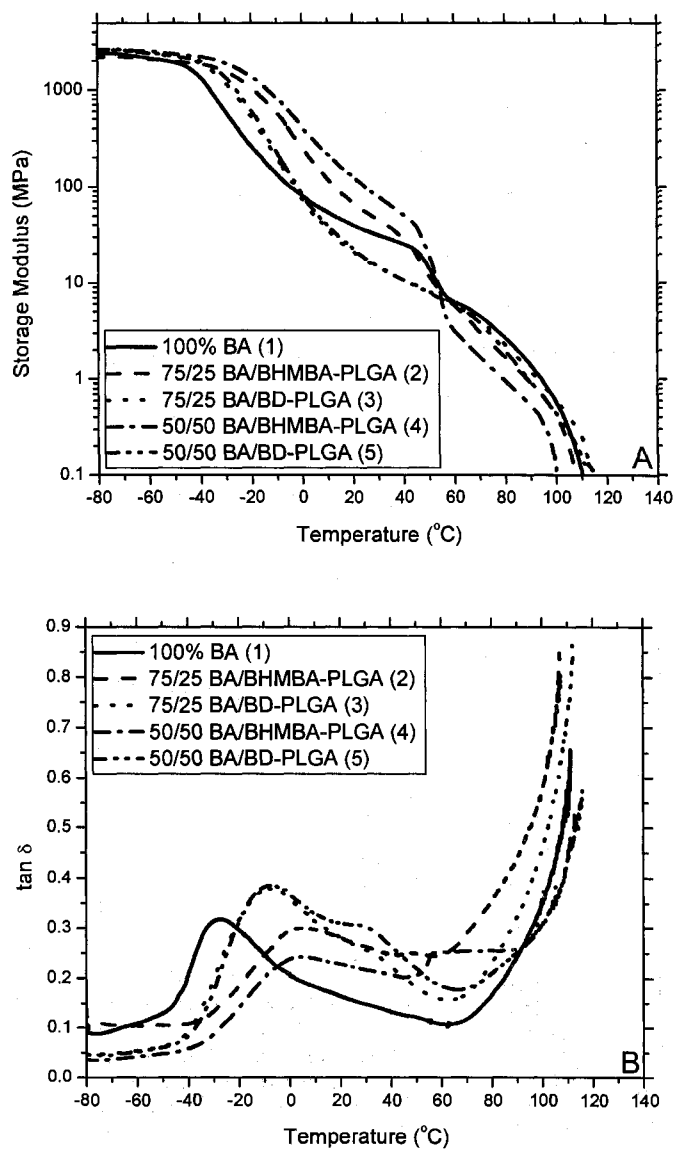


**Figure IV-3.** DMA plots of storage modulus vs. temperature (A) and  $\tan \delta$  vs. temperature (B) for 8% HS TPUs. The number in parenthesis corresponds to the entry number of Table IV-1.

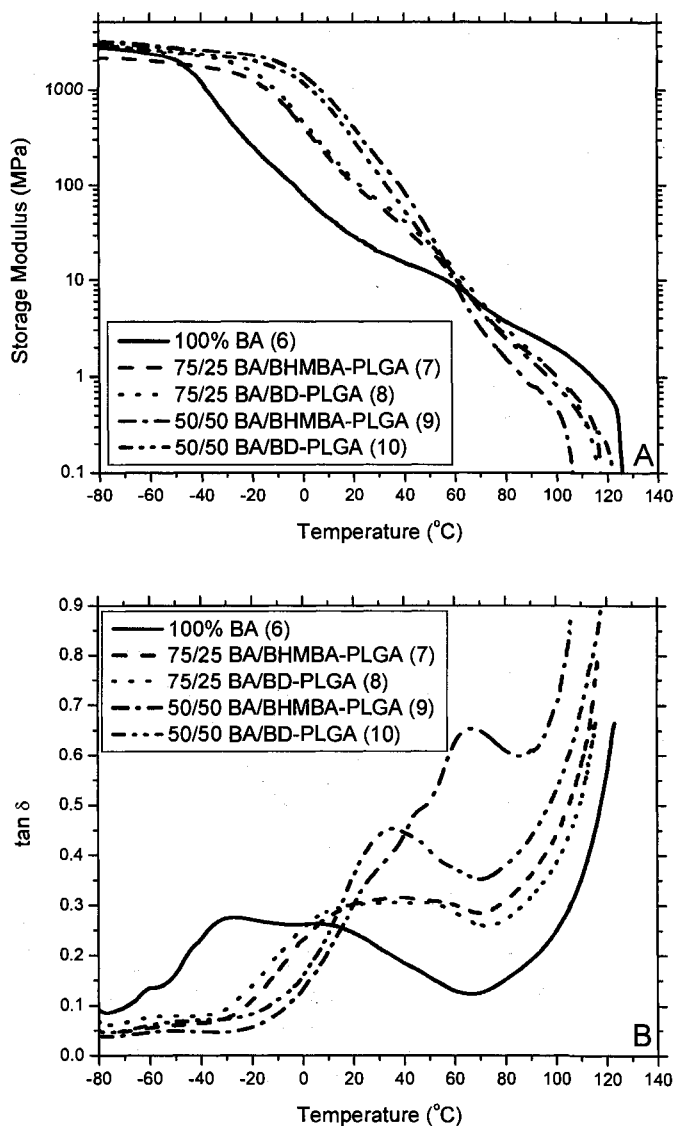


**Figure IV-4.** DMA plots of storage modulus vs. temperature (A) and tan  $\delta$  vs. temperature (B) for 12% HS TPUs. The number in parenthesis corresponds to the entry number of Table IV-1.

The 8% HS TPUs show a strong dependence on the type of PLGA and are seemingly independent of the amount of PLGA. The T<sub>g</sub>, as indicated by the peak of the tan  $\delta$  plot, and the storage modulus of the 50/50 and 75/25 BA/BD-PLGA are similar even though there is a different amount of PLGA. The same trend is apparent with the BHMBA-PLGA TPUs as well.



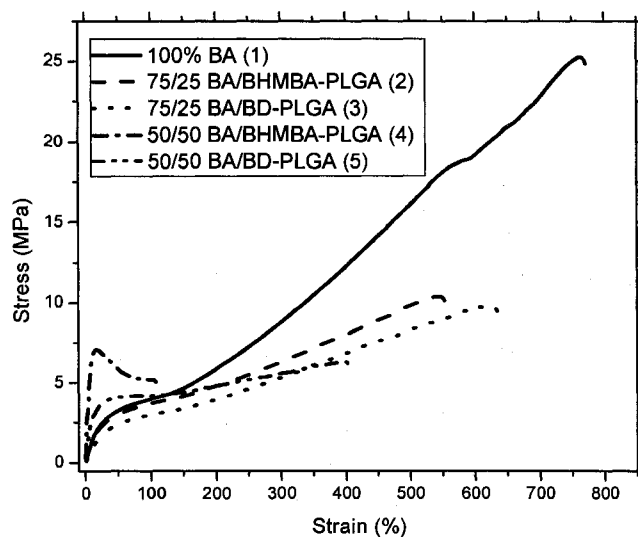
The opposite is true for the 12% HS TPUs where the  $T_g$  is more dependent on the amount of PLGA incorporated. At 25% loading of PLGA, the  $T_g$ s of the TPUs synthesized with BD- and BHMBA-PLGA are very similar, as are the storage moduli. At 50% PLGA the  $T_g$  of BD-PLGA TPU is much higher than that of BHMBA-PLGA. The storage moduli of the 50% PLGA TPUs are similar up to about 60°C; whereas at higher temperatures the TPU with BHMBA-PLGA has a lower modulus at high temperature.

As would be expected, the overall effect of the HS is evident whereby the 8% HS TPUs had lower  $T_g$ s as compared to the 12% HS. Also, the 8% HS TPUs had lower modulus at high temperatures as compared to the 12% HS. For instance, the temperature at which the TPUs have a storage modulus of 1 MPa is higher for the TPUs with 12% HS where all but one formulation reach this point at or above 100°C. The 8% HS TPUs reach the same storage modulus at slightly lower temperatures, just below 100°C.

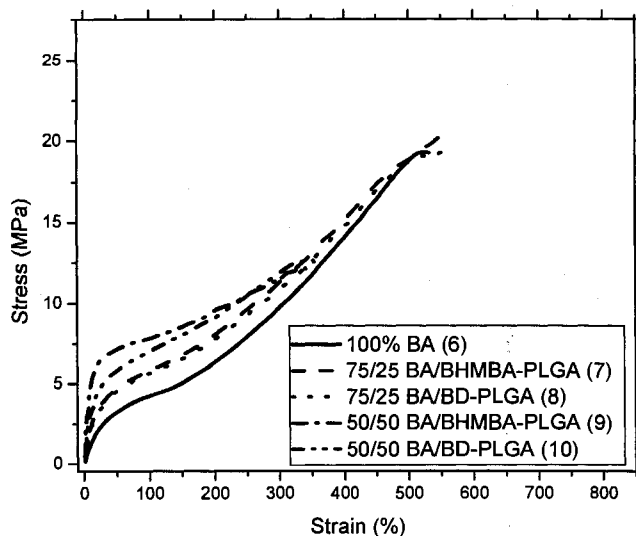
In all cases the onset of the  $T_g$  is below zero, typical of an elastomer. The potential usable temperature ranges start well below zero and go up to about 60-80°C, depending on the formulation.

Figure IV-5 and Figure IV-6 display the stress vs. strain plots of the 8% and 12% HS TPUs respectively. Table IV-1 lists the modulus, energy to break, peak stress, and ultimate strain. Each value listed in the table is an average of three specimens. In all cases except entry 4, the peak stress was also the ultimate stress. The 100% BA TPUs were both very tough, flexible materials with very high elongations and energy to break, in part due to the phase-separated morphology typical of TPUs. Though it appears that the 8% HS 100% BA TPU had a higher ultimate elongation and energy to break, it is important to note that the 12% HS 100% BA TPU pulled out of the grips during the test

for each of the three samples tested without breaking. Other than entry 4, there is not a drastic change in the physical properties with varying PLGA initiators. As would be expected with increasing PLGA content, the modulus of the resultant TPU increases while the ultimate elongation and energy to break decrease. All of the 8% HS PLGA-containing TPUs show reduced physical properties as compared to the 100%BA analogue. In the case of the 12% HS TPUs, the TPUs containing 25% PLGA have surprisingly similar physical properties to the 100% BA analogue; although the 100% BA analogue did not break and would actually have higher elongation and energy to break. Again, at the 50% loading of PLGA there is a reduced ultimate elongation and energy to break with an increased modulus. Perhaps the best formulation to balance physical properties and PLGA (hydrolytic degradability) content would be a 12% HS TPU with 25% PLGA polyol.



**Figure IV-5.** Stress vs. strain tensile test of 8%HS TPUs. The number in parenthesis corresponds to the entry number of Table IV-1.



**Figure IV-6.** Stress vs. strain tensile test of 12%HS TPUs. The number in parenthesis corresponds to the entry number of Table IV-1.

The degradation experiments probed only the hydrolytic degradation of the polymers; no biotic media were purposefully added to the degradation samples. The seawater used for this study was filtered and sterilized as purchased from Aldrich. Figure IV-7 and Figure IV-8 illustrate the percent mass remaining vs. immersion time of the TPUs at 37°C. There are two reasons for using 37°C as the degradation temperature; it accelerates the rate of degradation such that it occurs in a more reasonable time frame and it also allows the data to be compared to the literature based on studies using physiological conditions of the human body. The 100% BA TPUs exhibited essentially no degradation throughout the test. There is a very small initial decrease in mass, likely due to the diffusion of residual DMF solvent out of the sample. All of the 8%HS PLGA-containing TPUs had similar degradation profiles with about 20% mass lost in 100 days.

The 12% HS PLGA-containing TPUs show a dependence on the amount of PLGA in the TPU. The 12% HS 25% PLGA-containing TPUs degraded slower than the

8% HS PLGA-containing TPUs, but the 12% HS 50% PLGA-containing TPUs degraded more rapidly, with 60-70% mass remaining at 100 days. The effect of the PLGA initiator is also apparent in the 12% HS PLGA-containing TPUs; at both PLGA loadings the BHMBA initiated polyol system degraded slightly more rapidly than the corresponding BD initiated polyol system. The BHMBA initiator results in a pendant acid group in the middle of the PLGA chain which enhances the rate of degradation. This is in agreement with previous study of polyester degradation.<sup>156</sup> In all cases, the incorporation of PLGA into the TPU formulation enhances hydrolytic degradation.

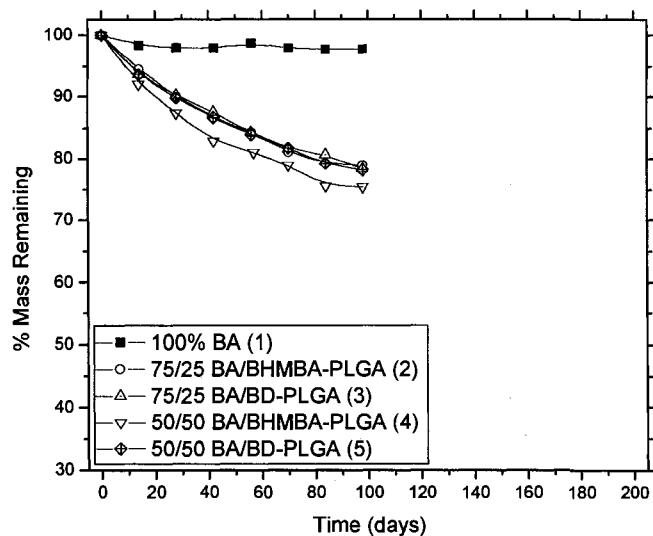


**Figure IV-7.** Remaining mass of 8%HS TPUs vs. immersion time in seawater at 37°C. The number in parenthesis corresponds to the entry number of Table IV-1.

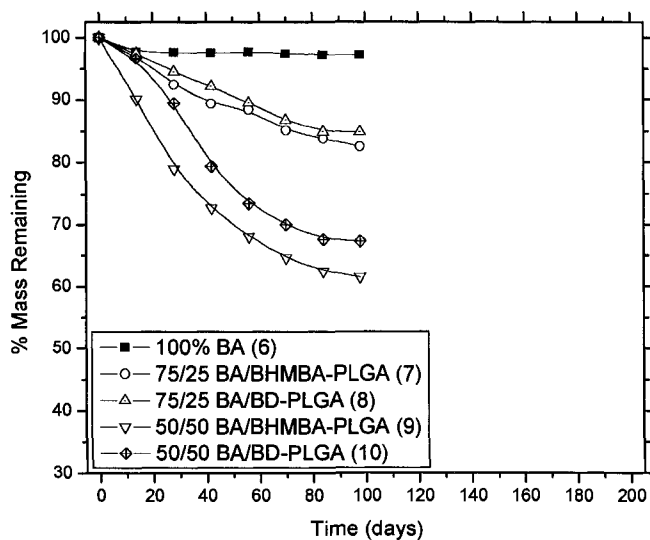


**Figure IV-8.** Remaining mass of 12%HS TPUs vs. immersion time in seawater at 37°C. The number in parenthesis corresponds to the entry number of Table IV-1.

### Conclusions

A series of thermoplastic polyurethane elastomers based on H<sub>12</sub>MDI have been synthesized and span a wide range of mechanical, thermal, and degradation properties. The PLGA-containing TPUs displayed excellent physical properties and were also capable of undergoing hydrolytic degradation, as tested in seawater. The use of completely aliphatic reagents minimized the potential for toxic degradation byproducts. It was demonstrated that the TPU properties can be tuned by controlling the synthetic variables such as HS content and polyol composition. The exceptional combination of properties of these TPUs make them attractive for a number of applications, even where degradable materials may not have been previously considered.

CHAPTER V  
PRIMARY VS. SECONDARY POLY(D,L-LACTIDE) POLYOLS IN  
THERMOPLASTIC POLYURETHANES

Introduction

When synthesizing TPUs with a mixed polyol system of BA and PLGA there was a general trend observed that the more PLGA incorporated into the formulation the lower the molecular weight of the resultant TPU. It is suspected that the reduced reactivity of the secondary hydroxyl endgroup is causing the reduced molecular weight. This chapter section describes the synthesis of mono- and difunctional PDLLA and PDLLA modified to have primary hydroxyl endgroups. The reaction of the monofunctional PDLLA polymers with H<sub>12</sub>MDI was monitored using real-time FTIR, allowing determination of the second order rate constant. Then, the difunctional PDLLA polymers were used in 50/50 molar ratio with BA as soft segments in a TPU formulation.

Results and Discussion

In order to determine if the primary (BA) and secondary (PLGA) hydroxyl functionality of the polyols in the mixed polyol system affects the final molecular weight of the TPU, a model system was studied. PDLLA, which naturally has a secondary hydroxyl end group, and a modified PDLLA to have a primary end group (PDLLA-1OH), were used in similar TPU formulations.

The PDLLA-1OH was synthesized by a number of post polymerization reactions. The first step was to remove all attached catalyst by a 1 M HCl wash procedure. Then, the PDLLA was reacted with succinic anhydride to yield a carboxylic acid end group.

Next, the carboxylic acid was converted to an acid chloride by reaction with oxalyl chloride. Finally, the acid chloride terminated polymer was reacted with a large excess of BD. The large excess minimized the possibility of chain coupling.

Figure V-1 through Figure V-4 show the  $^1\text{H}$  NMR spectrum of the polymer after each end group modification reaction. Figure V-1 shows the  $^1\text{H}$  NMR spectrum of the PDLLA as synthesized with BD initiator, with its naturally occurring secondary hydroxyl end group. The endgroup is visible from the methylene proton of the ultimate lactoyl unit at 4.2 ppm. The diacid terminated PDLLA in Figure V-2 has no 'e' proton visible as it becomes part of the 'c' protons of the polymer. Also, the methylene protons of the anhydride residue are visible at 2.6 ppm. Once the acid group is converted to an acid chloride the two sets of methylene protons of the anhydride moiety become unique and are at 2.6 ppm and 3.1 ppm in Figure V-3. Finally, Figure V-4 shows the  $^1\text{H}$  NMR spectrum of PDLLA with a BD unit as the endgroup. This is most clearly seen by the presence of the methylene protons labeled 'k', representative of the terminal BD residue.

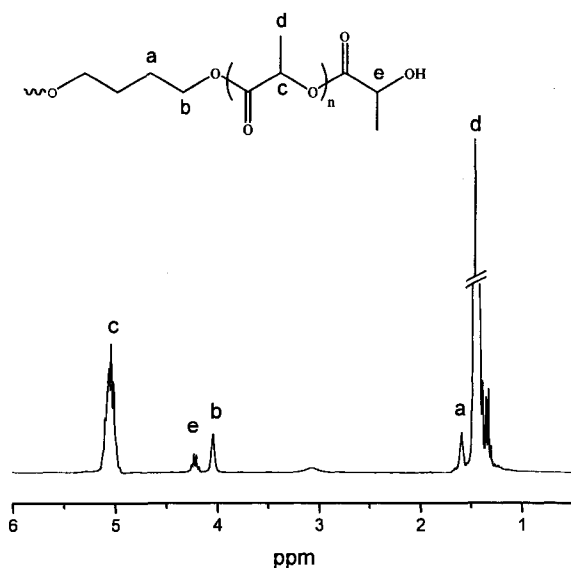


**Figure V-1.**  $^1\text{H}$  NMR of BD initiated PDLLA.

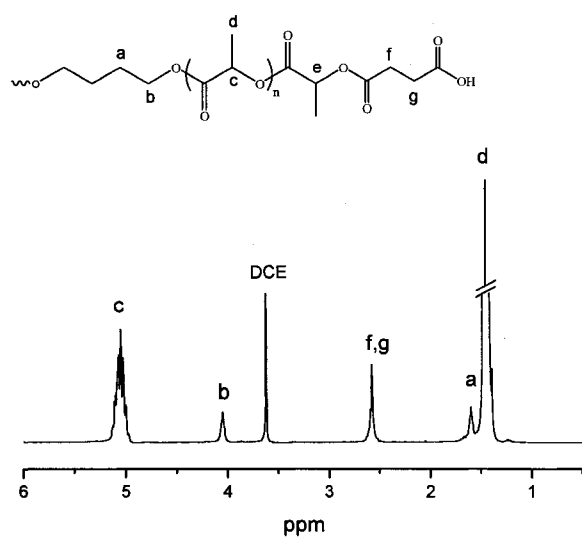


**Figure V-2.** <sup>1</sup>H NMR of BD initiated PDLLA-COOH (DCE = dichloroethane).

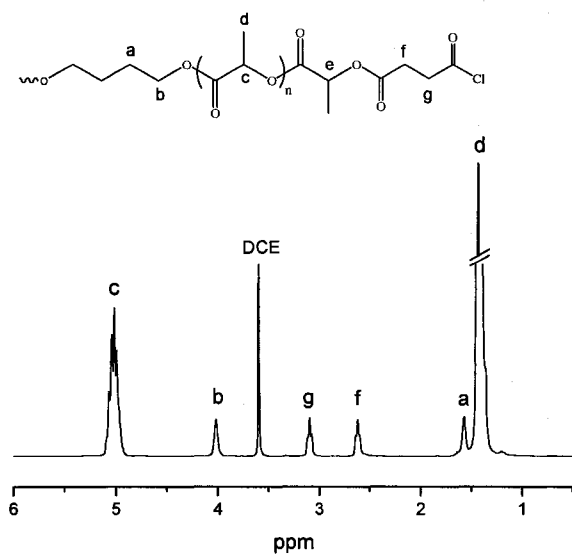


**Figure V-3.** <sup>1</sup>H NMR of BD initiated PDLLA-COCl (DCE = dichloroethane).



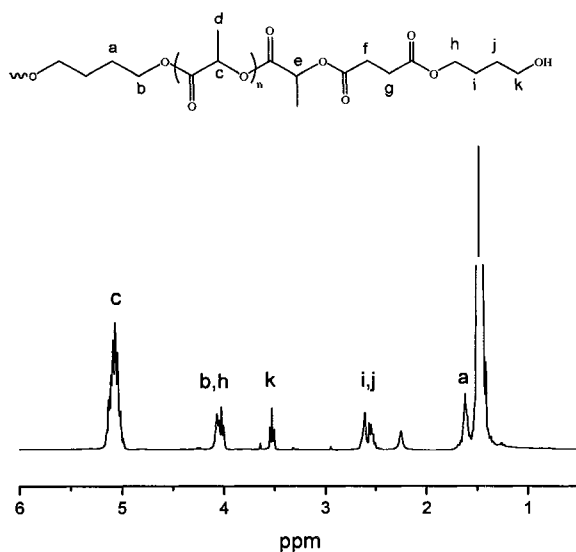


**Figure V-4.**  $^1\text{H}$  NMR of BD initiated PDLA-1OH.

GPC was used to confirm that the post-polymerization reactions did not degrade the polymer. Figure V-5 shows the GPC chromatogram of the normal and primary hydroxyl-terminated PDLA. There is a slight increase in the molecular weight after modification and there is no visible degradation of the polymer.

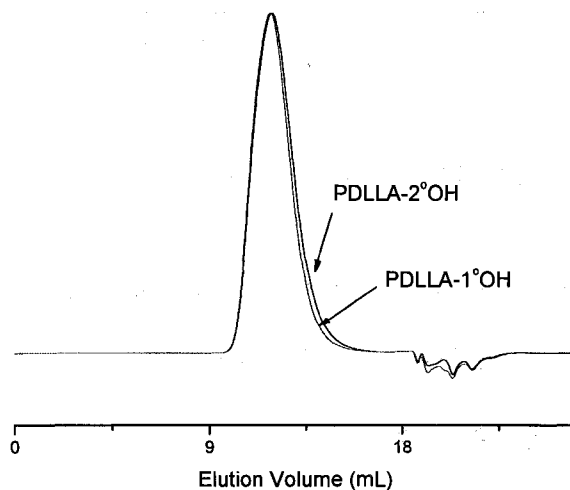


**Figure V-5.** GPC of primary and secondary PDLA.

The kinetics of the DBTDL-catalyzed reaction of the two PDLLAs with  $H_{12}$ MDI was studied using monofunctional PDLLA. The use of monofunctional PDLLA was necessary to minimize the effects of increasing molecular weight on the reaction. However, it was desirable to use a 5,000 g/mol PDLLA to facilitate the post-polymerization endgroup modification reactions. Specifically, the purification procedures are more facile with a higher molecular weight polymer but, if the molecular weight is too high it becomes difficult to confirm the products using NMR.

The second order kinetic plot of the reaction of PDLLA-1OH and -2OH is shown in Figure V-6. The rate constants calculated from the slope of the  $1/[NCO]$  vs. time plot of the reaction with PDLLA-1OH and -2OH were  $1.01 \times 10^{-3}$  and  $4.70 \times 10^{-4}$  L/(mol\*s) respectively. As would be expected, the reaction with the primary hydroxyl endgroup is faster than with the secondary hydroxyl endgroup.

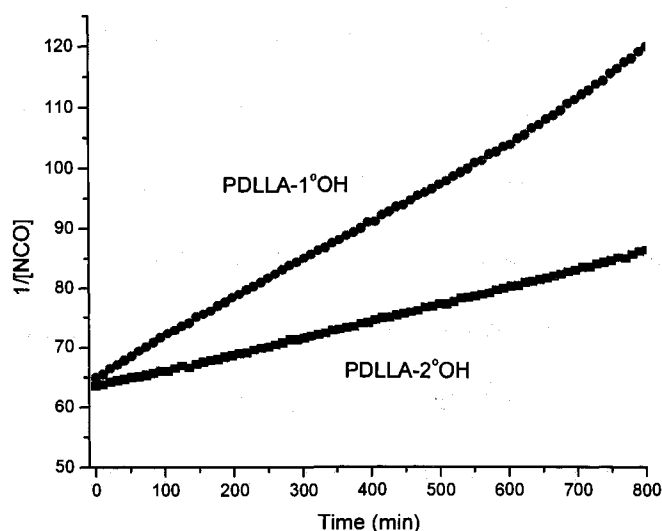


**Figure V-6.** Second order kinetic plot of  $1/[NCO]$  vs. time of the reaction of modified PDLLA (PDLLA-1°OH) and unmodified PDLLA (PDLLA-2°OH) with  $H_{12}$ MDI and 300 ppm Sn of DBTDL.

In order to determine if the difference in reaction rate affected the molecular weight of the resultant TPUs, two TPUs were synthesized using either PDLLA-1OH or PDLLA-2OH. Both TPUs were formulated to have a 12%HS and a 50/50 molar ratio of BA and one of the PDLLA polyols. The relative molecular weight of the polyols and TPUs was determined using HFIP GPC. The molecular weight of the normal, secondary hydroxy PDLLA was 2,860 g/mol and the resultant TPU was 5,630 g/mol, about double that of the polyol. The molecular weight of the PDLLA-1OH was 3,020 g/mol and the resultant TPU was 11,800 g/mol, about four times that of the polyol. The result with PDLLA-2OH is consistent with the TPUs synthesized with 50 mol% PLGA where the relative molecular weights were consistently below 10,000 g/mol.

### Conclusions

PDLLA has been synthesized to include primary hydroxyl endgroups as opposed to the normal secondary hydroxyl endgroups. The reactivity of the primary vs. secondary hydroxyl PDLLAs with  $H_{12}$ MDI was investigated using real-time FTIR monitoring of the catalyzed reaction. The second order rate constant of the reaction with PDLLA-1OH was more than 2 times that of the reaction with the normal PDLLA-2OH. Also, TPUs were synthesized with 50 mol% of either PDLLA-2OH or PDLLA-1OH. The TPU synthesized with PDLLA-1OH was about four times the molecular weight of the PDLLA-1OH polyol, while the PDLLA-2OH TPU was only about twice the molecular weight of the PDLLA-2OH. The increased reactivity of the primary hydroxyl endgroup does result in higher molecular weight TPUs as opposed to those synthesized with the normal secondary hydroxyl endgroup.

## CHAPTER VI

### REACTIVE EXTRUSION OF THERMOPLASTIC POLYURETHANES

#### Introduction

Biodegradable polymers were originally developed for biomedical applications within the human body, such as surgical sutures, and have traditionally been designed as high-strength fibers or rigid plastic, such as poly(L-lactic acid) (PLLA) and poly(glycolic acid). However, there are many other applications that would benefit from materials that degrade into non-toxic byproducts, and degradable polymers also represent one solution to the problem of plastic waste disposal. One way to synthesize degradable polymers that have a wide range of physical and thermal properties is to incorporate degradable polyesters into thermoplastic polyurethanes (TPUs).

The properties of TPUs are readily tunable to span a range of physical properties from elastomeric, to plastic, to high-strength fiber, by varying the amount and composition of the hard segments (HS) and soft segments (SS). The SS, a polyol, is usually either a polyether or polyester; thus polyurethanes offer the possibility of incorporating biodegradable polyesters into a family of polymers whose properties can be readily tuned for a variety of applications, including soft plastic and elastomeric.

One key element in the synthesis of degradable TPUs is an aliphatic diisocyanate, such that the potential diamine degradation products are less toxic compared to the aromatic analogue.<sup>157</sup> Among other diisocyanates, methyl 2,6-diisocyanatocaproate (LDI) has been investigated because it is based on the naturally occurring amino acid L-lysine.<sup>157-159</sup> Another aliphatic isocyanate, dicyclohexylmethane-4,4'-diisocyanate (H<sub>12</sub>MDI) was also used.<sup>35,36</sup> The use of the more symmetrical diisocyanate allows for

increased crystallization of the HS. The focus of the following investigations was to synthesize LDI and H<sub>12</sub>MDI based TPUs via reactive extrusion, a technique that can easily be scaled-up, unlike a bench-scale batch technique. Additionally, the optimization of the reactive extrusion process is of great importance to yield high molecular weight polymers.

### Optimization of Reactive Extrusion (REX) Synthesis Parameters

#### *LDI-based Thermoplastic Polyurethane*

The processing conditions of the REX process were optimized using a design of experiments (DOE). The DOE probed four parameters critical to the TPU polymerization at two levels each. The four factors investigated were screw speed (A), [catalyst] (B), throughput (C), and temperature profile (D). The DOE used was a half factorial design as displayed in Table VI-1. The screw speed was set at 250 or 350 RPM, the [catalyst] was 500 or 1000 ppm Sn, the throughput was 9.193 or 12.257 g/min and the temperature profiles were set at 120 or 130°C. The flow rates of each reagent that made up the total throughputs are listed in Table VI-2. The temperature profiles that were labeled 120 or 130°C are listed in Table VI-3. An 8-10 min equilibration time was allowed between one minute sample collections of each run of the DOE. The order of the runs was row number 1, 4, 6, 7, 3, 8, 2, 5 from Table VI-1. The parameter that was monitored to evaluate the DOE was molecular weight of the resultant TPU from each run (row). The DOE was designed and analyzed using DOE PRO XL v3.0.

**Table VI-1.** Design of experiments used for reactive extrusion of LDI-TPUs.

Factor	A	B	C	D=ABC
Row #	Screw Speed	[cat]	Throughput	Temp. Profile
1	250	500	9.193	120
2	250	500	12.257	130
3	250	1000	9.193	130
4	250	1000	12.257	120
5	350	500	9.193	130
6	350	500	12.257	120
7	350	1000	9.193	120
8	350	1000	12.257	130

**Table VI-2.** Reagent flow rates.

	(g/min)	(g/min)
Total Throughput	9.913	12.257
1,4-Butanediol	0.72	0.96
LDI	2.45	3.27
TONE 5249	6.00	8.00
DBTDL 500 ppm Sn (mL/hr)	1.37	1.83
DBTDL 1000 ppm Sn (mL/hr)	2.74	3.67

**Table VI-3.** Extruder temperature profiles.

Setting	Zone (°C)				
	1 (Die)	2	3	4	5 (Feed)
120	120	120	120	115	90
130	120	130	130	115	90

### *H<sub>12</sub>MDI-based Thermoplastic Polyurethane*

A second DOE was performed using H<sub>12</sub>MDI instead of LDI and poly(butylene adipate) (BA) instead of the poly( $\epsilon$ -caprolactone) (TONE 5249) polyol. The DOE probed three parameters critical to the TPU polymerization at two levels each. The factors investigated were selected to probe the effects stoichiometry, HS content, and post-curing while using the information learned from the DOE of the LDI-based TPU synthesis. The three factors investigated were NCO/OH ratio (A), HS content (B), and post-cure temperature (C). The DOE used was a half factorial design as displayed in Table VI-4. The flow rates of the reagents for each row are listed in Table VI-5, where the total throughput was held nearly constant since throughput was not a factor in the DOE. Likewise, the temperature and screw speed were also held constant at the 120°C setting of Table VI-3 and 250 RPM respectively.

**Table VI-4.** Design of experiments used for reactive extrusion of H<sub>12</sub>MDI-TPUs.

Factor	A	B	C
Row #	NCO/OH	HB	Post Cure Temp.
1	1.02	6	80
2	1.02	12	25
3	1.04	6	25
4	1.04	12	80

**Table VI-5.** Reagent flow rates for H<sub>12</sub>MDI TPU DOE.

Row	1,4-BD (g/min)	H <sub>12</sub> MDI (g/min)	BA (g/min)	DBTDL (mL/hr)	Total (g/min)
1	0.425	2.206	7.080	2.91	9.766
2	0.725	2.960	6.040	2.91	9.777
3	0.423	2.242	7.050	2.91	9.767
4	0.720	2.998	6.000	2.91	9.770

## Results and Discussion

### *Synthesis*

When engineering a degradable polymer, consideration must be given to the anticipated degradation products. For this reason, less toxic aliphatic diisocyanates, such as LDI and H<sub>12</sub>MDI, were favored over an aromatic diisocyanate such as 4,4'-methylenebis(phenylisocyanate) (MDI). LDI is particularly favored since it is derived from the naturally occurring amino acid, L-lysine.

Relative HS content is controlled by the relative amounts of chain extender and polyol. The HS content for the TPUs reported herein was set at 12% based upon the findings of a previous study.<sup>158</sup> The [NCO]/[OH] stoichiometric ratio is generally set between 1.0-1.1<sup>40</sup> to account for side reactions that may occur involving the isocyanate groups; in this study it was set at 1.05.

Precise metering of the reagents was required to attain the proper stoichiometry necessary to synthesize high molecular weight polymers. Initial attempts to accurately meter the molten polyol with a peristaltic pump were unsuccessful, resulting in very low molecular weight polymer. The use of gear pumps for the metering of the reagents was a very important aspect of the reactive extrusion process.

An initial indication of the molecular weight of the polymers synthesized with each run of the DOE was the observed melt strength of the extrudate. Higher molecular weight TPUs had a melt strength that made it possible to collect strands of polymer; whereas lower molecular weight TPUs were less viscous and were collected in jars.

Before the DOE experiments were started, the extruder was allowed to equilibrate at the temperatures listed in Table VI-3 for the 120 setting. Once the extruder barrel had



been allowed to adequately heat soak, metering of the reagents was started. As the reaction proceeded, an exotherm was observed such that the actual barrel temperatures were above the set temperatures. This was an indication that the polymerization was taking place. An observed increase of the torque and die pressure also indicated an increasing molecular weight in the extruder.

### *Characterization and Analysis*

*LDI based TPUs.* A sample from each run of the LDI-TPU was analyzed for molecular weight using the aforementioned THF GPC system. The Mn for each sample and the average for each run is listed in Table VI-7.

Analysis of the results as preformed with DOE PRO XL v3.0 indicated the importance of each variable and the interactions among variables. A summary of the analysis is provided in the ANOVA table in Table VI-6. The significance of a factor or two-way interaction of factors is represented by F, P, and percent contribution. The more significant a factor the higher the F value and lower the P value. The significance is also listed as percent contribution where the higher the percentage the more important the factor. This is graphically represented in the Pareto chart in Figure VI-1. The most important factor for this DOE was the throughput followed by temperature profile and two interactions of factors that included catalyst concentration. The coefficients from the Pareto chart were then used to generate the predictive equation  $\hat{y} = 36944 - 3021(A) + 132(B) + 9901(C) - 4582(D) - 3421(AB) + 3883(BC)$ , where  $\hat{y}$  is the predicted Mn of the TPU and A-D represent the setting of the four factors. The optimized conditions, yielding the highest molecular weight, were those of row four of the DOE. It is not

always the case that the optimum setting is one of the runs of the DOE; however, that was the case for this experiment.

The TPU from row four had a  $T_g = -58^\circ\text{C}$  and  $T_m = 41^\circ\text{C}$  as indicated by the second heating scan using DSC. This is a slightly lower  $T_g$  and comparable  $T_m$  to a similar material synthesized using a solution-based batch synthesis.<sup>34</sup> This polymer would be useful in low temperature applications up to near body temperature.

**Table VI-6.** ANOVA table of LDI-TPU DOE.

**ANOVA TABLE**

Source	SS	df	Mn			
			MS	F	P	% Contrib
Screw Speed	145986806.3	1	145986806.3	9.521	0.015	5.59%
[cat]	278256.3	1	278256.3	0.018	0.896	0.01%
Throughput	1568358006.3	1	1568358006.3	102.280	0.000	60.08%
Temp. Profile	335897256.3	1	335897256.3	21.906	0.002	12.87%
AB	187210806.3	1	187210806.3	12.209	0.008	7.17%
AC	8925156.3	1	8925156.3	0.582	0.467	0.34%
BC	241258556.3	1	241258556.3	15.734	0.004	9.24%
Error	122671350.000	8	15333918.750			4.70%
Total	2610586193.750	15				

**Table VI-7.** Molecular weight of LDI-TPU DOE runs.

Row #	Mn (g/mol)		
	1st	2nd	Avg.
1	34020	34440	34230
2	36020	41170	38595
3	24420	24390	24405
4	69040	56220	62630
5	26410	28310	27360
6	50550	43580	47065
7	22430	21930	22180
8	38410	39770	39090

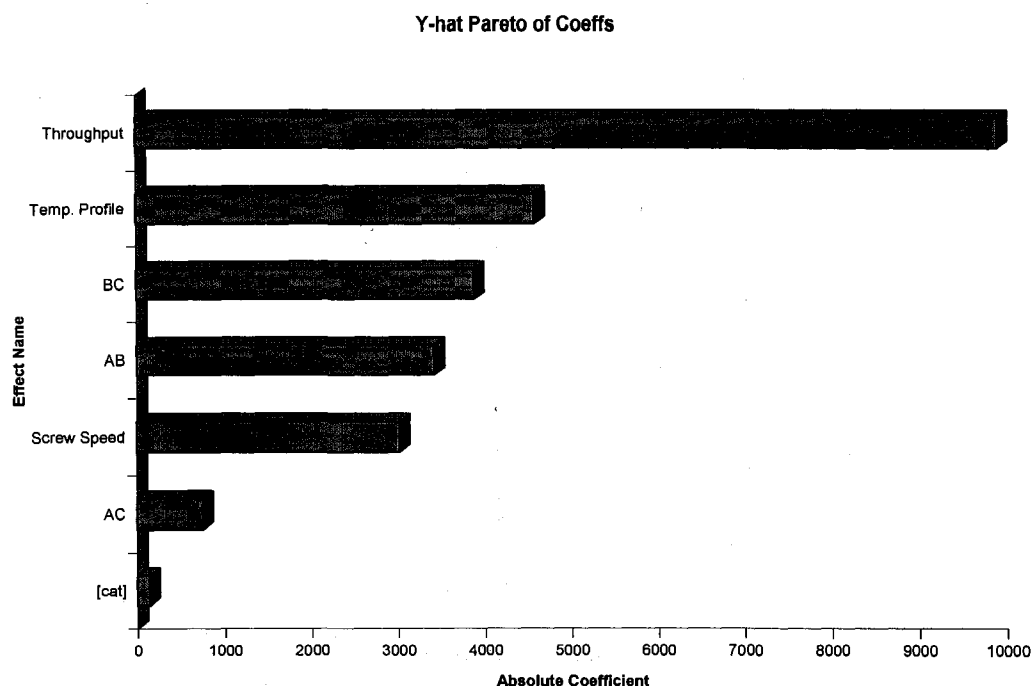


**Figure VI-1.** Pareto chart showing the importance of each variable from the LDI-TPU DOE.

*H<sub>12</sub>MDI based TPUs.* The H<sub>12</sub>MDI-TPUs could not be dissolved in THF so they could not be analyzed using THF-GPC. HFIP-GPC was used to analyze the molecular weight and molecular weight distributions relative to PMMA standards. A sample from each run was analyzed except for run three. The second replicate of the run three sample was insoluble in HFIP indicating a very high molecular weight. For the sake of the DOE analysis, the Mn for run three of the insoluble material was assigned the Mn of the first replicate. The Mn for each run is listed in Table VI-8.

**Table VI-8.** Molecular weight of H<sub>12</sub>MDI-TPU DOE runs.

Run	Mn (g/mol)		
	1st	2nd	Avg.
1	27650	14609	21129.5
2	14291	6999	10645
3	89878	insoluble	89878
4	66238	56612	61425

The same type of analysis was performed on the H<sub>12</sub>MDI-TPUs as was performed above with the LDI-TPUs. A summary of the DOE analysis is provided in the ANOVA table and Pareto chart in Table VI-9 and Figure VI-2 respectively. The most important factor was the NCO/OH ratio with almost 90% contribution to the Mn. The effect of post cure temperature was minimal with a contribution of less than 2%. A predictive equation to predict Mn ( $\hat{y}$ ) was generated from the coefficients of the analysis:  $\hat{y} = -2994310 + 2988213 (\text{NCO/OH}) - 3245 (\text{HB}) - 163 (\text{Post Cure Temp.})$ . The optimized setting for this DOE was that of run 3 in Table VI-4.

**Table VI-9.** ANOVA table of H<sub>12</sub>MDI-TPU DOE.**ANOVA TABLE**

Source	SS	Mn		F	P	% Contrib
		df	MS			
NCO/OH	7143531156.1	1	7143531156.1	180.906	0.000	86.89%
HB	758064453.1	1	758064453.1	19.198	0.012	9.22%
Post Cure Temp.	161433496.1	1	161433496.1	4.088	0.113	1.96%
Error	157950410.500	4	39487602.625			1.92%
Total	8220979515.875	7				

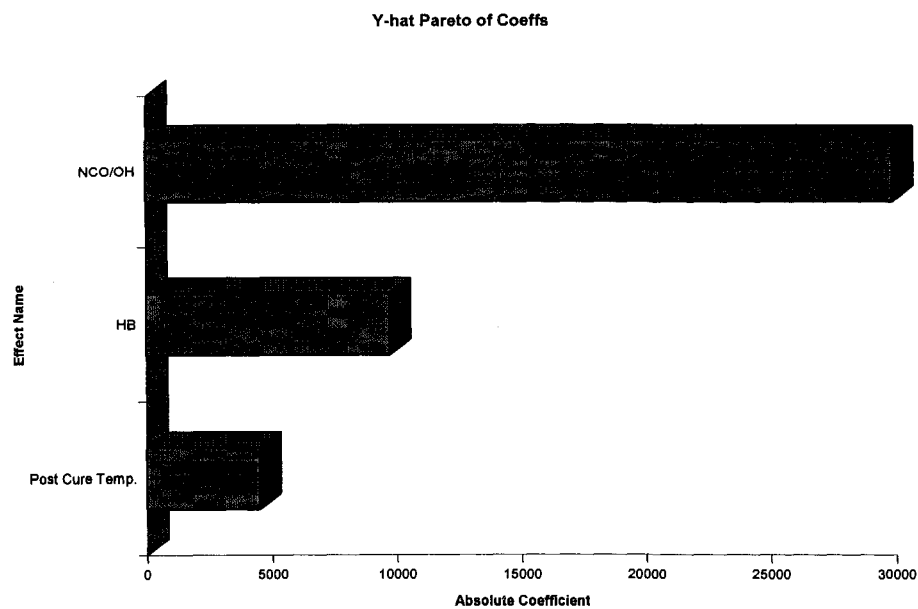


**Figure VI-2.** Pareto chart showing the importance of each variable from the H<sub>12</sub>MDI-TPU DOE.

The  $T_g$  of the polymer from the optimized settings was  $-29^{\circ}\text{C}$  as indicated by a peak in the  $\tan \delta$  vs. temperature plot of the DMA displayed in Figure VI-3. Also, this material showed a storage modulus of 1 MPa at  $100^{\circ}\text{C}$ , much higher than that of the LDI based material.

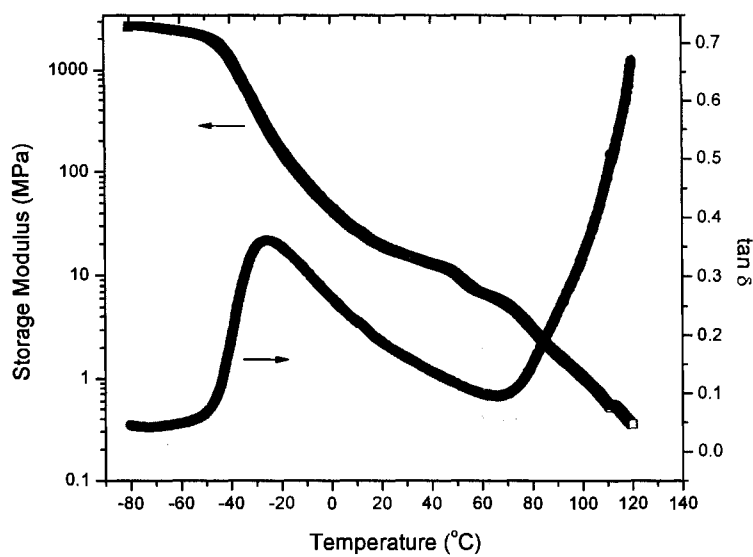


**Figure VI-3.** DMA of row 3, 2<sup>nd</sup> run.

### Conclusions

Through the use of DOE the optimum settings required to get high molecular weight TPUs using reactive extrusion were determined for an LDI and H<sub>12</sub>MDI system. This synthetic method provided a rapid means of synthesis that is more closely related to industrial processes than a bench-scale batch technique. A large volume of material can be synthesized in a short period of time, on the order of 10 g/min, using this method. However, the large volume of material needed for a run requires one to have a good understanding of the desired formulation(s) to minimize waste. The potential degradation products of the entirely aliphatic systems studied were designed to have little potential for toxic components when compared to typical aromatic-based TPUs. Both systems yielded very tough elastomeric polymers that have the potential for use in degradable applications as well as biomedical applications.

CHAPTER VII  
REACTION KINETICS OF DICYCLOHEXYLMETHANE-4,4'-DIISOCYANATE  
WITH 1- AND 2-BUTANOL: A MODEL STUDY FOR POLYURETHANE  
FORMATION

Introduction

Recently, a number of reports have issued concerning biodegradable polyurethanes containing hydrolytically unstable polyester soft segments, for example, poly( $\epsilon$ -caprolactone), poly(D,L-lactide), poly(glycolide), and/or copolymers therefrom.<sup>32-35,37-39</sup> For these materials, aliphatic isocyanates are overwhelmingly preferred due to the toxicity of aromatic amines, which are the presumed degradation products of an aromatic polyurethane. However, the reaction of an aliphatic isocyanate with an alcohol is kinetically slower than the corresponding reaction of an aromatic isocyanate, particularly when secondary alcohols are involved, such as those present in poly(D,L-lactide)-based polyols. The study described in this chapter employs real-time FTIR spectroscopic analysis to study the kinetics of the reaction of H<sub>12</sub>MDI with model primary and secondary alcohols in *N,N*-dimethylformamide (DMF) solution, using either DBTDL, SnOct, or triethylamine (TEA) as catalyst. This system was designed to replicate the polymerization conditions used to synthesize thermoplastic polyurethanes (TPUs). The isocyanate peak (2260-2270 cm<sup>-1</sup>) is easily identified and monitored in the IR spectrum allowing for straightforward calculation of reaction progress.

## Results and Discussion

FTIR spectroscopy was used to monitor kinetics of the isocyanate/alcohol reaction in real time. The urethane system studied consisted of H<sub>12</sub>MDI and either 1- or 2-BuOH in DMF solvent, using SnOct, DBTDL, or TEA as catalyst. This system was designed as a model for polyurethane systems consisting of mixed polyols which may have primary or secondary hydroxyl functionality or in some cases both.<sup>35</sup> The reaction was monitored by following the disappearance of the isocyanate peak centered at 2266 cm<sup>-1</sup>. Figure VII-1 shows partial FTIR spectra collected during a representative reaction of H<sub>12</sub>MDI and 2-BuOH with DBTDL catalyst (300 ppm Sn). In theory, the reaction could also be quantified by the appearance of the urethane peak, but the isocyanate peak is of much greater intensity and is less affected by neighboring peaks. However, there is a small peak that develops at 2339 cm<sup>-1</sup> that does affect the area of the isocyanate peak.

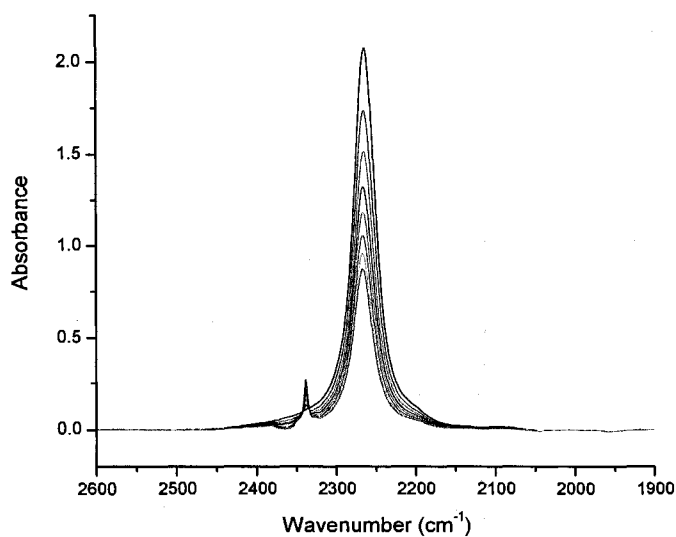


**Figure VII-1.** Partial FTIR spectrum for the reaction of H<sub>12</sub>MDI with 2-BuOH using DBTDL (300 ppm Sn) catalyst showing the progression of isocyanate consumption (Table VII-1, Exp. 4).



For this reason, the reaction was quantified using peak height, rather than peak area. To correlate peak height to an absolute concentration of isocyanate, a calibration using solutions of H<sub>12</sub>MDI of known concentrations was performed. Figure VII-2 shows the calibration plot of peak height at 2266 cm<sup>-1</sup> vs. concentration. The calibration equation used for the analysis of each reaction was:

$$H = 19.17832 [\text{NCO}] - 0.01131 \quad \text{Equation VII-1}$$

where  $H$  is the 2266 cm<sup>-1</sup> peak height. As predicted from the Beer-Lambert Law, there is a linear relationship between the isocyanate concentration and the observed peak height. For each reaction, the actual isocyanate concentration was calculated from the peak height using the calibration Equation VII-1. A plot of 1/[NCO] vs. time was linear over a broad range of conversion for the catalyzed isocyanate/alcohol reactions studied, and from these plots a second order rate constant,  $k$ , was extracted. For the two uncatalyzed (control) reactions, the second-order plots were non-linear, and in these cases, the initial reaction rate was measured.

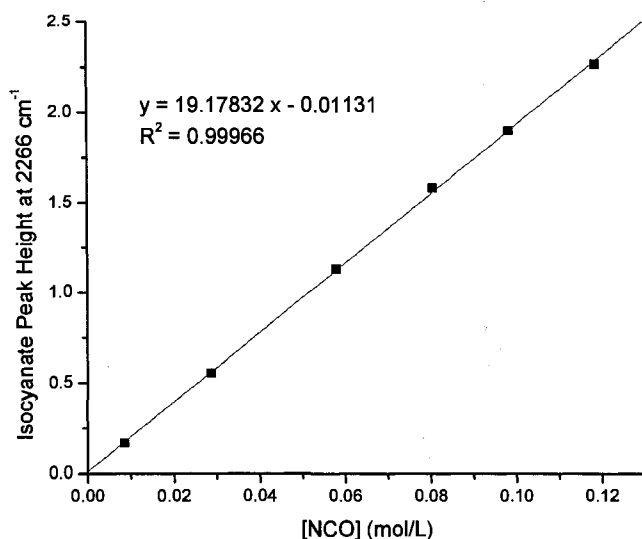


**Figure VII-2.** Isocyanate peak height at 2266 cm<sup>-1</sup> vs. isocyanate concentration for H<sub>12</sub>MDI in DMF at 40°C.

**Table VII-1.** Reaction Formulations and Second -Order Rate Constants for Isocyanate/Alcohol Reactions in *N,N*-Dimethylformamide<sup>a</sup> at 40°C with [NCO]/[OH]=1.00.

Exp.	[H <sub>12</sub> MDI] (mol/L)	1-BuOH [OH] (mol/L)	2-BuOH [OH] (mol/L)	Catalyst, [Catalyst] (mol/L x 10 <sup>5</sup> )	<i>k</i> (L mol <sup>-1</sup> s <sup>-1</sup> x 10 <sup>4</sup> )
1	0.051	0.10	-	-	c
2	0.052	-	0.10	-	d
3	0.051	0.10	-	DBTDL <sup>b</sup> , 5.3	5.90
4	0.051	-	0.10	DBTDL <sup>b</sup> , 5.3	1.79
5	0.051	0.10	-	SnOct <sup>b</sup> , 5.3	0.23
6	0.051	-	0.10	SnOct <sup>b</sup> , 5.3	0.13
7	0.051	0.10	-	TEA, 5.1	0.31
8	0.050	-	0.10	TEA, 5.2	0.11

<sup>a</sup> About 0.08 L of DMF was contained in each reaction vessel.

<sup>b</sup> 300 ppm Sn.

<sup>c</sup> Non-linear second order plot; initial rate = 2.6 x 10<sup>-7</sup> mol L<sup>-1</sup> s<sup>-1</sup>.

<sup>d</sup> Non-linear second order plot; initial rate = 7.8 x 10<sup>-8</sup> mol L<sup>-1</sup> s<sup>-1</sup>.

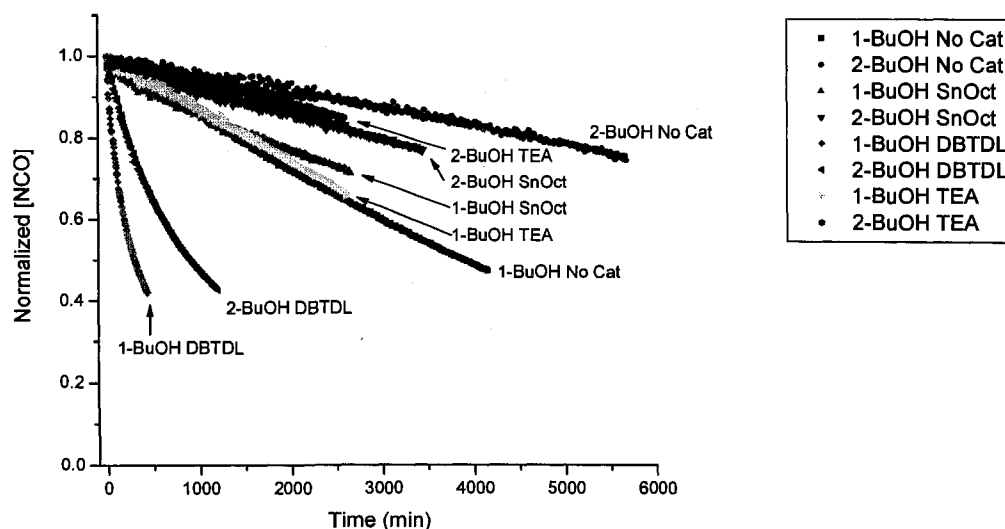


**Figure VII-3.** Normalized isocyanate concentration ( $[NCO]/[NCO]_0$ ) vs. time for the experiments listed in Table VII-1.

The reaction of  $H_{12}$ MDI with 1- or 2-BuOH was evaluated with three different catalysts, DBTDL, SnOct, and TEA. The experimental formulations are listed in Table VII-1. The effect of each catalyst can be seen in Figure VII-3, which shows the normalized isocyanate concentration vs. time plot for all of the experiments listed in Table VII-1. Normalized [NCO] was plotted to compensate for slight variations in  $[NCO]_0$  among the various experiments. As would be expected, in all systems the primary alcohol reaction was faster than the corresponding secondary alcohol reaction. DBTDL, one of the most commonly used organometallic urethane catalysts, showed the greatest increase in reaction rate compared to the control (no catalyst) as indicated by the highest conversion in the shortest time. Both SnOct and TEA caused a slight increase in reaction rate of the secondary alcohol; however, TEA showed no significant catalysis in the reaction with the primary alcohol and SnOct appeared to have slightly retarded the reaction, presumably due to the introduction of 2-ethylhexanoic acid. These last two

reactions, along with the uncatalyzed 1-BuOH reaction, were repeated to ensure their reproducibility. The duplicate reactions yielded the same results; the TEA catalyzed reaction was similar to the uncatalyzed reaction and the SnOct catalyzed reaction was slightly retarded. Figure VII-4 shows second-order plots of the DBTDL-catalyzed reaction, which are representative. The second-order rate constant,  $k$ , was determined as

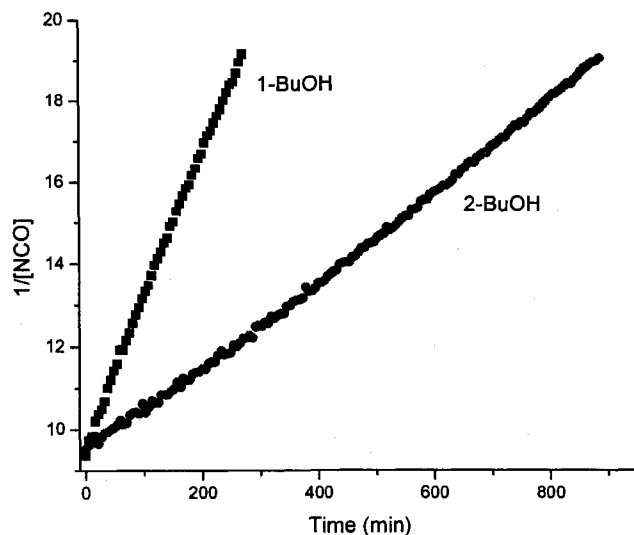


**Figure VII-4.** Second-order rate plot of H<sub>12</sub>MDI and BuOH in DMF with DBTDL catalyst (300 ppm Sn; Table VII-1, Exp. 3 and 4).

the slope of the linear plot, and these are listed in Table VII-1 for all of the catalyzed reactions. The catalyzed reactions had  $k_{\text{primary OH}}/k_{\text{secondary OH}}$  rate constant ratios of 3.3, 1.8, and 2.8 for DBTDL, SnOct, and TEA respectively. Second-order plots for the uncatalyzed reactions (not shown) displayed upward curvature, presumably due to autocatalysis as a result of the formed urethane linkages. Thus, for these two reactions, only the initial reaction rates are listed (footnote to Table VII-1). Comparison of initial rates showed that for both alcohols,  $5.3 \times 10^{-5}$  mol/L (300 ppm Sn) DBTDL caused an

increase in initial reaction rate on the order of  $2 \times 10^1$  compared to the uncatalyzed reactions.

Additionally, a series of reactions of  $H_{12}$ MDI and 1-BuOH was carried out in which the DBTDL concentration was varied from 25-800 ppm as listed in Table VII-2. This set of experiments was designed to determine the relationship between [DBTDL] and rate constant as well as to probe the time scale limitations of the flow cell apparatus. Figure VII-5 shows the second-order rate plots. As would be expected, the rate of reaction increased with increasing catalyst concentration. Second order rate constants were calculated by linear regression of the kinetic data in Figure VII-5 and were plotted as a function of [DBTDL] in Figure VII-6. The resulting plot has an apparent positive y-intercept, consistent with a finite rate for the uncatalyzed reaction. The rate constant increased linearly with increasing [DBTDL] in the concentration range of 100-700 ppm Sn. This linear behavior indicates that the overall rate of the urethane forming reaction is governed by the catalyzed reaction of the isocyanate and alcohol; whereas the uncatalyzed and/or urethane catalyzed reactions do not significantly contribute to the overall rate. However, between 0 and 100 ppm Sn the data displayed downward curvature, with earlier catalyst increments causing disproportionately greater increases in the value of the rate constant. This is consistent with a change in mechanism, and possibly reaction order, from an uncatalyzed or self-catalyzed reaction to the DBTDL-catalyzed reaction characteristic of the broad linear region from 100-700 ppm Sn. There is a deviation from linearity above 700 ppm Sn which may indicate the upper limit of reaction rate that can be monitored using this specific flow cell apparatus.

**Table VII-2.** Reaction Formulations and Second-Order Rate Constants for Isocyanate/Alcohol Reactions in N,N-Dimethylformamide at 40°C with  $[\text{NCO}]/[\text{OH}]=1.00$  with varying [DBTDL].

Exp.	$[\text{H}_{12}\text{MDI}]$ (mol/L)	1-BuOH, [OH] (mol/L)	[Catalyst] (mol/L x $10^5$ ), ppm Sn	$k$ (L mol <sup>-1</sup> s <sup>-1</sup> x $10^4$ )
9	0.052	0.10	0.4, 25	1.90
10	0.051	0.10	0.9, 50	2.53
11	0.052	0.10	1.8, 100	3.72
12	0.051	0.10	3.6, 200	4.84
3	0.051	0.10	5.3, 300	5.90
13	0.051	0.10	7.0, 400	6.71
14	0.051	0.10	8.9, 500	7.72
15	0.051	0.10	10.7, 600	8.83
16	0.051	0.10	12.4, 700	9.54
17	0.051	0.10	14.1, 800	9.12

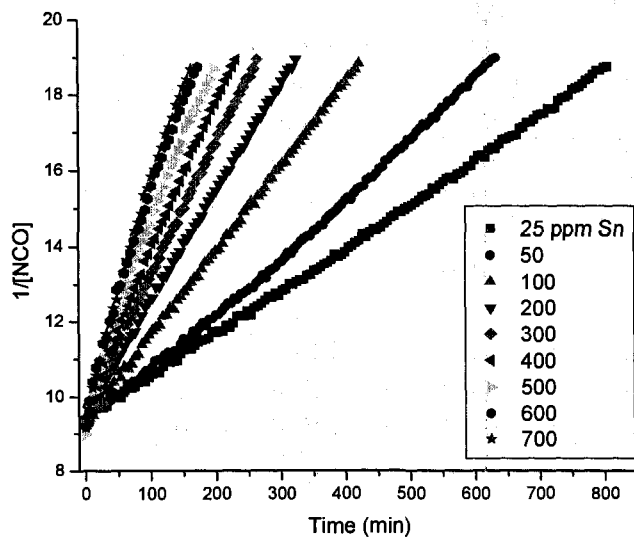


**Figure VII-5.** Second-order rate plot of  $\text{H}_{12}\text{MDI}$  and 1-BuOH in DMF with varying concentrations of DBTDL catalyst at 40°C.

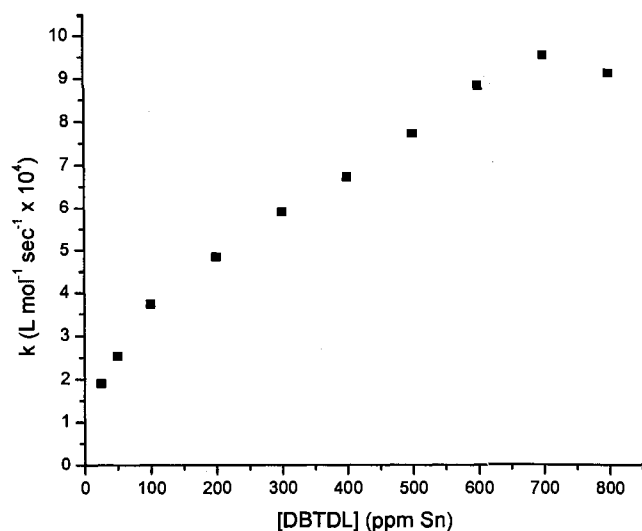


**Figure VII-6.** Second-order rate constant vs. [DBTDL], for reaction of H<sub>12</sub>MDI with 1-BuOH in DMF at 40°C.

Lastly, to examine the precision of our method, the reaction of H<sub>12</sub>MDI with 1-BuOH catalyzed by DBTDL at a concentration of 500 ppm Sn was performed in triplicate. The rate constants observed were 7.72 (initial experiment as listed in Table VII-2), 7.54, and 7.83 x 10<sup>-4</sup> l/mol-s. The observed rate constants showed a variation of less than 2.4% as compared to the initial value or less than 2.6% as compared to the average value of 7.63 x 10<sup>-4</sup> L/mol-s. These results indicate that the results are precise and reproducible.

### Conclusions

These experiments demonstrate the importance of the configuration of reagents used in urethane and poly(urethane) systems. The urethane reaction with a primary alcohol is much faster than that of a secondary alcohol in all cases and is quantified by the second order rate constant ratio,  $k_{\text{primary OH}}/k_{\text{secondary OH}}$ , which was 3.3 in the case of

DBTDL at 300 ppm Sn. The difference in reactivity was also apparent in the time to reach 50% conversion of isocyanate groups. The reactions catalyzed by DBTDL at 300 ppm Sn were 240 min and 860 min to reach 50% conversion of isocyanate for reaction with 1- and 2-BuOH respectively. Additionally, DBTDL was shown to be the most effective catalyst while SnOct and TEA showed similar catalytic activity that was minimal compared to DBTDL. This difference in reactivity must be addressed when using a system that contains both primary and secondary alcohols. Previous work<sup>35</sup> demonstrates the importance of alcohol structure, where a polyurethane formulated with a polyol having primary endgroups was of higher molecular weight than a mixed polyol system of primary and secondary polyols synthesized under the same reaction conditions. Lastly, the overall rate of the urethane forming reaction with [DBTDL] of less than 100 ppm Sn was affected by the rates of the uncatalyzed, urethane catalyzed and DBTDL catalyzed reactions. However, above 100 ppm Sn, the rate of the uncatalyzed and urethane catalyzed reactions were insignificant compared to the DBTDL catalyzed reaction, whereby [DBTDL] controlled the overall rate.



## CHAPTER VIII

POLYMERIZATION KINETICS OF *RAC*-LACTIDE INITIATED WITH  
ALCOHOL/STANNOUS OCTOATE COMPLEXES USING *IN SITU* ATTENUATED  
TOTAL REFLECTANCE-FOURIER TRANSFORM INFRARED SPECTROSCOPY:  
AN INITIATOR STUDY

## Introduction

FTIR has also proven to be a powerful tool for investigating the kinetics of lactone polymerizations. Lactide conversion can be conveniently monitored by following the reduction of the  $933\text{ cm}^{-1}$  peak or the  $1240\text{ cm}^{-1}$  peak which result from the  $-\text{CO-O}$  ring breathing and C-O-C stretch respectively.<sup>148,149</sup> Hillmeyer and coworkers<sup>134</sup> and our previous study<sup>136</sup> utilized the peak height of the  $1240\text{ cm}^{-1}$  to monitor the conversion of lactide using a remote *in-situ* ATR probe inserted into the reactor. The  $1240\text{ cm}^{-1}$  peak was selected because it has the benefit of much greater intensity than that of the  $933\text{ cm}^{-1}$  peak. Additionally, the use of an *in-situ* probe allows for real-time data collection and eliminates the need for the laborious collection of reaction aliquots. Our previous study utilized a calibration curve of known monomer/polymer solutions, designed to simulate a polymerization at various conversions, in order to equate the  $1240\text{ cm}^{-1}$  peak height to a lactide monomer concentration. This type of calibration allows for an accurate determination of monomer concentration up to high monomer conversion, but is especially accurate at low conversions. This is advantageous for calculating kinetic rate constants where accurate concentration measurements are needed at low conversion for kinetic plots.

Recently, Braun and coworkers<sup>160</sup> used transmission FTIR of reaction aliquots to monitor the bulk polymerization of lactide. They used the peak area of the peak centered at  $1454\text{ cm}^{-1}$ , asymmetric bending of C-H<sub>3</sub>, to normalize the peak at  $933\text{ cm}^{-1}$ . This method has the benefit of not requiring a separate calibration experiment, however, as pointed out by the authors, there is some sensitivity toward short-range order of the C-H<sub>3</sub> and the appearance of a double band at high lactide concentrations. Accordingly, the authors also indicate that this method is most appropriate at high monomer conversions, greater than 75%.

Both the calibration and internal normalization methods of determining monomer concentration have certain benefits. The calibration method allows for the accurate determination of monomer concentration over a wide range of conversion, while the internal normalization method does not require a separate calibration experiment. In this article we investigated the polymerization kinetics of alcohol/stannous octoate initiated *rac*-lactide (*rac*-LA) systems in refluxing tetrahydrofuran. Since monomer concentration at low conversion is important for kinetic calculations, we have extended the calibration technique from our previous study.<sup>136</sup> The polymerization was remotely monitored in real-time using an *in-situ* ATF-FTIR probe. Four different alcohol coiniciators, with functionalities from one to four, were used to study the effects of polymer architecture on the rate of polymerization.

## Results and Discussion

### *Calibration of Method*

Similar to our previous study, it was necessary to determine the functional relationship between the apparent peak height at  $1240\text{ cm}^{-1}$  and the *rac*-LA concentration in the presence of an appropriate concentration of polymer repeat units. This was accomplished in a manner similar to that previously described<sup>136</sup> with the exceptions that THF was used as the solvent and spectra were collected at reflux.

Figure VIII-1 shows a comparison plot of the *rac*-lactide concentration versus the  $1240\text{ cm}^{-1}$  peak height as well as the second-order polynomial fits and equations generated upon analysis. The plot clearly illustrates the influence of temperature on the  $1240\text{ cm}^{-1}$  peak height and the necessity of calibrating the system and subsequently analyzing the data at the appropriate temperature. As a result, the calibration equation generated for [*rac*-LA] versus the  $1240\text{ cm}^{-1}$  peak height at THF reflux was used in the analysis of each polymerization reported herein:

$$[\textit{rac}\text{-LA}] = -0.07246 + 4.20336 H_{1240} - 1.04493 H_{1240}^2 \quad \text{Equation VIII-1}$$

where  $H_{1240}$  is the  $1240\text{ cm}^{-1}$  peak height. Equation VIII-1, established by gravimetric calibration, represents the *rac*-LA concentration as a function of the peak height during polymerization in refluxing THF.

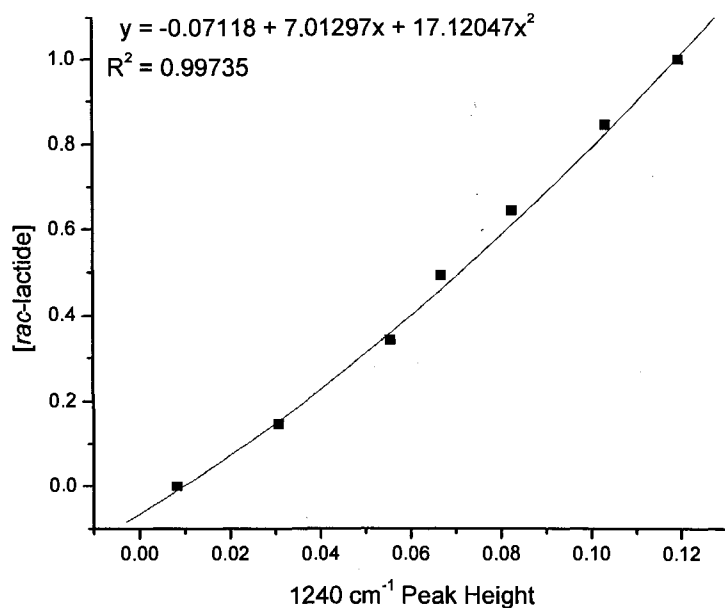
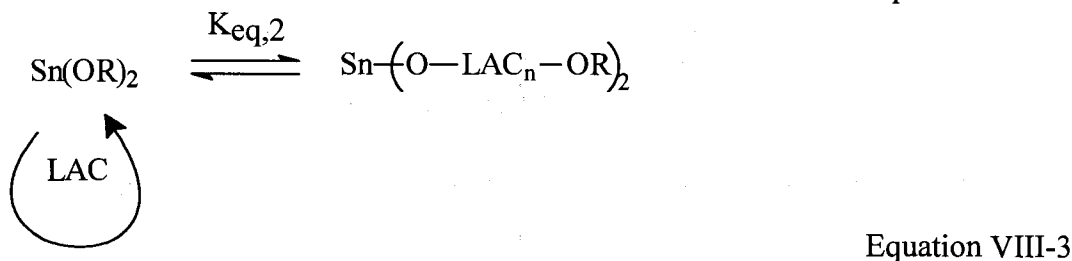
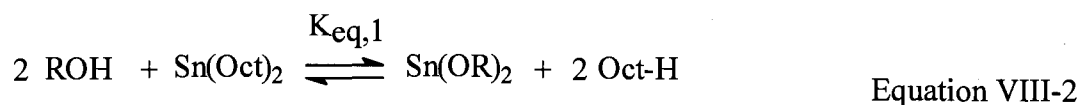


**Figure VIII-1.** ATR-FTIR calibration curve and equation for the rac-LA concentration at reflux (72°C) in THF.

*ROP of rac-LA Initiated with Alcohol/Sn(Oct)<sub>2</sub>*

ROP of lactone monomers catalyzed by Sn(Oct)<sub>2</sub> is an equilibrium process that is defined by the following simplified equations:



where  $K_{\text{eq},1}$  represents the equilibrium constant that dictates whether the reaction is controlled by the ROH/Sn(Oct)<sub>2</sub> ratio or, conversely, the Sn(Oct)<sub>2</sub>/ROH ratio.  $K_{\text{eq},2}$ , on the other hand, represents the equilibrium constant for the insertion of lactone monomer,

LAC, into the Sn-O bond (i.e., propagation). Essentially, this equilibrium (Equation VIII-3) prevents 100% conversion of LAC.

The diminution of the  $1240\text{ cm}^{-1}$  peak height of the infrared spectrum over time is illustrated in Figure VIII-2. Similarly, the  $933\text{ cm}^{-1}$  peak height also diminishes as the polymerization proceeds but, is difficult to monitor at high conversion because of the relatively low initial intensity. Conversely, the peak centered at  $1184\text{ cm}^{-1}$  increases as polymerization proceeds, slightly impinging on the  $1240\text{ cm}^{-1}$  peak. The development of the  $1184\text{ cm}^{-1}$  peak affects the area of the  $1240\text{ cm}^{-1}$  peak, thus peak height is used for analysis.

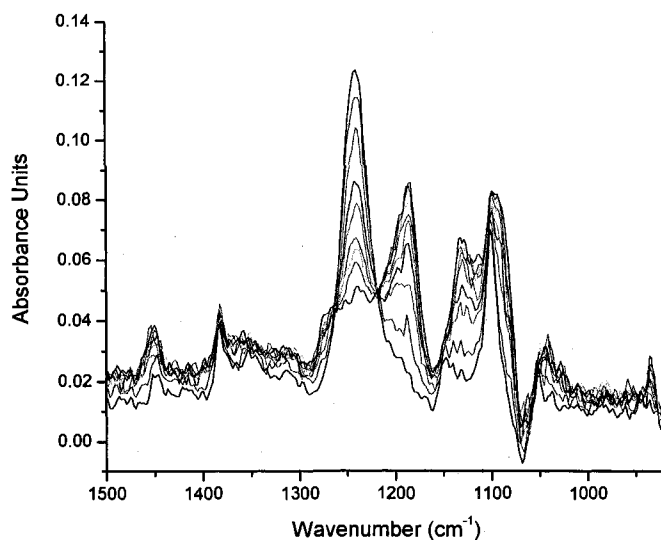


**Figure VIII-2.** Partial ATR-FTIR spectra demonstrating the progression of for *rac*-LA polymerization initiated with  $\text{PrOH/Sn}(\text{Oct})_2$  (Table VIII-2, Experiment 1).

A representative plot of  $1240\text{ cm}^{-1}$  peak height vs. time is displayed in Figure VIII-3. Using the aforementioned calibration equation, the peak height is then converted to [*rac*-LA]. Also, note the horizontal asymptote at long reaction time (high conversion) indicative of the monomer/polymer equilibrium described above.

Similar to our previous study,<sup>136</sup> we determined the equilibrium monomer concentration,  $[M]_{eq}$ , for a typical polymerization, where  $[rac-LA]_0 = 1.0$  M,  $[pentaerythritol]_0 = 0.013$  M,  $[Sn(Oct)_2]_0 = 0.0051$  M, and temperature = 72°C. GPC was utilized to independently determine  $[M]_{eq}$  at long reaction times. In order to determine the response factors of *rac*-LA and poly(*rac*-LA) a series of samples were prepared and analyzed by SEC-MALLS as listed in Table VIII-1. The average response factors of *rac*-LA and poly(*rac*-LA) were 1.04 and 0.98 respectively, yielding an average response factor ratio of 1.04:1 (*rac*-LA:poly(*rac*-LA)). Reaction aliquots were diluted in THF and analyzed via SEC-MALLS and the area of the monomer and polymer peaks were used to determine that 5.06% monomer was present. Since the original monomer

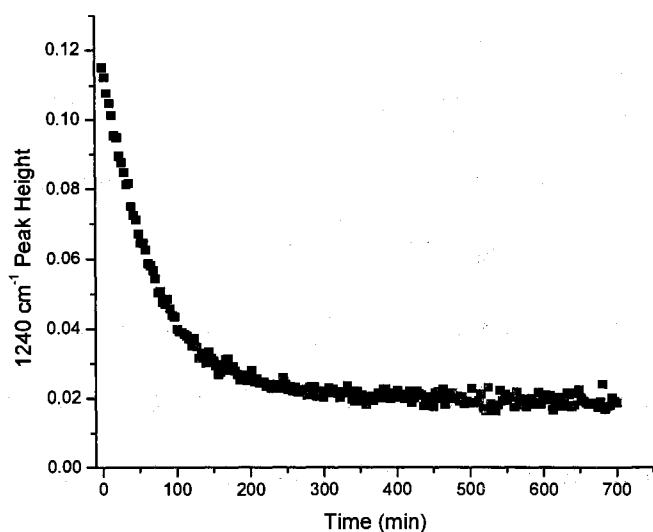


**Figure VIII-3.** Reduction of the 1240  $cm^{-1}$  peak height with time for *rac*-LA polymerization initiated with PrOH/ $Sn(Oct)_2$  (Table VIII-2, Experiment 1).

concentration was 1.03 M, it follows that  $[M]_{eq}$  was 0.052 M. Therefore,  $[M]_{eq} = 0.052$  M was used to calculate kinetic rate constants throughout this work. Furthermore, the

apparent rate constants ( $k_{\text{app}}$ ) observed for polymerizations in refluxing THF were comparable to those observed in toluene at 90°C from our previous report.<sup>136</sup>

**Table VIII-1.** Testing of refractive index (RI) response of *rac*-LA and poly(*rac*-LA).

Entry	<i>rac</i> -LA (g)	poly( <i>rac</i> -LA) (g)	Weight Fraction <i>rac</i> -LA	Weight Fraction Poly( <i>rac</i> -LA)	<i>rac</i> -LA, RI response <sup>a</sup>	Poly( <i>rac</i> -LA), RI response <sup>b</sup>	Calculated Weight Fraction <i>rac</i> -LA <sup>c</sup>	Calculated Weight Fraction Poly( <i>rac</i> -LA) <sup>d</sup>	<i>rac</i> -LA Response Factor <sup>e</sup>	poly( <i>rac</i> -LA) Response Factor <sup>e</sup>	Response Factor Ratio ( <i>rac</i> -LA : Poly( <i>rac</i> -LA))
1	0.8990	0.0960	0.9035	0.0965	0.2370	0.0275	0.8960	0.1040	1.01	0.93	1.09
2	0.8011	0.2076	0.7942	0.2058	0.2089	0.0523	0.7999	0.2001	0.99	1.03	0.97
3	0.6994	0.2879	0.7084	0.2916	0.1800	0.0777	0.6985	0.3015	1.01	0.97	1.05
4	0.5999	0.3871	0.6078	0.3922	0.1562	0.1038	0.6008	0.3992	1.01	0.98	1.03
5	0.5034	0.4805	0.5116	0.4884	0.1295	0.1304	0.4983	0.5017	1.03	0.97	1.05
6	0.3992	0.5774	0.4088	0.5912	0.1046	0.1558	0.4017	0.5983	1.02	0.99	1.03
7	0.3032	0.6707	0.3113	0.6887	0.0775	0.1827	0.2980	0.7020	1.04	0.98	1.06
8	0.2019	0.7753	0.2066	0.7934	0.0555	0.2061	0.2122	0.7878	0.97	1.01	0.97
9	0.1064	0.8703	0.1089	0.8911	0.0259	0.2357	0.0992	0.9008	1.10	0.99	1.11

a Area of monomer peak of RI chromatogram

b Area of polymer peak of RI chromatogram

c *rac*-LA RI response/(*rac*-LA RI response+Poly(*rac*-LA))

d Poly(*rac*-LA)/(*rac*-LA RI response+Poly(*rac*-LA))

e Weight Fraction/Calculated Weight Fraction



For a series of polymerizations conducted with constant initial *rac*-LA and PrOH concentrations, the effect of the initial Sn(Oct)<sub>2</sub> concentration is illustrated in Figure VIII-4. The expected increase in reaction rate is demonstrated by  $k_{app}$ , which resulted from an increase in the initial Sn(Oct)<sub>2</sub> concentration. For this set of experiments, the concentration of tin (II) alkoxide is equal to the initial Sn(Oct)<sub>2</sub> concentration for low Sn(Oct)<sub>2</sub>/PrOH ratios, but reaches an asymptotic value as Sn(Oct)<sub>2</sub>/ROH approaches unity as shown in Figure VIII-5. This behavior has been explained previously by Penczek et al.<sup>87</sup> and similarly demonstrated using real-time ATR-FTIR spectroscopy in our laboratory,<sup>136</sup> where the polymerization kinetics are governed by the equilibrium described in Equation VIII-3. Increasing the initial Sn(Oct)<sub>2</sub> concentration effectively enhances the polymerization rate because there is an increase in active species (Sn(OR)<sub>2</sub>) up to Sn(Oct)<sub>2</sub>/ROH ~ 0.5; however, further increase in [Sn(Oct)<sub>2</sub>]<sub>0</sub> does not generate any more active species.

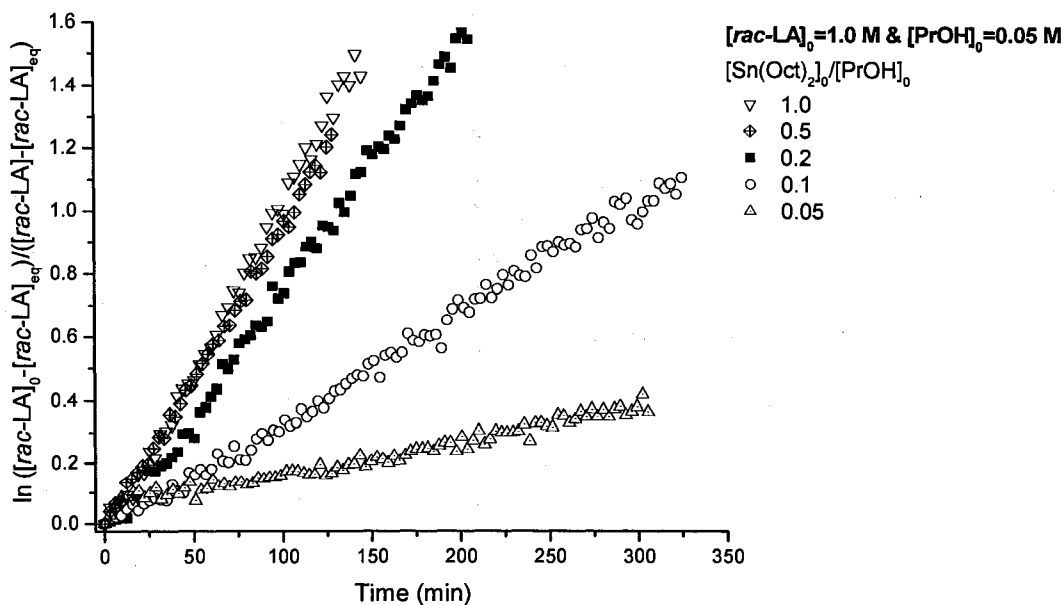


**Figure VIII-4.** First-order kinetic plots of *rac*-LA polymerizations initiated with PrOH/Sn(Oct)<sub>2</sub>, demonstrating the effect of the initial Sn(Oct)<sub>2</sub> concentration ([*rac*-LA]<sub>0</sub>=1.0 M, [PrOH]<sub>0</sub>=0.05 M; Table VIII-2, Entries 1, 5, 9, 11, and 12).

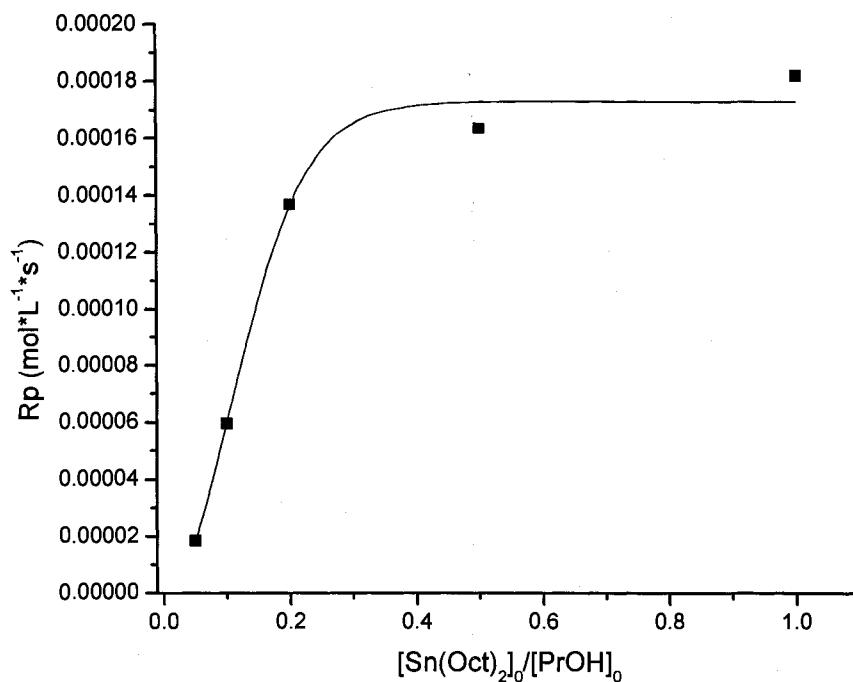


**Figure VIII-5.**  $R_p$  of *rac*-LA as a function of  $[\text{Sn}(\text{Oct})_2]_0/[\text{PrOH}]_0$  ( $[\text{PrOH}]_0 = 0.050$  M,  $[\text{rac-LA}]_0 = 1.0$  M).

The effect of polymer architecture on the rate of polymerization was studied through the use of four different alcohol initiators; monofunctional *n*-propyl alcohol, difunctional ethylene glycol, trifunctional trimethylolpropane and tetrafunctional pentaerythritol. Although the functionality of the alcohol coinitiator was varied, in all cases the alcohol was primary. The kinetic rate plots in Figure VIII-6 demonstrate the rates of polymerization for  $[\text{Sn}(\text{Oct})_2]/[\text{ROH}] = 0.05, 0.1, \text{ and } 0.5$ , where for a given  $[\text{Sn}(\text{Oct})_2]/[\text{ROH}]$  the rate of polymerization is practically unchanged for the varying architectures. The  $k_{\text{app}}$  for each plot in Figure VIII-6 is listed in Table VIII-2, entries one through ten. At  $[\text{Sn}(\text{Oct})_2]/[\text{ROH}] = 0.5$  (Table VIII-2, entries 1-4) there was a slight variation in  $k_{\text{app}}$ , however the variation is minor and within the same order of magnitude.

At lower  $[\text{Sn}(\text{Oct})_2]/[\text{ROH}]$ , there is no discernable difference in  $k_{\text{app}}$  with varying architecture.

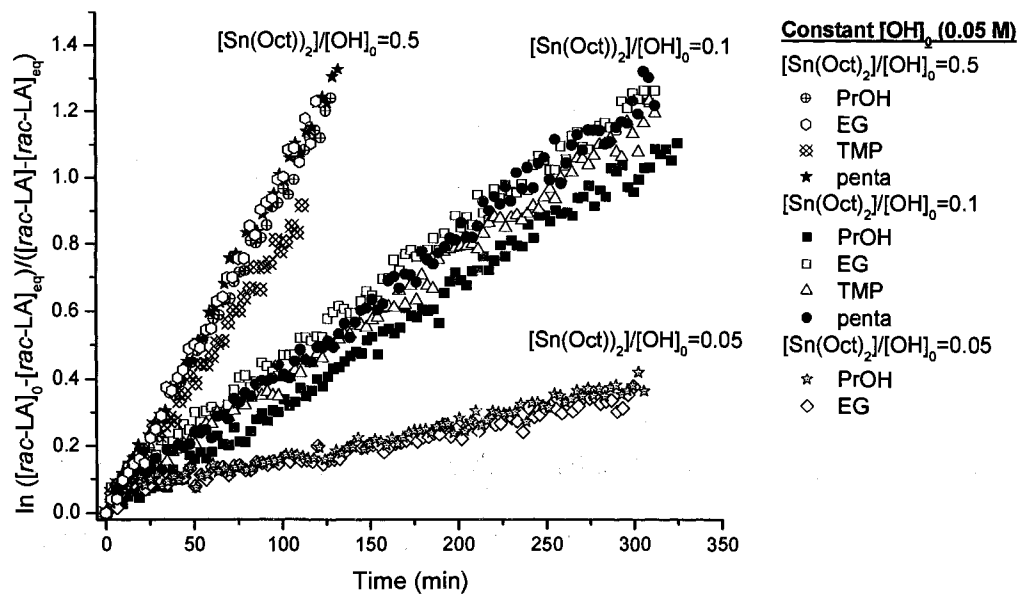


**Figure VIII-6.** First-order kinetic plots of *rac*-LA polymerizations initiated with various alcohols/ $\text{Sn}(\text{Oct})_2$ , demonstrating the effect of the initiator architecture.

**Table VIII-2.** Reaction Formulations and  $k_{app}$  Values for *rac*-LA Polymerizations with Sn(Oct)<sub>2</sub> Catalysis at 72°C in THF.

Entry-Rxn#	[ <i>rac</i> -LA] <sub>0</sub> (M)	[PrOH] <sub>0</sub> (M x 10 <sup>2</sup> )	[EG] <sub>0</sub> (M x 10 <sup>2</sup> )	[TMP] <sub>0</sub> (M x 10 <sup>2</sup> )	[penta] <sub>0</sub> (M x 10 <sup>2</sup> )	[Sn(Oct) <sub>2</sub> ] <sub>0</sub> (M x 10 <sup>2</sup> )	[SnOct] <sub>0</sub> / [OH] <sub>0</sub>	$k_{app}$ (s <sup>-1</sup> x 10 <sup>4</sup> )
1	1.0	5.1				2.5	0.5	1.6
2	1.0		2.5			2.5	0.5	1.7
3	1.0			1.7		2.5	0.5	1.3
4	1.0				1.3	2.5	0.5	1.7
5	1.0	5.2				0.51	0.1	0.58
6	1.0		2.4			0.51	0.1	0.64
7	1.0			1.7		0.51	0.1	0.61
8	1.0				1.3	0.51	0.1	0.66
9	1.0	5.1				0.25	0.05	0.18
10	1.0		2.6			0.26	0.05	0.16
11	1.0	5.1				5.0	1.0	1.8
12	1.0	5.2				1.0	0.2	1.3
13	1.0	-	-	-	-	1.0		0.003

## Conclusions

The polymerization of *rac*-LA was monitored in real-time using mid-infrared ATR-FTIR spectroscopy. First-order, semilogarithmic plots showed the polymerizations to be internally first order. Similar to previous studies,<sup>87,136</sup> it was demonstrated that the rate of polymerization was enhanced with additional Sn(Oct)<sub>2</sub> where  $[\text{Sn}(\text{Oct})_2]_0/[\text{OH}]_0 \leq 1$ . Furthermore, the polymer architecture was varied by the use of a coinicator alcohol with functionality from one to four. This variation in architecture had little to no effect on the observed rate of polymerization.

## CHAPTER IX

### CONVENTIONAL AND MACROINITIATOR COPOLYMERIZATION

#### Introduction

The purpose of the experiments in this chapter was to probe the copolymerization behavior of D,L-lactide (DLLA) and  $\epsilon$ -caprolactone (CL). A number of researchers in our group noticed that very long reaction times were required to reach full conversion of the CL monomer during a conventional copolymerization. The rate of DLLA conversion was seemingly unaffected. These observations indicate the reactivity of a growing lactide chain end is more likely to react with DLLA than with CL.

To avoid prolonged polymerization time for the copolymer a two-step synthesis method was developed where the CL comonomer charge of the copolymer was polymerized first using the full compliment of initiator and catalyst. The resulting poly(CL) oligomer was used as a macroinitiator of the DLLA comonomer charge of the copolymer. The experiments described herein aim to determine the relative rates of conversion of the two monomers using a traditional copolymerization and the macroinitiator method. Also, NMR was used to determine the relative “randomness” of the polymer chain synthesized by the macroinitiator vs. conventional copolymerization methods.

#### Results and Discussion

Four reactions were carried out to determine the effects of the macroinitiator method on rate of polymerization and monomer sequence distribution. Two compositions of copolymer were studied: 90/10 and 50/50 mol% DLLA/CL. In each

case a conventional copolymerization was carried out along with the macroinitiator method. The conventional method was carried out by fully melting and mixing the monomers with the initiator prior to starting the polymerization by the addition of catalyst at the selected polymerization temperature; the conventional copolymerization was considered the control experiment to compare to the macroinitiator polymerization.

GPC was utilized to determine monomer conversion of reaction aliquots, such that DLLA and CL could be monitored independently of each other. A calibration curve was created for each monomer by measuring the RI peak height of monomer solutions with a known concentration. The calibration curves and equations for DLLA and CL are displayed in Figure IX-1 and Figure IX-2 respectively.

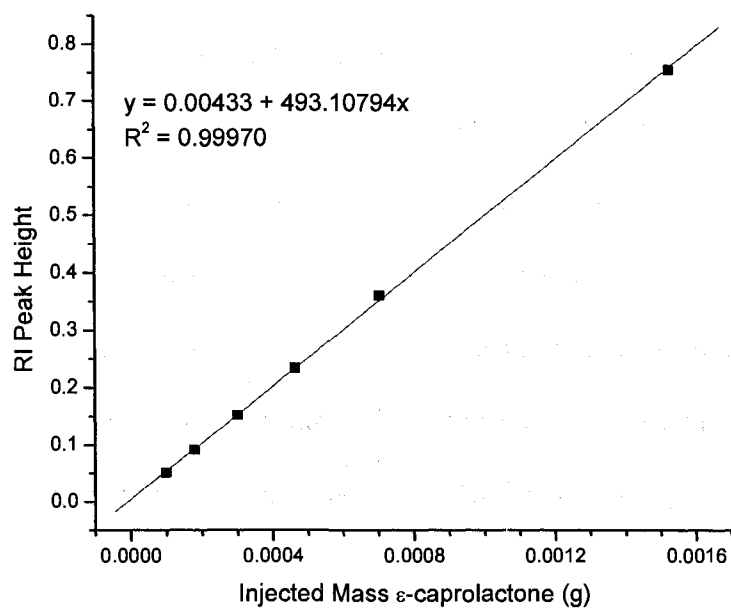


**Figure IX-1.** Refractive Index calibration plot of D,L-lactide.

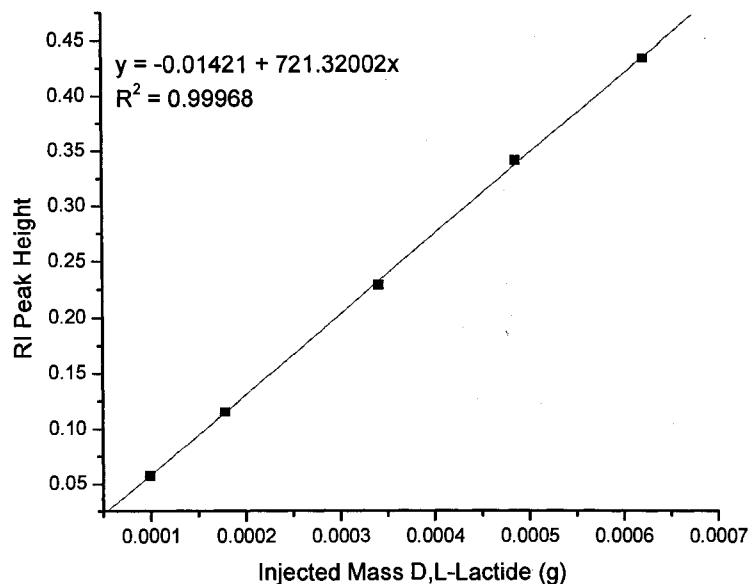


**Figure IX-2.** Refractive Index calibration plot of  $\epsilon$ -caprolactone.

The equations in Figure IX-1 and Figure IX-2 were then used to calculate the mass of each monomer in a reaction aliquot to determine conversion. A representative GPC chromatogram of a reaction aliquot is displayed in Figure IX-3. The polymer, DLLA, and CL peaks are centered at 13.5, 18.2, and 19.3 mL, respectively. The mass of each monomer in the aliquot was calculated using the peak height of the monomer and the corresponding calibration equation. Since the total injected mass of each sample was known, conversion of each monomer was determined using the calibrations above. For example, the total injected mass of the aliquot in Figure IX-3 was  $2.1873 \times 10^{-3}$  g and the calculated mass of DLLA and CL was  $1.2578 \times 10^{-4}$  and  $8.6163 \times 10^{-4}$  respectively. Then weight fraction of each monomer in the aliquot was calculated and compared to the initial monomer concentrations to determine conversion.

The conversions calculated from the aliquots of each reaction are plotted vs. reaction time in Figure IX-4 through Figure IX-7 for each of the four reactions. The conversion vs. time plot for the conventional copolymerization reaction of 90/10 mol%



DLLA/CL (Figure IX-4) indicates that the DLLA conversion reached equilibrium (maximum it will achieve for DLLA) in about 120 min, while the CL conversion was only about 75% at 480 min. Using the macroinitiator method, as displayed in Figure IX-5, the CL was completely converted in 60 min, after which it was added to the DLLA. The DLLA then reached maximum conversion in an additional 90 min for a total reaction time of 150 min to reach maximum conversion of both monomers.

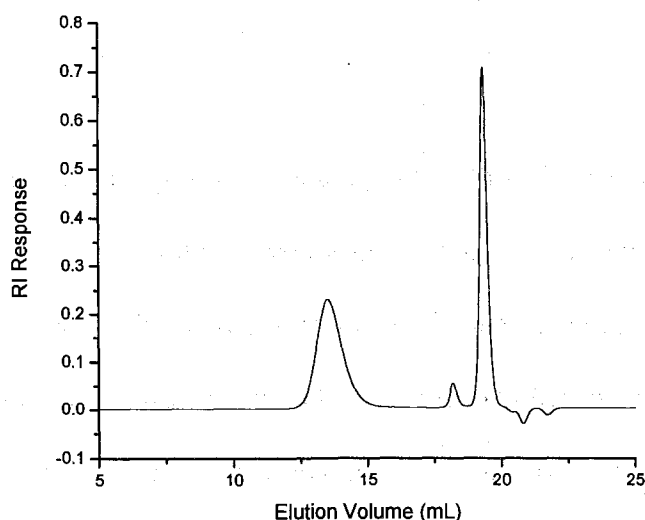


**Figure IX-3.** GPC chromatogram (refractive index trace) of 50/50 mol% DLLA/CL conventional copolymerization at 6 minutes.

The same trends were observed for the 50/50 mol% DLLA/CL polymerizations in Figure IX-6 and Figure IX-7. DLLA reached maximum conversion in 120 min; while CL required 720 min in a conventional copolymerization. The macroinitiator method fully converted CL in 60 min and then was added to DLLA, which reached maximum conversion in an additional 120 min for a total reaction time of 180 min to fully convert both monomers, as opposed to 720 min for the conventional copolymerization.

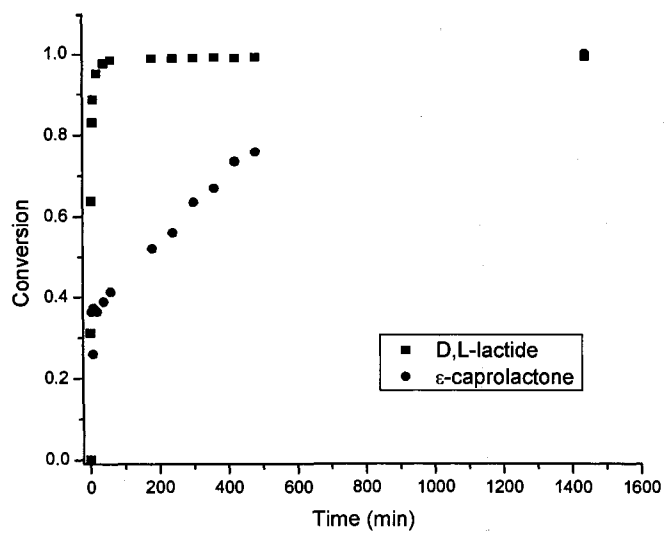


**Figure IX-4.** Conversion vs. time for conventional copolymerization of 90/10 mol% DLLA/CL.

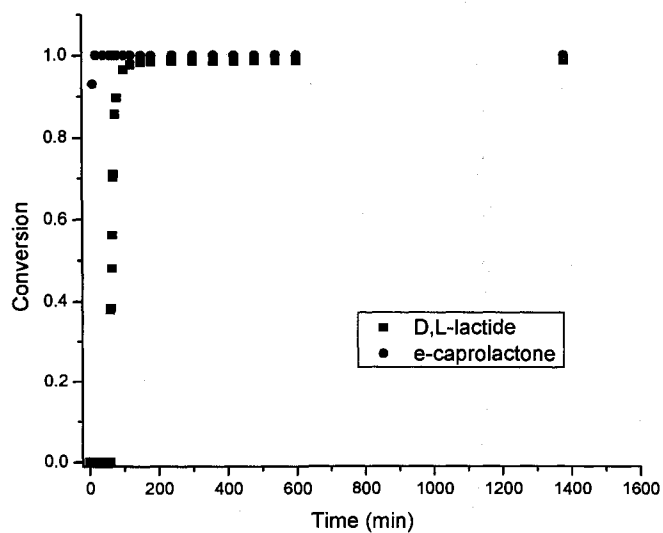


**Figure IX-5.** Conversion vs. time for macroinitiator copolymerization of 90/10 mol% DLLA/CL.

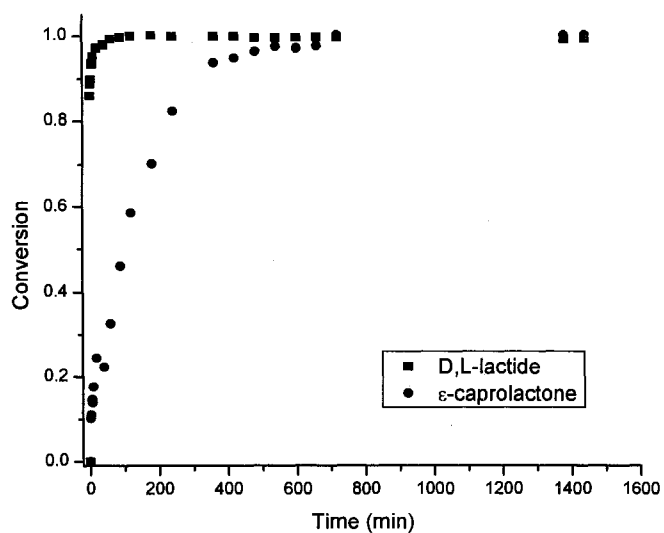


**Figure IX-6.** Conversion vs. time for conventional copolymerization of 50/50 mol% DLLA/CL.

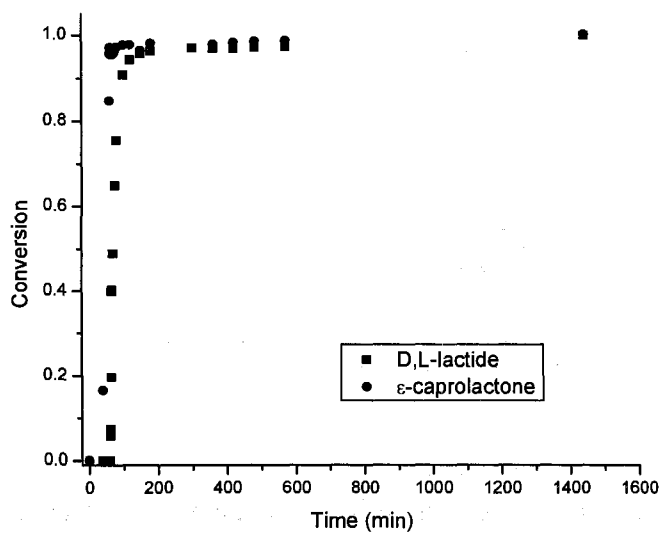


**Figure IX-7.** Conversion vs. time for macroinitiator copolymerization of 50/50 mol% DLLA/CL.

Differential scanning calorimetry (DSC) was used to determine the randomness of the copolymers. Completely random copolymers are predicted to display one  $T_g$  somewhere between that of the two respective homopolymers as defined by the Fox

equation. A block copolymer is predicted to exhibit two individual  $T_g$ s since the polymer behaves like two homopolymers. The 90/10 mol% DLLA/CL copolymers both showed only one  $T_g$ , at 21 and 25°C for the conventional and macroinitiator methods, respectively as displayed in Figure IX-8 and Figure IX-9. The difference in  $T_g$  does suggest that there are differences in the randomness of the copolymers, but neither were blocky enough to exhibit two distinct  $T_g$ s. The 50/50 mol% DLLA/CL copolymers both also showed only one  $T_g$ ; however, the  $T_g$  of the copolymer from the macroinitiator method was a very broad transition compared to that of the conventional copolymer. The  $T_g$  of the conventional copolymer was -20°C and the  $T_g$  of the macroinitiator copolymer was -28°C. The lower  $T_g$ s as compared to the 90/10 system are characteristic of the higher CL content which has a lower  $T_g$  than poly(DLLA). Not surprisingly, there was a larger difference in  $T_g$  between the two methods of copolymerization than was observed in the 90/10 system. The temperature difference and the shape of the transition both indicate that there are differences in the backbone sequencing in the 50/50 systems.

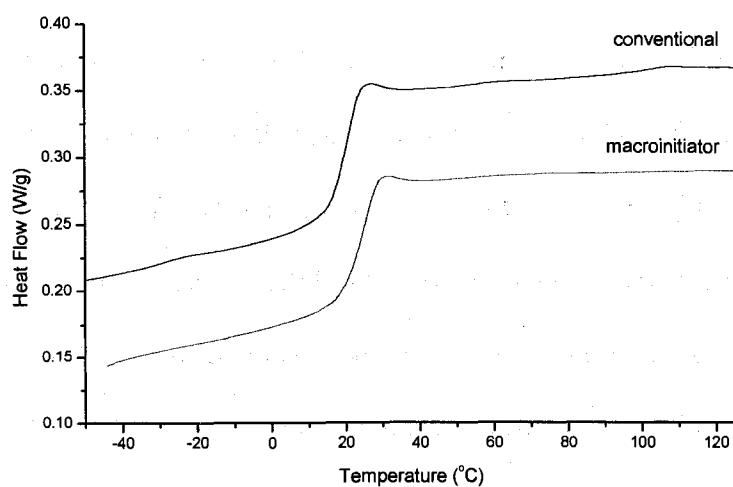


**Figure IX-8.** DSC of 90/10 mol% DLLA/CL copolymers.

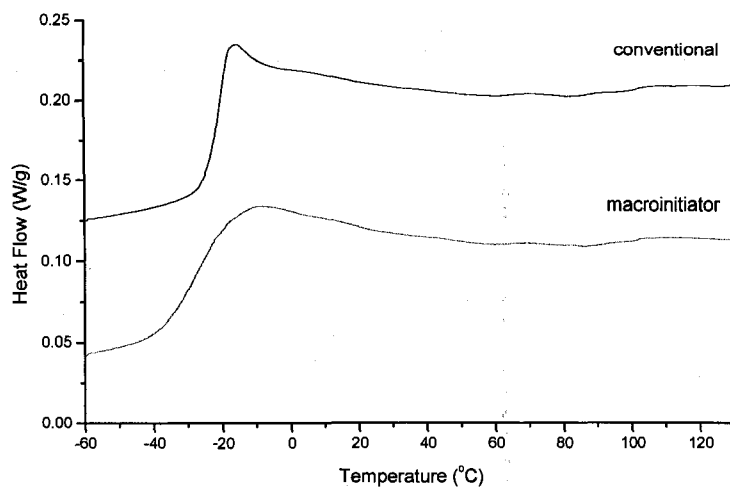


**Figure IX-9.** DSC of 50/50 mol% DLLA/CL copolymers.

$^{13}\text{C}$  NMR was used to analyze the monomer sequencing to determine if the resultant copolymer from the macroinitiator method was comparable to that obtained from the conventional copolymerization. One might expect a blocky nature in the case of the macroinitiator method for both compositions since the rates of conversion of the CL were very slow in conventional copolymerizations and very fast using the macroinitiator method. Figure IX-10 and Figure IX-11 show the carbonyl region of the  $^{13}\text{C}$  NMR spectrum of the 90/10 and 50/50 mol% DLLA/CL copolymers, respectively. Since the goal of the macroinitiator copolymerization method is to produce a polymer similar to that of a conventional copolymerization in a shorter time, the NMR displayed is that of each polymer when both monomers reached maximum conversion. Evidence of transesterification was observed in all of the copolymers, indicated by a monomer sequence with one or three lactoyl units (L,  $\text{C}_3\text{H}_4\text{O}_2$ ) between two caproyl units (C). Interestingly, only the 50/50 conventional copolymer showed the CLC sequence, indicating cleavage of the backbone yielding one L between two Cs.<sup>161,162</sup>

Based on the sequencing of C in Figure IX-10, it is evident that the conventional 90/10 copolymer is more random, since it has no CCC sequences like those observed in the copolymer from the macroinitiator method. Also, there was no sequence in the macroinitiator copolymer where one C was between two lactidyl groups. Both 90/10 copolymers exhibited very little observable transesterification (an odd number of L units between C units) due to the low CL content.

The 50/50 copolymers, displayed in Figure IX-11, show more pronounced differences between the conventional and macroinitiator methods. Most obvious is the very blocky nature of the macroinitiator copolymer with the vast majority of the sequences being CCC or LLL. Conversely, the 50/50 conventional copolymer shows a wide array of sequences including a number of sequences only obtainable by transesterification. The wide distribution of monomer sequencing indicates a very random copolymer.

Since the 50/50 DLLA/CL macroinitiator synthesis yielded a very blocky copolymer, the macroinitiator synthesis was repeated with a reaction temperature of 150°C to promote transesterification reactions. The conversion plot in Figure IX-12 shows that maximum DLLA conversion was reached at a total reaction time of 180 min, similar to the reaction at 130°C. The DSC trace of the copolymer after 24 h reaction time (Figure IX-13) indicated a very broad T<sub>g</sub> centered at -28.9°C, also very similar to the 130°C reaction. The <sup>13</sup>C NMR spectrum of the copolymer after 24 h reaction time (Figure IX-14) was also very similar to the 130°C reaction, indicating a very blocky copolymer. Thus, the copolymer produced after 24 h of reaction time at 150°C was not

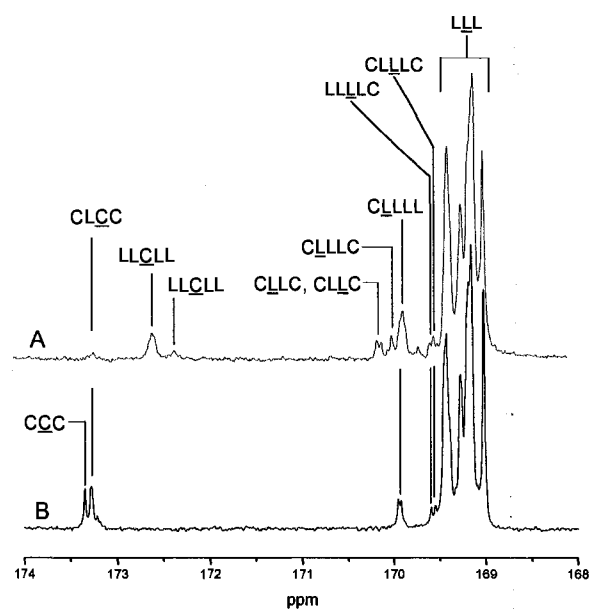


**Figure IX-10.** Carbonyl region of the  $^{13}\text{C}$  NMR of conventional (A) and macroinitiator (B) 90/10 mol% DLLA/CL.

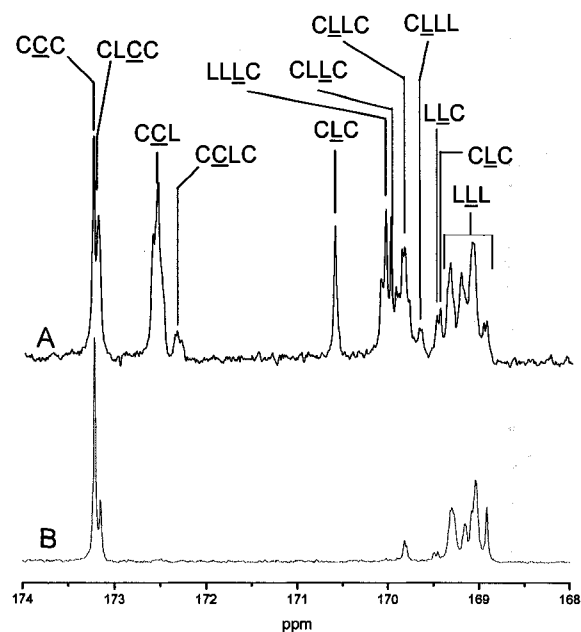


**Figure IX-11.** Carbonyl region of the  $^{13}\text{C}$  NMR of conventional (A) and macroinitiator (B) 50/50 mol% DLLA/CL.

significantly different from the copolymer produced in 180 min at 130°C. Even at very long reaction times at 150°C, 72 and 97 h, there was essentially no difference.

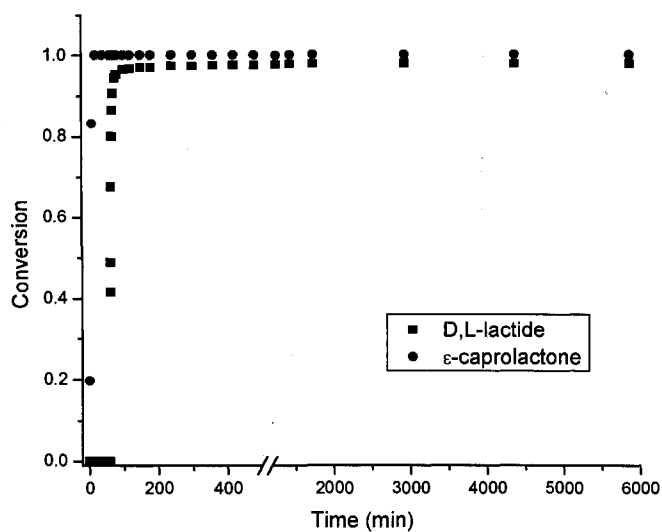


**Figure IX-12.** Conversion of macroinitiator copolymerization of 50/50 mol% DLLA/CL synthesized at 150°C.

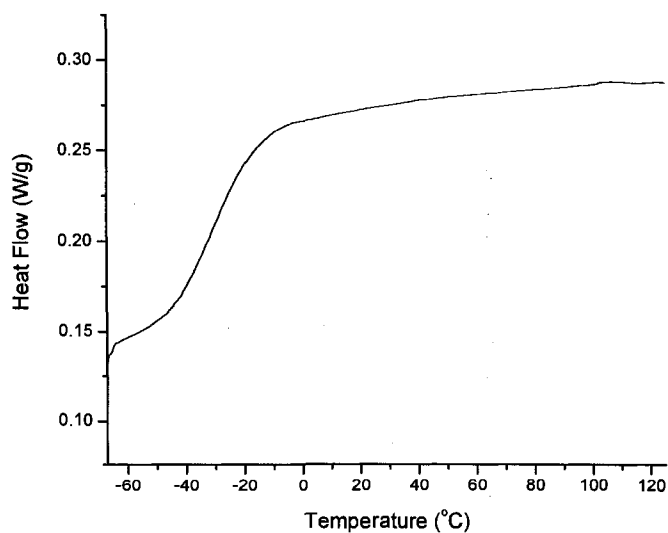


**Figure IX-13.** DSC of 50/50 mol% DLLA/CL macroinitiator copolymer synthesized at 150°C, 24 h reaction time.



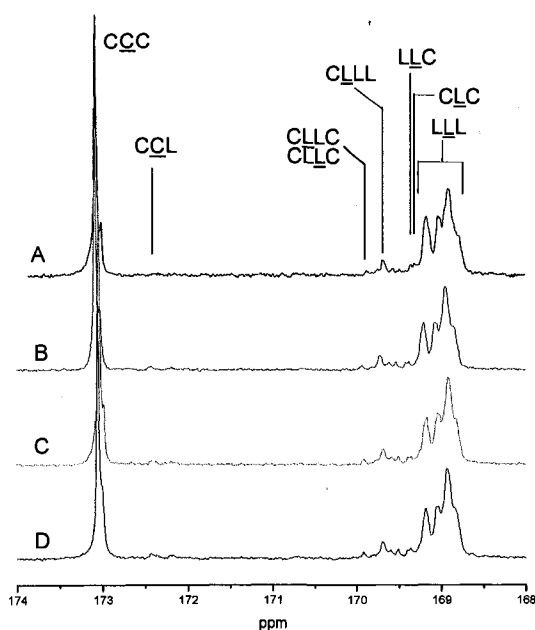


**Figure IX-14.** Carbonyl region of the  $^{13}\text{C}$  NMR of macroinitiator 50/50 mol% DLLA/CL synthesized at  $150^\circ\text{C}$ ; reaction time: 24 h (A), 48 h (B), 72 h (C), and 97 h (D).

### Conclusions

For comonomer compositions low in CL, as with the 90/10 mol% DLLA/CL copolymer, it is possible to obtain copolymers by the macroinitiator method that have very similar properties to the copolymer synthesized by the conventional method. However, there are observable differences in the monomer sequencing as measured by  $^{13}\text{C}$  NMR spectroscopy and slight differences in the observed  $T_g$  by DSC.

In comparison, a copolymer of equimolar DLLA/CL composition varied greatly depending on which method of synthesis was used. The macroinitiator method copolymer had a very broad  $T_g$  region in the DSC thermogram unlike the conventional copolymer that had a very distinct, sharp transition. Also, NMR spectroscopy indicated that the macroinitiator copolymer had a very blocky nature while the conventional copolymer had a wide array of monomer sequences indicative of a random copolymer.

In both cases, the copolymer synthesized by the macroinitiator method was different than the copolymer synthesized by the conventional method. However, as would be expected, this effect is diminished as CL composition decreases.

Attempts to promote randomization of copolymers produced by the macroinitiator method, by higher polymerization temperature and/or longer reaction time, were unsuccessful. Increasing the temperature from 130 to 150°C and extending the reaction time to as long as 97 h for the 50/50 DLLA/CL macroinitiator synthesis resulted in essentially the same copolymer obtained at 130°C after 180 min., This suggests that significant transesterification with  $\text{Sn}(\text{Oct})_2$  catalyst is not so easily promoted.

## APPENDIX A

### HYDROLYTIC DEGRADATION OF POLY(D,L-LACTIDE) AND RESPIROMETRY DEGRADATION OF D,L-LACTIDE-BASED POLYOLS AND POLYURETHANES

#### Introduction

The objective was to investigate the hydrolytic degradation of acid-functionalized poly(D,L-lactide) (PDLLA) in two degradation media: phosphate buffer solution (pH 7.4) and seawater both at 37°C. The buffer solution was selected because of precedent in the literature based on physiological conditions of the human body. Seawater was selected because of potential applications where degradable materials would be discarded into the ocean. Three different functionalities of PDLLA were synthesized; hydroxy-terminated (control, PDLLA-OH), acid-terminated (PDLLA-COOH), and pendant acid (PDLLA-BHMBA). In all cases a difunctional initiator was used, either 1,4-butanediol (1,4-BD) or 2,2-bis(hydroxymethyl)butyric acid (BHMBA). Additionally, select samples of PDLLA, PLGA, and TPUs were tested per an agreement with the U.S. Army Natick Soldier Research, Development and Engineering Center (NSRDEC) and the United States Navy for biodegradation in the marine environment through respirometry experimentation in accordance with ASTM D6691.

#### Results and Discussion

##### *Synthesis*

In order to determine if the procedure of washing the polymer with 1M HCl, as outlined in the Experimental chapter, was sufficient to cleave SnOct from the polymer chain ends, elemental analysis was carried out on three samples; crude polymer,

precipitated polymer, and 1M HCl washed polymer. The results as received from Galbraith Laboratories are listed in Table A-1. Precipitation of the polymer did not remove any tin, in fact the observed tin concentration actually increases slightly because monomer was removed, reducing the overall mass while unchanging the amount of tin connected to polymer chains. Only when the polymer was treated with the 1M HCl wash procedure was the tin removed by cleavage of the stannyl-ether bonds.

Removal of SnOct from the chain ends of the polymer was important for subsequent chain end modification reactions. In the case of the acid terminated polymer synthesis, reaction of the hydroxyl endgroup with succinic anhydride was necessary to achieve the desired product. The  $^{13}\text{C}$  NMR spectra of the carbonyl region showing the conversion of hydroxyl (PDLLA-OH) to carboxylic acid (PDLLA-COOH) endgroups are shown in Figure IX-151.

**Table A-1.** Tin level of PDLLA with various post-polymerization preparations.

Polymer Preparation	Sn level (ppm)
None (Crude)	232
Precipitation	249
1M HCl wash	4.2

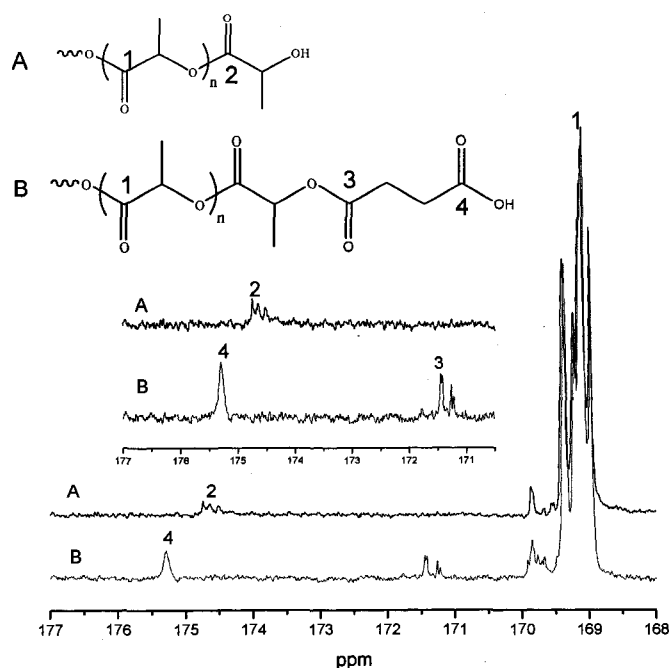


**Figure IX-15.**  $^{13}\text{C}$  NMR of PDLLA-OH and PDLLA-COOH.

### Degradation Analysis

*Buffer Solution Degradation.* The three polymers investigated were approximately 10,000 g/mol as listed in Table A-2. Degradation was conducted using phosphate buffered solution at a pH of 7.40, held at a constant temperature of 37°C.

**Table A-2.** Experimental Conditions for Polymerizations of D,L-Lactide<sup>a</sup>

Sample	Name	DLLA (mol)	Initiator, [Initiator] (mmol)	$M_{n,theo}$ (g/mol)	$M_{n,exp}$ (g/mol)	MWD ( $M_w/M_n$ )
1	PDLLA-OH	0.447	1,4-BD, 6.50	10,002	11,300	1.14
2	PDLLA-COOH	NA	NA	10,202 <sup>b</sup>	11,300	1.16
3	PDLLA-BHMBA	0.342	BHMBA, 5.00	10,010	11,500	1.02

<sup>a</sup> For all polymerizations,  $\text{Sn}(\text{Oct})_2$  was used as a catalyst at 300 ppm Sn and  $T = 130^\circ\text{C}$

<sup>b</sup> Theoretical  $M_n$  calculated from PDLLA-OH plus the addition of succinic acid endgroups

Figure IX-16 shows the percent remaining mass vs. degradation time for the 10,000 g/mol series of polymers. The data indicate that mass loss occurred much sooner for the acid-functionalized PDLLA's compared to the control polymers containing only hydroxyl end groups (PDLLA-OH). This was expected based on the acid catalytic effect and increased water uptake caused by the presence of the hydrophilic carboxylic acid groups. However, it was unexpected that PDLLA-BHMBA, with a single pendent acid group per molecule, would show a similar or even slightly accelerated mass loss profile compared to PDLLA-COOH, which has two acid groups per molecule.

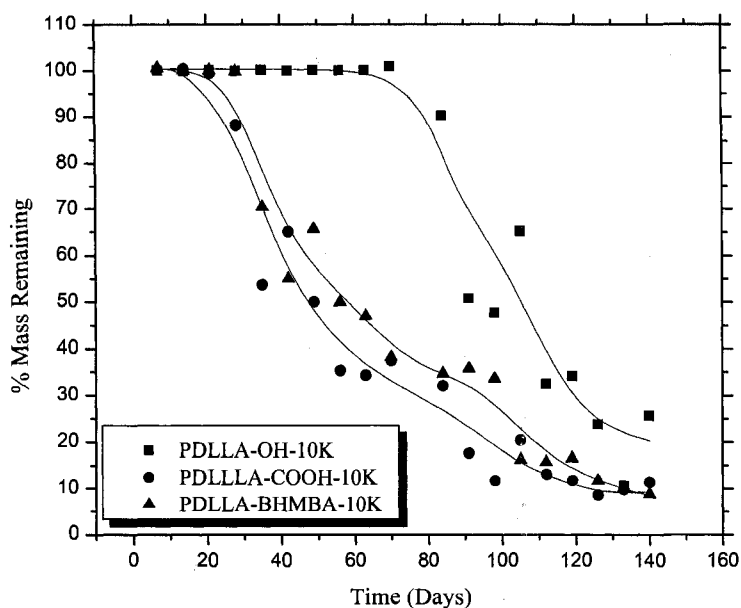


**Figure IX-16.** Remaining mass of dried samples vs. immersion time in phosphate-buffered saline at 37°C.

It is inherent that as PDLLA hydrolytically degrades it forms an acid-terminated fragment and a hydroxyl-terminated fragment. The presence of these acid terminated fragments can be followed by monitoring the pH of the buffer solution vs. time. Figure IX-17 shows pH vs. time data for the series of polymers. Comparison of the pH data

with the mass loss data shows a correlation between the onset of fragmentation and drop in pH.

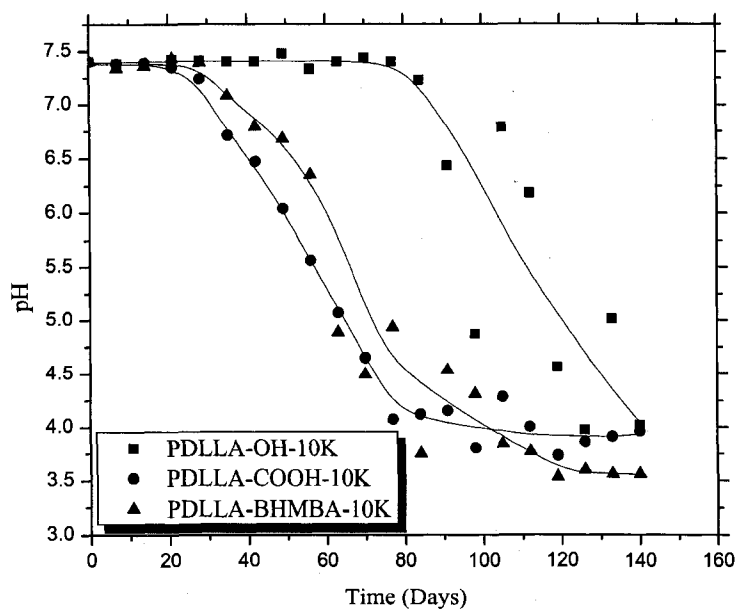


**Figure IX-17.** Buffer solution pH vs. time for degradation of PDLA-OH, PDLA-COOH, and PDLA-BHMBA.

A comparison of the above 10,000 g/mol degradation data with 5,000; 20,000; and 40,000 g/mol PDLAs shows that as molecular weight increases, the degradation is enhanced by the pendant acid of PDLA-BHMBA more than the acid terminated PDLA-COOH.<sup>156</sup>

*Seawater Degradation.* Additional degradation studies were carried out using 5,000 g/mol PDLA-BHMBA and PDLA-COOH in seawater at 37°C. Figure IX-18 shows the percent remaining mass vs. degradation time for the 5,000 g/mol series of polymers. The data indicates the degradation rates of the PDLA-BHMBA and PDLA-COOH were very similar. This was in agreement with the results from the buffer solution where at low molecular weights the pendant and diacid functional polymers degraded very similarly. Figure IX-19 shows the pH vs. time plots where the onset of

mass loss correlates well to a drop in pH as seen in the buffer solution degradation studies.

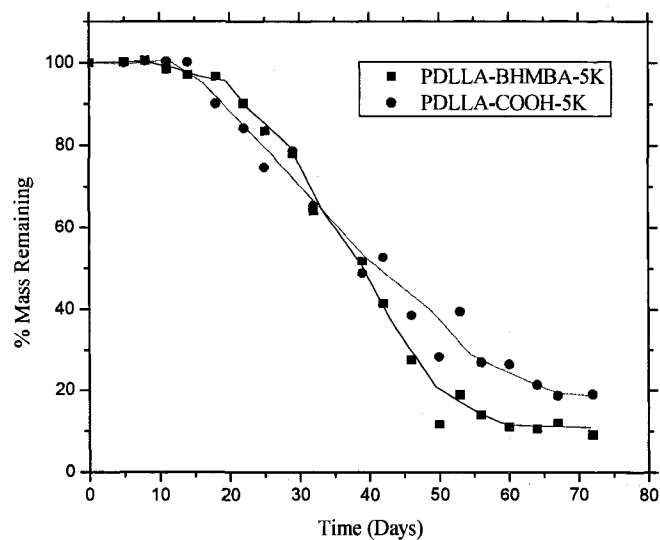


**Figure IX-18.** Remaining mass of dried samples vs. immersion time in sewer water at 37°C.

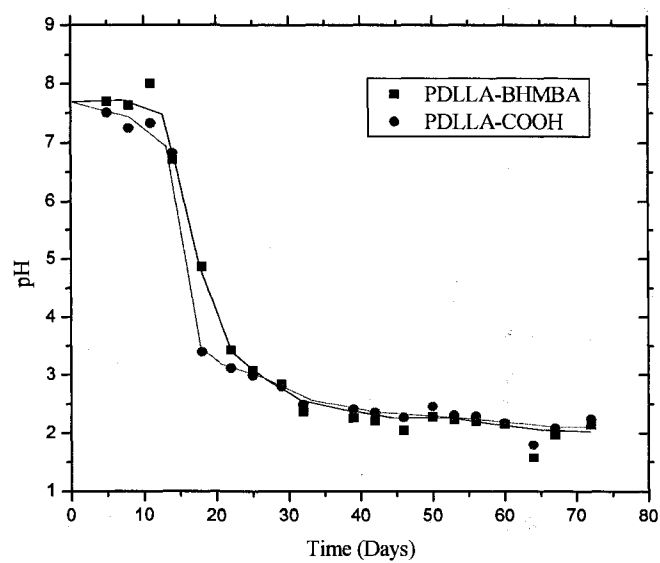


**Figure IX-19.** pH vs. time for degradation of 5,000 g/mol PDLLA-COOH, and PDLLA-BHMBA.



*Biodegradation in the Marine Environment Through Respirometry*

*Experimentation According to ASTM D6691.*<sup>163</sup> The polymer samples listed in Table A-3 were tested for biodegradation (or mineralization) as a function of time in accordance with ASTM D6691, “Standard Test Method for Determining Aerobic Biodegradation of Plastics Materials in the Marine Environment by a Defined Microbial Consortium,”<sup>164</sup> per an agreement with the U.S. Army Natick Soldier Research, Development and Engineering Center (NSRDEC) and the United States Navy. This test utilizes an inoculum of 13 marine microorganisms that is added to the samples in a synthetic sea water solution at 30°C. Carbon dioxide evolution as a function of time was measured using Columbus Instruments respirometers with respect to positive (glucose, Figure IX-28) and negative (baseline, Figure IX-27) controls for a period of 30 days.

The measured biodegradation results for the samples tested are presented in Figure IX-20 through Figure IX-25.<sup>163</sup> Each sample was run in triplicate and the data for each is displayed. Carbon dioxide evolution from the negative control was considered the baseline and was subtracted from the final test results. The negative control consisted of the same marine medium but without any test sample. The results of the negative control are illustrated in Figure IX-27.

A set of positive controls were also run with the test using glucose (40% Carbon), a known biodegradable material in the marine environment. The positive control test data using glucose is presented in Figure IX-28 provides a comparable biodegradable material for these tests.

All samples were sent to Galbraith Laboratories in Knoxville, Tennessee for carbon content determination. The average value of two samples is reported in Table A-3

and serves as the initial carbon content. In order to determine the percentage of sample that has mineralized (biodegraded) during the test, the initial amount of carbon in the sample must be known. The average percent mineralization of the polymer samples during the test was then calculated using this data.

Figure IX-20 and Figure IX-21 compare the biodegradation of 2,000 g/mol PLGA initiated with BHMBA and BD respectively. The BHMBA-PLGA reaches 80  $\mu$ moles of CO<sub>2</sub> evolved and about 7% mineralization. There is a large degree of scatter in the data of the BD-PLGA sample where the 3 samples did not agree well. This scatter is illustrated by the large error bars on the mineralization plot and makes it difficult to draw conclusions about the rate of degradation compared to the BHMBA analogue.

Figure IX-22 and Figure IX-23 compare the biodegradation of 5,000 g/mol BHMBA-PDLLA and PDLLA-COOH respectively. BHMBA-PDLLA has one pendant acid group located at the center of the polymer chain while PDLLA-COOH has an acid group at each of the two endgroups. The BHMBA-PDLLA reaches 50  $\mu$ moles of CO<sub>2</sub> evolved and about 4% mineralization and the PDLLA-COOH reaches 45  $\mu$ moles of CO<sub>2</sub> evolved and about 2.5% mineralization. In this case it is clear that the BHMBA initiated polymer, with a centrally located pendant acid group, has an enhanced degradation rate as compared to the polymer with two terminal acid groups. This supports the findings of Cooper and coworkers who found that BHMBA can enhance the rate of degradation as well as or better than an acid terminated analogue.<sup>156</sup>

Figure IX-24 and Figure IX-25 compare the biodegradation of two similar H<sub>12</sub>MDI based TPUs with 12% hard segment and a mixed polyol as the soft segment. The soft segment was comprised of 50% BA and 50% BHMBA-PLGA (Figure IX-24) or

50% BD-PLGA (Figure IX-25). The TPU made with BHMBA-PLGA reaches an average of about 135  $\mu\text{moles}$  of  $\text{CO}_2$  evolved and about 12% mineralization. The TPU made with BD-PLGA reaches an average of about 120  $\mu\text{moles}$  of  $\text{CO}_2$  evolved and about 13% mineralization. The two TPUs show very similar rates of degradation, both of which are greater than that of the PDLLA and PLGA sample mentioned earlier, with the exception of the BD-PLGA. This is in contrast to hydrolytic degradation studies where the low molecular weight polyols degrade much faster than the corresponding TPUs. This would indicate that the TPUs are readily degraded by the bacteria in the simulated marine environment as compared to the polyols.

Figure IX-26 shows the biodegradation of a scaled up batch of 50/50 BA/BHMBA-PLGA (531-48A1), made by Noveon with polyol from the Storey group, which reaches an average of about 75  $\mu\text{moles}$  of  $\text{CO}_2$  evolved and about 5.5% mineralization. The carbon dioxide evolved and mineralization is similar to that of the polyols discussed above. This suggests that the TPU has about the same degradability as the above polyols in this type of test. Also, this indicates that the material is no more toxic to the biotic medium than the corresponding polyols through the duration of this test.

**Table A-3.** Carbon Content Analysis Results of Samples.<sup>163</sup>

Sample Number	Sample Description	Carbon Content (%)
847-1A	2000g/mol BHMBA-PLGA	44.25
847-1B	2000g/mol BD-PLGA	18.23
847-4B	5000g/mol BHMBA-PDLLA	45.34
847-5B	5000g/mol PDLLA-COOH	48.80
531-40A-1	HMDI TPU 12% HB 50BA/50BHMBA-PLGA	55.69
531-40B-1	HMDI TPU 12% HB 50BA/50D-PLGA	42.98
531-48A-1	Scaled-up HMDI TPU 50BA/50BHMBA-PLGA	58.61

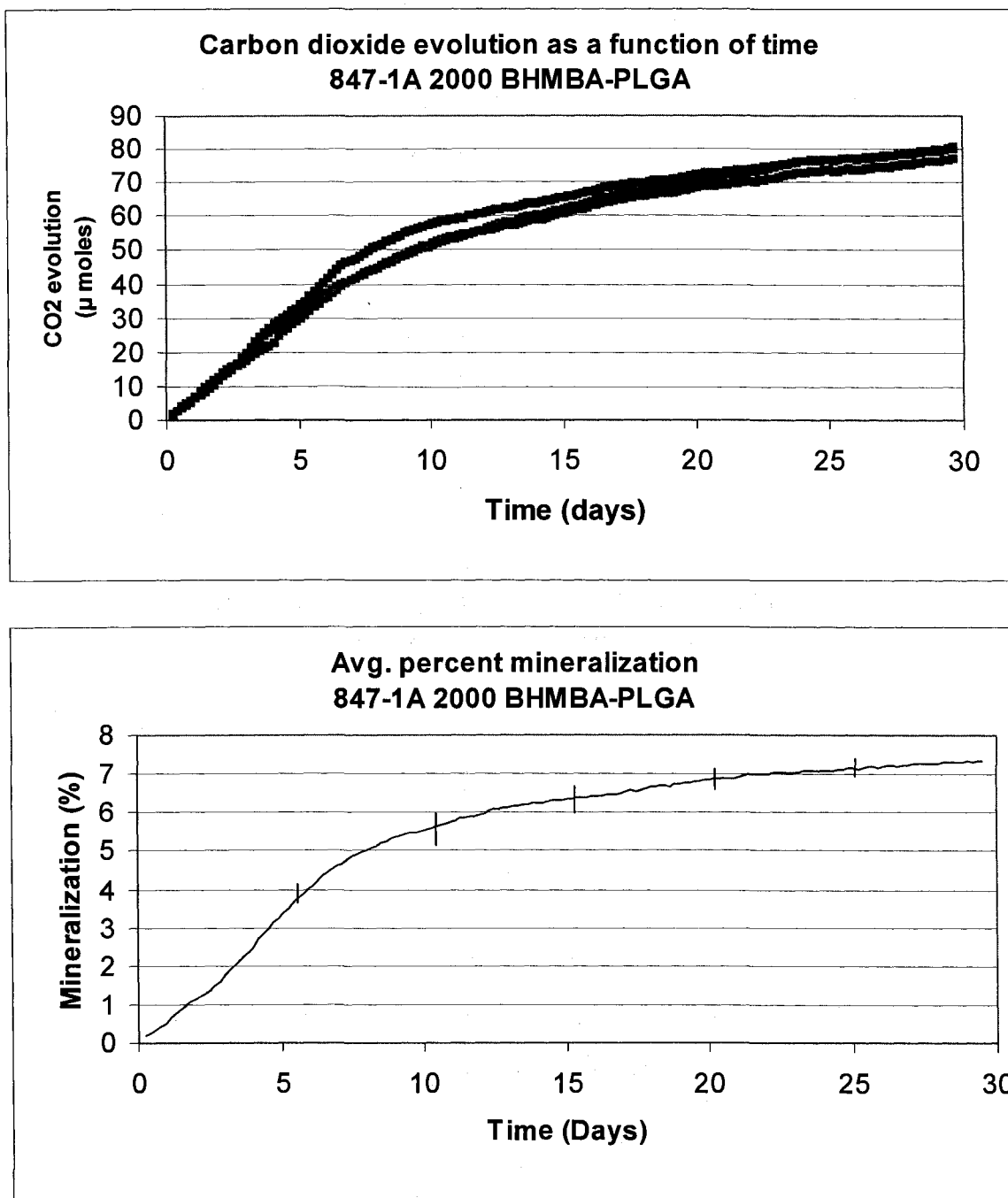


**Figure IX-20.** Biodegradation Results for Sample 847-1A 2000 BH MBA-PLGA.

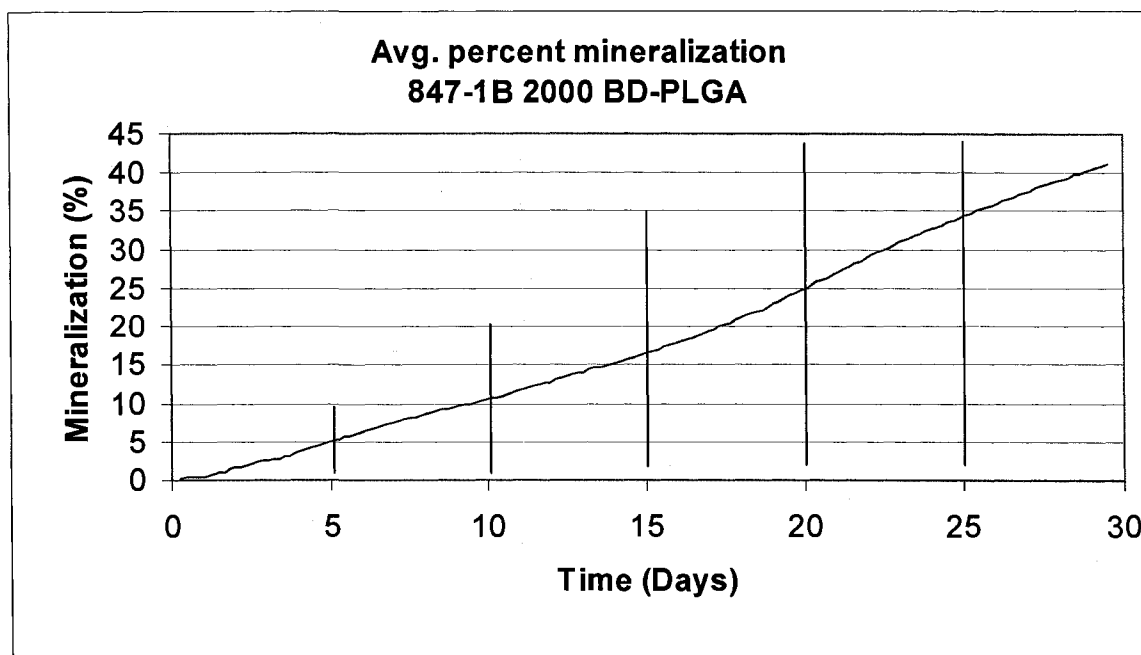
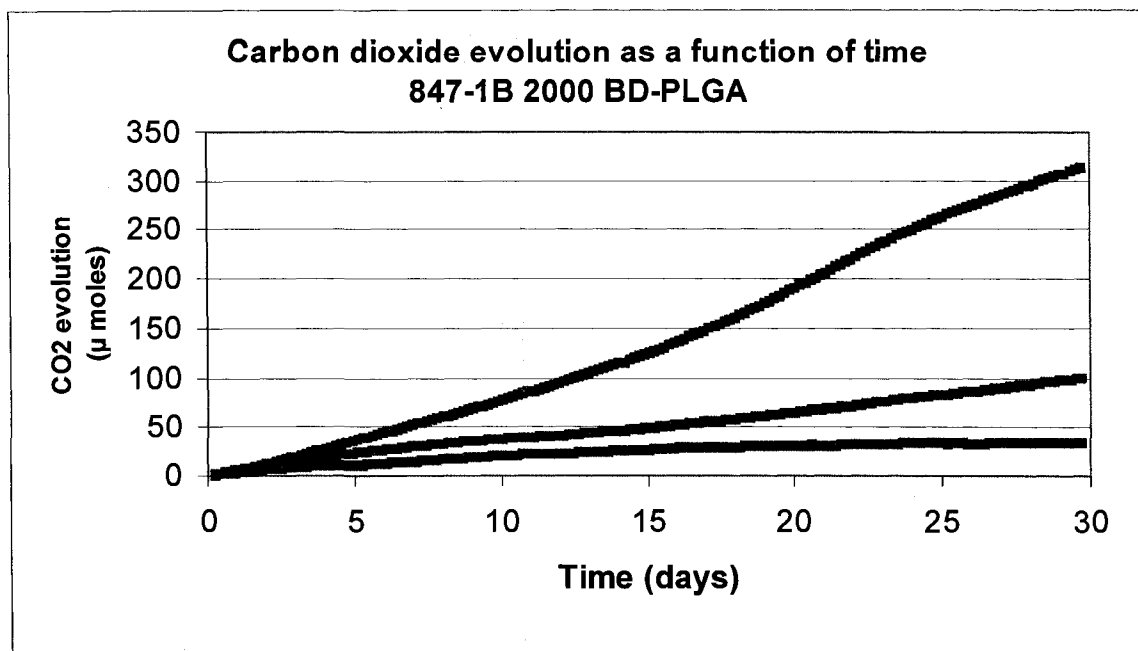


**Figure IX-21.** Biodegradation Results for Sample 847-1B 2000 BD-PLGA.

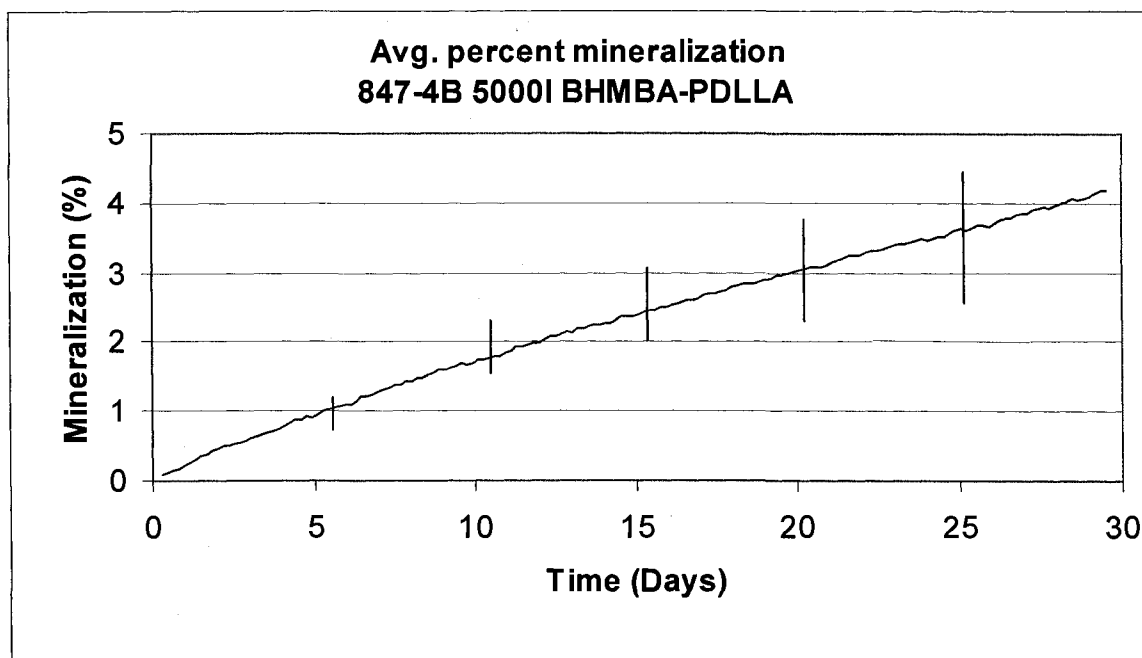
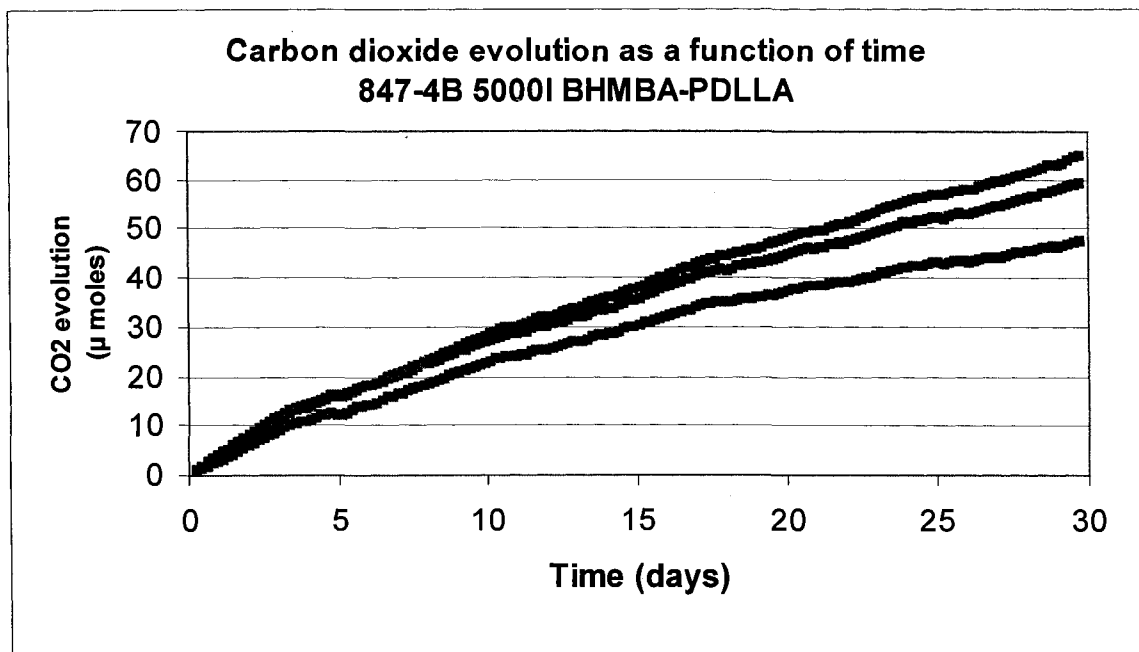


**Figure IX-22.** Biodegradation Results for Sample 847-4B 5000I BHMBA-PDLLA.

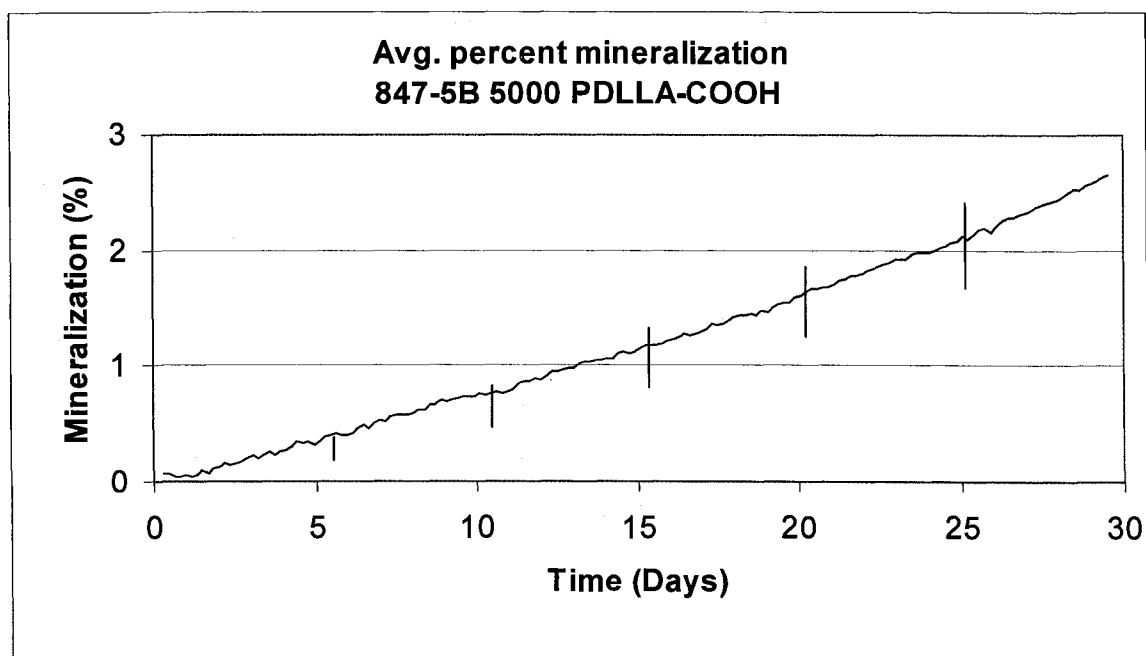
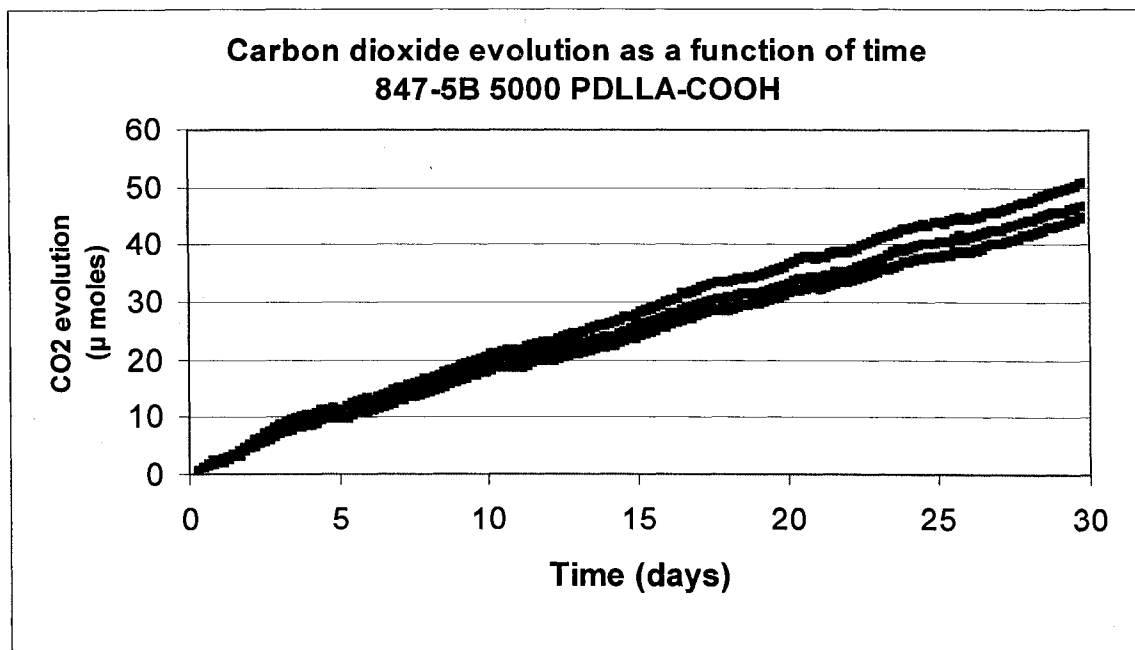


**Figure IX-23.** Biodegradation Results for Sample 847-5B 5000 PDLLA-COOH.

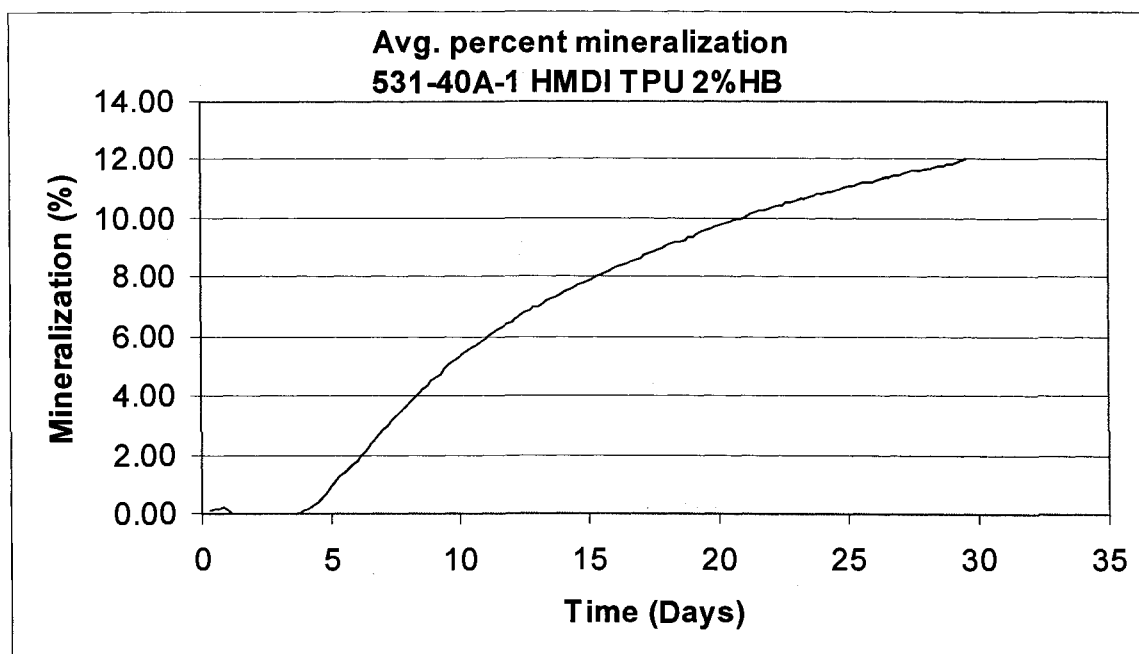
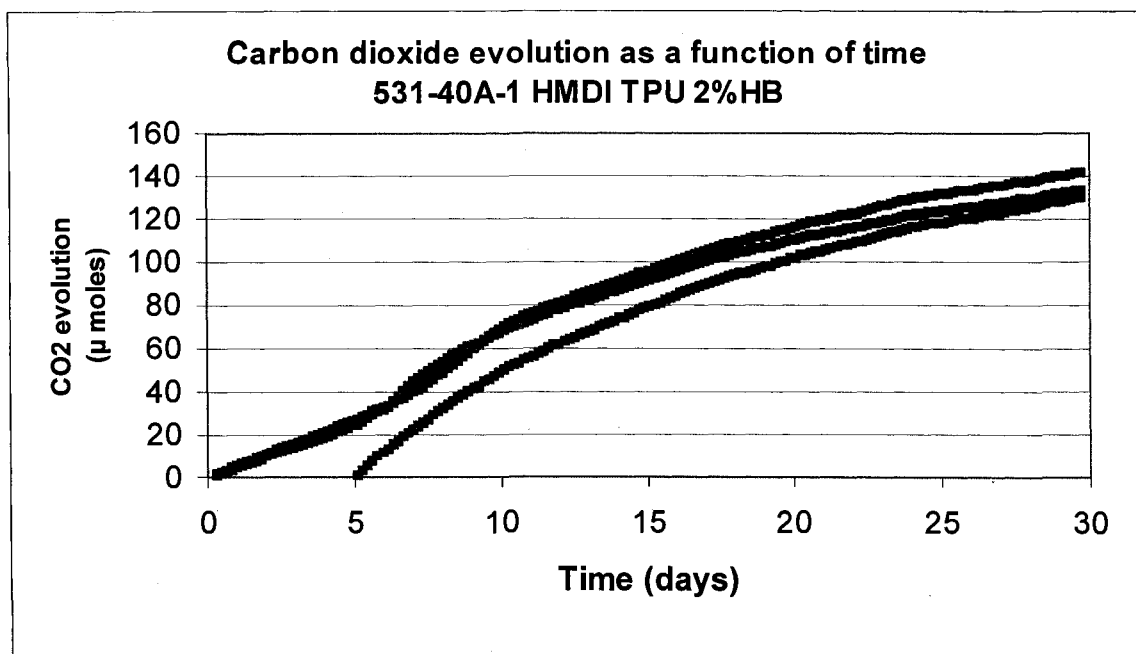


**Figure IX-24.** Biodegradation Results for Sample 531-40A-1 HMDI TPU 12% HB.



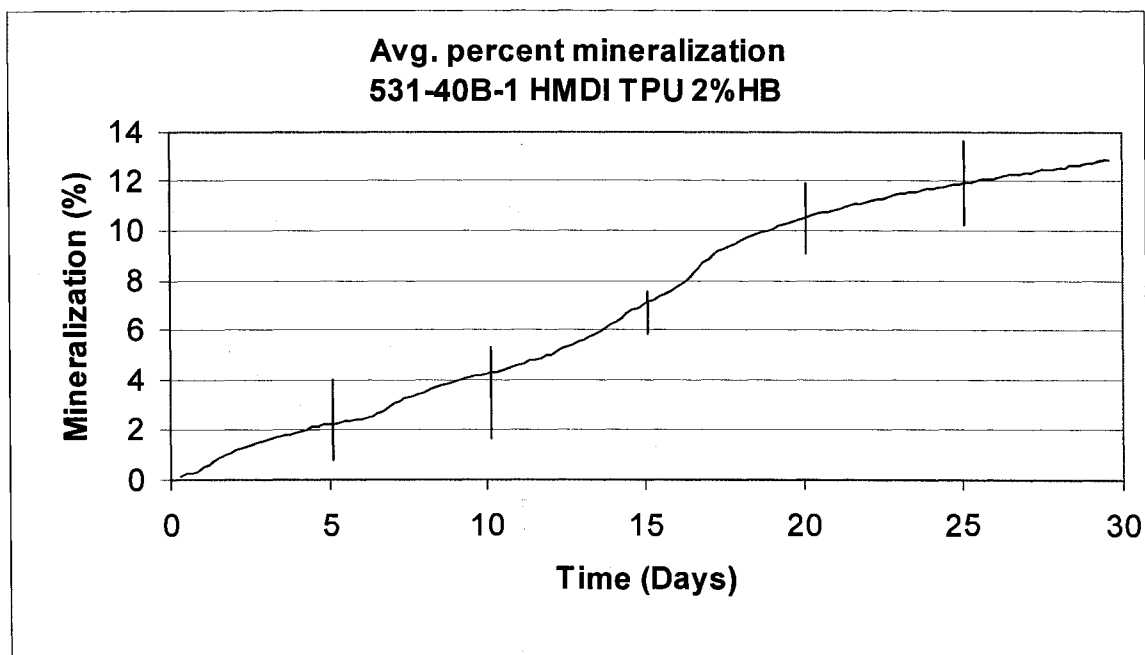
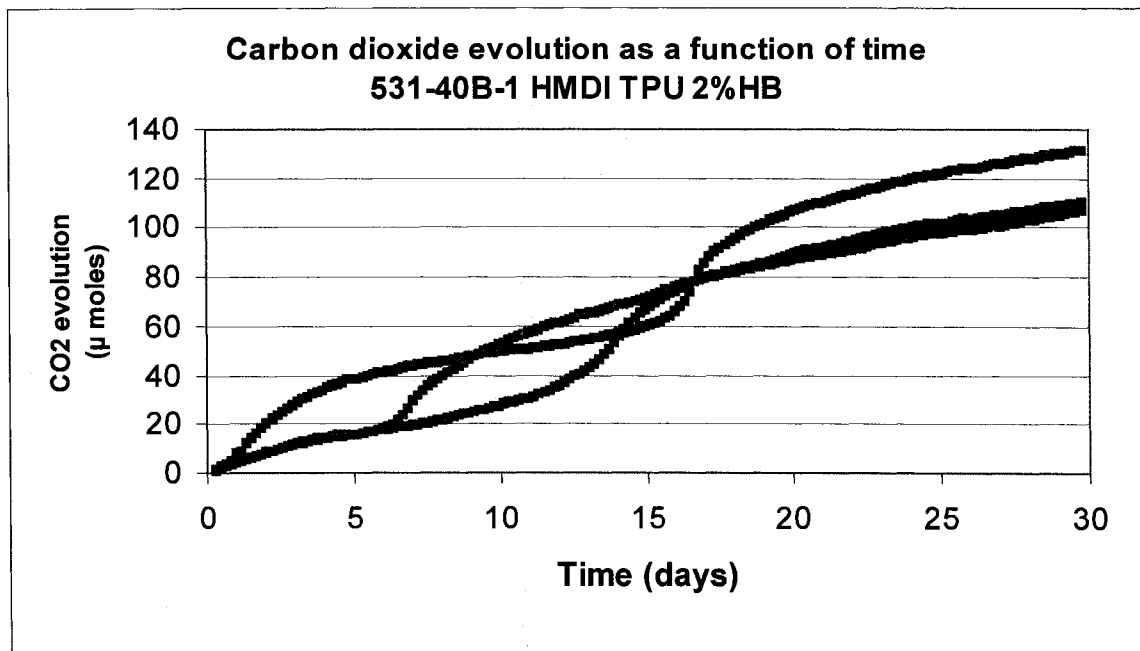


**Figure IX-25.** Biodegradation Results for Sample 531-40B-1 HMDI TPU 12% HB.

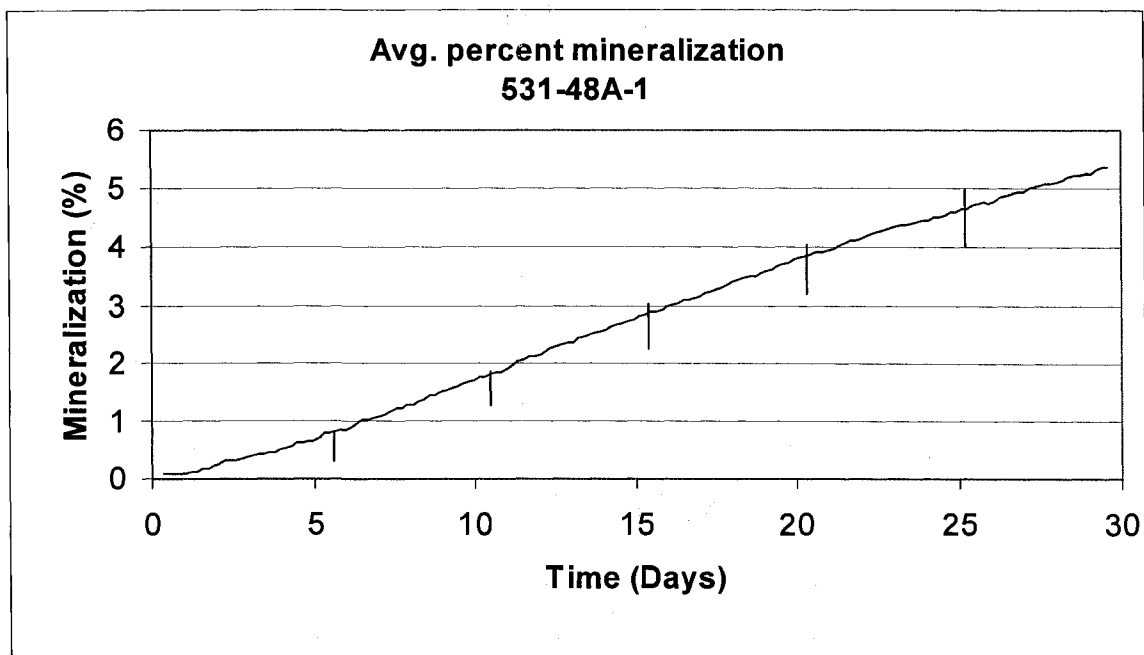
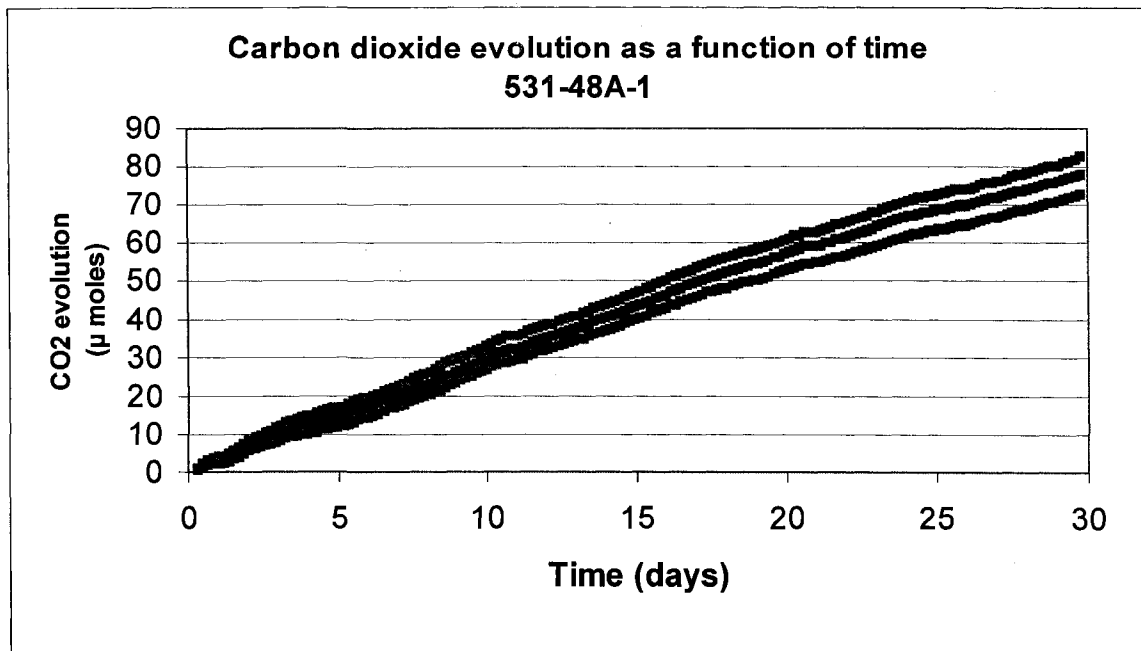


**Figure IX-26.** Biodegradation Results for Sample 531-48A-1, the scaled up TPU.

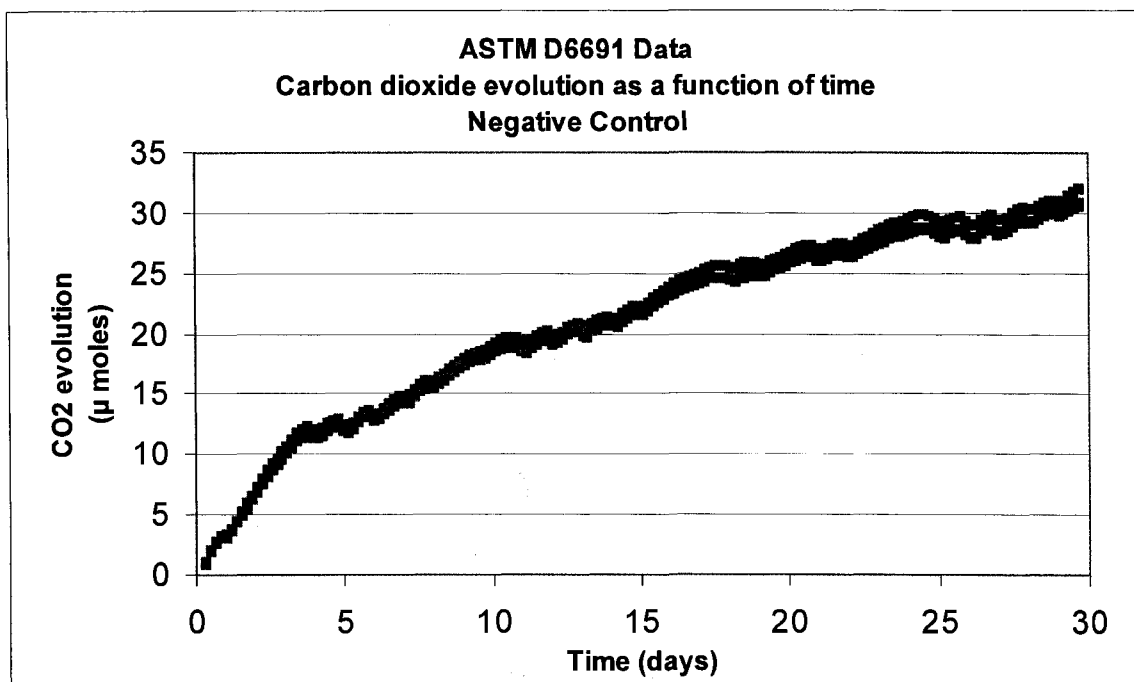


**Figure IX-27.** Carbon Dioxide Evolution of Negative Control Samples (Baseline).

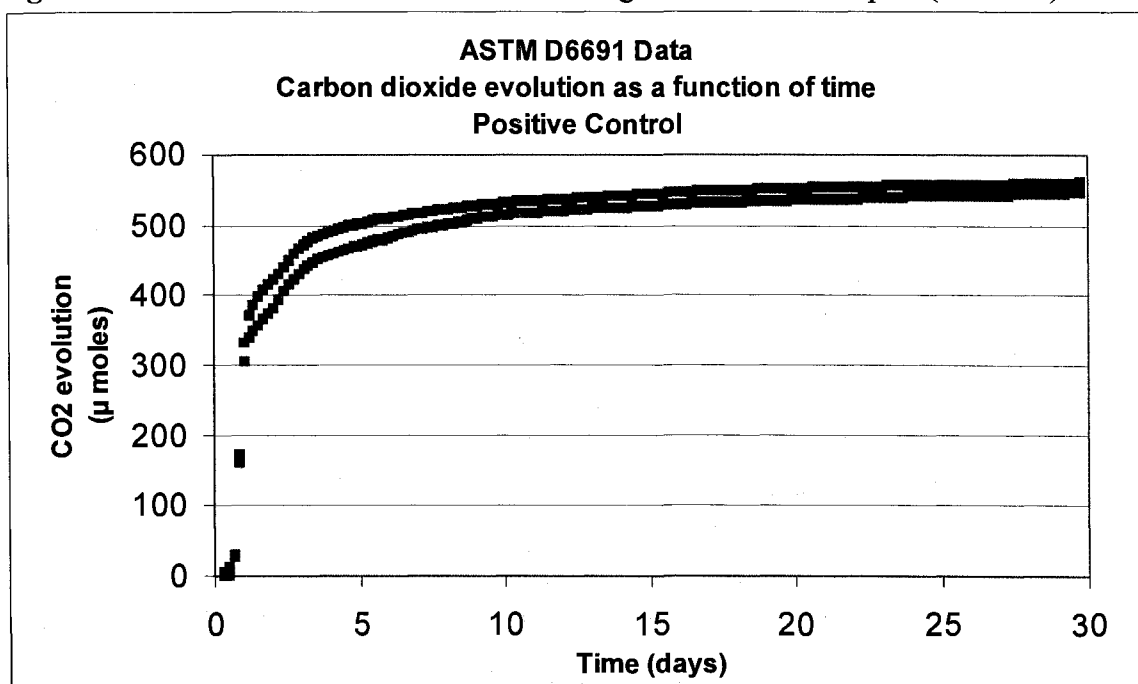


**Figure IX-28.** Carbon Dioxide Evolution of Positive Control Sample (Glucose).

## Conclusions

These degradation results show that not only are the D,L-lactide based polyols degradable but, so are the polyurethanes synthesized using those polyols. In fact, the observed rates of degradation are quite encouraging for meeting the goal of developing a material that will sufficiently degrade in a seawater environment.

## REFERENCES

1. Municipal Solid Waste Generation, Recycling, and Disposal in the United States: Facts and Figures for 2006. EPA-530-F-07-030, US Environmental Protection Agency, 2007.
2. Mayer, J. M.; Kaplan, D. L. *Trends in Polymer Science* **1994**, *2*, 227.
3. Carter, B. K.; Wilkes, G. L. *Polymers as Biomaterials*; Plenum Press: New York, 1984.
4. Hawkins, W. L. *Polymer Degradation and Stabilization*; Springer-Verlag: New York, 1984.
5. Kaplan, D. L.; Mayer, J. M.; Ball, D.; Allen, A. L.; Stenhouse, P. *Biodegradable Polymers and Packaging*; Technomic Publishing Co., Inc.: Lancaster, 1993.
6. Narayan, R. *Degradable Materials: Perspective, Issues, and Opportunities*; CRC Press, Inc.: Boca Raton, 1990.
7. Holy, N. *Chemtech* **1991**, January 26.
8. WO 96/151173.
9. WO 96/15174.
10. WO 96/21689.
11. Gruber, P. R., et. al. USP 5142023.
12. Gruber, P. R., et. al. USP 5247058.
13. Gruber, P. R., et. al. USP 5247059.
14. Gruber, P. R., et. al. USP 5258488.
15. Gruber, P. R., et. al. USP 5274073.
16. Gruber, P. R., et. al. USP 5357035.
17. Gruber, P. R., et. al. USP 5484881.
18. Gruber, P. R.; Michael, O. Polylactides "NatureWorks" PLA. In *Biopolymers*; Steinbuchel, A., Doi, Y., Eds.; Wiley-VCH: Weinheim, 2002; Vol. 4, p 235-250.
19. Ishioka, R.; Kitakuni, E.; Ichikawa, Y. Aliphatic Polyesters: "Bionelle". In *Biopolymers*; Steinbuchel, A., Doi, Y., Eds.; Wiley-VCH: Weinheim, 2002, p 275-298.
20. Kawashima, N.; Ogawa, S.; Obuchi, S.; Matsuo, M.; Yagi, T. Polylactic acid "LACEA". In *Biopolymers*; Steinbuchel, A., Doi, Y., Eds.; Wiley-VCH: Weinheim, 2002; Vol. 4, p 251-274.
21. Takiyama, E., et. al. USP 5436056, 1995.
22. Takiyama, E., et. al. 5530058, 1996.
23. Takiyama, E., et. al. EPC 0572682, 1997.
24. Takiyama, E., et. al. EPC 0565235, 1999, 1999.
25. Takiyama, E., et. al. EPC 0569153, 1999.
26. Tsuji, H. Polylactides. In *Biopolymers*; Steinbuchel, A., Doi, Y., Eds.; Wiley-VCH: Weinheim, 2002; Vol. 4, p 129-178.
27. Ahn, K. D.; Kwon, I. C.; Kim, Y. H. *Polymer* **1987**, *11*, 97-107.
28. Hiltunen, K.; Harkonen, M.; Seppala, J. V.; Vaananen, T. *Macromolecules* **1996**, *29*, 8677-8682.
29. Leemhuis, M.; van Steenis, J. H.; van Uxem, M. J.; van Nostrum, C. F.; Hennink, W. E. *Eur. J. Org. Chem.* **2003**, *17*, 3344-3349.

30. Storey, R. F.; Donnalley, A. B.; Maggio, T. L. *Macromolecules* **1998**, *31*, 1523-1526.
31. Wiggins, J. S.; Mohammad, H. K.; Mauritz, K. A.; Storey, R. F. *Polymer* **2006**, *47*, 1960-1969.
32. Asplund, J. O. B.; Bowden, T.; Mathisen, T.; Hilborn, J. *Biomacromolecules* **2007**, *8*, 905-911.
33. Guan, J.; Fujimoto, K. L.; Sacks, M. S.; Wagner, W. R. *Biomaterials* **2005**, *26*, 3961-3971.
34. Hassan, M. K.; Mauritz, K. A.; Storey, R. F.; Wiggins, J. S. *J. Polym. Sci. A* **2006**, *44*, 2990-3000.
35. Moravek, S. J.; Cooper, T. C.; Hassan, M. K.; Wiggins, J. S.; Mauritz, K. A.; Storey, R. F. *Div. Polym. Chem., Polym. Preprs.* **2007**, *48(1)*, 568-569.
36. Moravek, S. J.; Cooper, T. R.; Hassan, M. K.; Wiggins, J. S.; Mauritz, K. A.; Storey, R. F. *Div. Polym. Chem., Polym. Preprs.* **2007**, *48(1)*, 597-598.
37. Tatai, L.; Moore, T. G.; Adhikari, R.; Malherbe, F.; Jayasekara, R.; Griffiths, I.; Gunatillake, P. A. *Biomaterials* **2007**, *28*, 5407-5417.
38. Van Minnen, B.; Stegenga, B.; van Leeuwen, M. B. M.; van Kooten, T. G.; Bos, R. R. M. *J. Biomed. Mat. Res, Part A* **2006**, *76A*, 377-385.
39. Yeganeh, H.; Lakouraj, M. M.; Jamshidi, S. *J. Polym. Sci. A* **2005**, *43*, 2985-2996.
40. Holden, G.; Legge, N. R.; Quirk, R.; Schroder, H. E. *Thermoplastic Elastomers 2nd Edition*; Hanser Publishers: New York, 1996.
41. Thompson, R. C.; Olsen, Y.; Mitchell, R. P.; Davis, A.; Rowland, S. J.; John, A. W. G.; McGonigle, D.; Russell, A. E. *Science* **2004**, *67*, 405-415.
42. Huang, S. J. *J. Macromol. Sci. Pure Appl. Chem.* **1995**, *32*, 593-597.
43. *High Polymers, Vol I, The Collected Papers of W. H. Carothers*; Mark, H.; Whitby, G. S., Eds.; Wiley-Interscience: New York, 1940.
44. Wirpsza, Z. *Polyurethanes: Chemistry, Technology and Applications*; Ellis Horwood Ltd.: New York, 1994.
45. Zawadzki, S. F.; Tabak, D.; Akcelrud, L. *Polym. Plast. Technolo. Engin.* **1993**, *32*, 155.
46. Benicewicz, B. C.; Hopper, P. K. *J. Bioact. Comp. Polym.* **1990**, *5*, 453.
47. Grijpma, D. W.; Pennings, A. J. *J. Macromol. Chem. Phys.* **1994**, *195*, 1633-1647.
48. Holland, S. J.; Tighe, B.; Gould, P. L. *J. Controlled Release* **1986**, *4*, 155-180.
49. Lewis, D. H. In *Biodegradable Polymers as Drug Delivery Systems*; Chasin, M., Langer, R., Eds.; Marcel Dekker: New York, 1990.
50. Vert, M.; Schwarch, G.; Coudane, J. *J. Macromol. Sci. Pure Appl. Chem., Part A* **1995**, *32*, 787.
51. Guilding, D. K.; Reed, A. M. *Polymer* **1979**, *20*, 1459.
52. Gregory, J. B.; Newberne, P. M.; Wise, D. L. *Polymeric Delivery Systems*; Gordon and Breach: New York, 1978; Vol. 5.
53. Li, S.; Garreau, H.; Vert, M. *J. Mater. Sci.: Mater. Med.* **1990**, *1*, 198.
54. Miller, R. A.; Brady, J. M.; Cutright, D. E. *J. Biomed. Mat. Res.* **1977**, *1*, 711.
55. Pitt, C. G.; Gratzl, M. M.; Kummel, G. L.; Surles, J.; Schindler, A. *Biomaterials* **1982**, *2*.
56. Tsuji, H.; Ikada, Y. *J. Appl. Polym. Sci.* **1998**, *67*, 405-415.

57. Tsuji, H.; Ikada, Y. *Polym. Degrad. Stabil.* **2000**, *67*, 179-189.
58. Fukuzaki, H.; Yoshida, M.; Kumakura, M. *Eur. Polym. J.* **1989**, *25*, 1019.
59. Hosseini, S.; Taheri, S.; Zadhoush, A.; Mehrabani-Zeinabad, A. *J. Appl. Polym. Sci.* **2007**, *103*, 2304.
60. Hocker, H.; Keul, H. *Adv. Mater.* **1994**, *6*, 21.
61. Hocker, H.; Keul, H. In *Encyclopedia of Advanced Materials*; Bloor, D., Brook, R. J., Flemming, M. C., Mahajan, S., Eds.; Permagon Press: Oxford, 1994.
62. Saiyasombat, W.; Molloy, R.; Nicholson, T. M.; Johnson, A. F.; Ward, I. M.; Poshyachinda, S. *Polymer* **1998**, *39*, 5581.
63. Rokicki, G. *Prog. Polym. Sci.* **2000**, *25*, 259.
64. Odian, G. *Principles of Polymerization*; Wiley-Interscience: New York, 1991.
65. Bischoff, C. A.; Walden, P. W. *Ann.* **1893**, *279*, 45.
66. Bischoff, C. A.; Walden, P. W. *Ber.* **1893**, *26*, 262.
67. Fitcher, F.; Beisswenger, A. *Ber.* **1903**, *36*, 1200.
68. Schmitt, E. E.; Rohistina, P. USP 3297033, 1967.
69. Schmitt, E. E.; Rohistina, P. USP 3463158, 1969.
70. Storey, R. F.; Sherman, J. W. *Macromolecules* **2002**, *35*, 1504.
71. 21CFR175.300, US Food and Drug Administration, 2007.
72. Nijenhuis, A., J.; Grijpma, D. W.; Pennings, A. J. *Macromolecules* **1995**, *2002*, 1504.
73. Schwarch, G.; Coudane, J.; Engel, R.; Vert, M. *J. Polym. Chem., Part A* **1997**, *35*, 3431.
74. Dahlman, J.; Rafler, G.; Fechner, G.; Meklis, B. *Br. Polym. J.* **1990**, *23*, 235.
75. Kricheldorf, H. R.; Kreiser-Saunders, I.; Boettcher, C. *Polymer* **1995**, *36*, 1253.
76. Duda, A.; Florjanczyk, Z.; Horfman, A.; Slomkowski, S.; Penczek, S. *Macromolecules* **1990**, *33*, 689.
77. Eenink, M. J. D., Twente University, 1987.
78. Kowalski, A.; Duda, A.; Penczek, S. *Macromol. Rapid Commun.* **1998**, *19*, 567.
79. Kowalski, A.; Libiszowski, J.; Duda, A.; Penczek, S. *Polym. Preprints* **1998**, *39*, (2), 74.
80. Kowalski, A.; Libiszowski, J.; Duda, A.; Penczek, S. *Macromolecules* **2000**, *33*, 1964.
81. Kricheldorf, H. R.; Kreiser-Saunders, I.; Stricker, A. *Macromolecules* **2000**, *33*, 702.
82. Storey, R. F.; Taylor, A. E. *J. Macromol. Sci. Pure Appl. Chem.* **1996**, *A33*, 77.
83. Storey, R. F.; Taylor, A. E. *J. Macromol. Sci. Pure Appl. Chem.* **1998**, *A35*, 723.
84. Weij, V. W. V. D. *Makromol. Chem.* **1980**, *181*, 2541.
85. Zhang, X.; MacDonald, D. A.; Goosen, M. F. A.; McAuley, K. B. *J. Polym. Chem.* **1994**, *32*, 2695.
86. Kowalski, A.; Duda, A.; Penczek, S. *Macromolecules* **2000**, *33*, 689.
87. Kowalski, A.; Duda, A.; Penczek, S. *Macromolecules* **2000**, *33*, 7359.
88. Hofman, A.; Slomkowski, S.; Penczek, S. *Makromol. Chem., Rapid Commun.* **1987**, *8*, 387.
89. Liu, Y.; Ko, B.; Lin, C. *Macromolecules* **2001**, *34*, 6196.
90. Ouhadi, I.; Stevens, C.; Teyssie, P. *Makromol. Chem.* **1975**, *1*, 191.

91. Vion, J. M.; Jerome, R.; Teyssie, P.; Aubin, H.; Prud'homme, R. *Macromolecules* **1986**, *19*, 1828.
92. McGuinness, D. S.; Marshall, E. L.; Gibson, V. C.; Steed, J. W. *J. Polym. Sci. Part A: Polym. Chem.* **2003**, *41*, 3798.
93. Kricheldorf, H. R.; Eggerstadt, S. *Macromol. Chem. Phys.* **1998**, *199*, 283.
94. Kricheldorf, H. R.; Hauser, K. *Macromolecules* **1998**, *31*, 614.
95. Kricheldorf, H. R.; Langanke, D. *Macromol. Chem. Phys.* **1999**, *200*, 1183.
96. Kricheldorf, H. R.; Lee, S. R. *Macromolecules* **1995**, *28*, 6718.
97. Kricheldorf, H. R.; Less, S. R. *Macromol. Chem. Phys.* **1998**, *199*, 273.
98. Kricheldorf, H. R.; Less, S. R.; Bush, S. *Macromolecules* **1996**, *29*, 1375.
99. Ryner, M.; Finne, A.; Albertsson, A.-C.; Kricheldorf, H. R. *Macromolecules* **2001**, *34*, 7281.
100. Stridsberg, K.; Albertsson, A.-C. *J. Polym. Sci. Part A: Polym. Chem.* **1999**, *37*, 3407.
101. Stridsberg, K.; Ryner, M.; Albertsson, A.-C. *Macromolecules* **2000**, *33*, 2862.
102. Kricheldorf, H. R.; Berl, M. *Macromolecules* **1988**, *21*, 286.
103. Ling, J.; Zhu, W.; Shen, Z. *Macromolecules* **2004**, *37*, 758.
104. Chen, H.-Y.; Huang, B.-H.; Lin, C.-C. *Macromolecules* **2005**, *38*, 5400.
105. Finne, A.; Reema; Albertsson, A.-C. *J. Polym. Sci. Part A: Polym. Chem.* **2003**, *41*, 3074.
106. Lohmeijer, B. G. G.; Pratt, R. C.; Leibfarth, F.; Logan, J. W.; Long, D. A.; Dove, A. P.; Nederberg, F.; Choi, J.; Wade, C.; Waymouth, R. M.; Hedrick, J. L. *Macromolecules* **2006**, *39*, 8574.
107. Holden, G.; Quirk, R. P.; Kricheldorf, H. R. *Thermoplastic Elastomers*; 3rd. ed.; Hanser Gardner Publications: Munich, 2004.
108. *The Polyurethanes Book*; Randall, D.; Lee, S., Eds.; Huntsman International LLC, Polyurethanes business, 2002.
109. Bruin, P.; Smedingam, J.; Pennings, A. J. *Biomaterials* **1990**, *11*, 291.
110. Bruin, P.; Veenstra, G. J.; Nijenhuis, A., J.; Pennings, A. J. *Makromol. Chem., Rapid Commun.* **1988**, *9*, 589.
111. De Groot, J. H.; Nijenhuis, A., J.; Bruin, P.; Pennings, A. J. *Colloid. Polym. Sci.* **1990**, *268*, 1073.
112. Gorna, K.; Gogolewski, S. *J. Biomed. Mat. Res, Part A* **2006**, *79A*, 128.
113. Guelcher, S. A. *Tissue Eng., Part B: Reviews* **2008**, *14*, 3.
114. Van Minnen, B.; van Leeuwen, M. B. M.; Kors, G.; Zuidema, J.; Van Kooten, T. G.; Bos, R. R. M. *J. Biomed. Mat. Res, Part A* **2008**, *85A*, 972.
115. Marchant, R. E.; Zhao, Q.; Anderson, J. M.; Hiltner, A. *Polymer* **1987**, *28*, 2032.
116. Szycher, M.; Poirer, V. L.; Dempsey, D. J. *J. Elastomers Plast.* **1983**, *15*, 81.
117. Milosevic, M.; Sting, D.; Rein, A. *Spectroscopy* **1995**, *10*, 44.
118. Deshmukh, S. C.; Aydil, E. S. *J. Vacuum Science and Technol., Part A: Vacuum, Surfaces, and Films* **1995**, *13*, 2355.
119. Miyazaki, S.; Shin, H.; Miyoshi, Y.; Hirose, M. *J. Appl. Phys., Part 1: Regular Papers, Short Notes, and Review Papers* **1995**, *34*, 787.
120. Miyoshi, Y.; Yoshida, Y.; Miyazaki, S.; Hirose, M. *J. Non-crystalline Solids, Part 2: Amorphous Semiconductors: Science and Technology* **1996**, *198*, 1029.
121. Pan, Y. V.; Barrios, E. Z.; Denton, D. D. *Appl. Phys. Lett.* **1996**, *68*, 3386.



122. Calabro, D. C.; Valyocsik, E. W.; Ryan, F. X. *Microporous Materials* **1996**, *7*, 243.
123. Puskas, J. E.; Lazendorfer, M. G.; Patten, W. E. *Polym. Bull.* **1998**, *40*, 55.
124. Storey, R. F.; Maggio, T. L. *Macromolecules* **2000**, *33*, 53.
125. Storey, R. F.; Jeskey, S. J. *ACS Dic. Poly. Chem., Polym. Preprs.* **2000**, *41(2)*, 1895.
126. Storey, R. F.; Thomas, Q. E. *Macromolecules* **2003**, *36*, 5065.
127. Pasquale, A. J.; Long, T. E. *Macromolecules* **1999**, *32*, 7954.
128. Hofmann, M.; Puskas, J. E.; Weiss, K. *Eur. Polym. J.* **2002**, *38*, 19-24.
129. Gorna, K.; Polowinski, S.; Gogolewski, S. *J. Polym. Sci. A* **2002**, *40*, 156-170.
130. Moravek, S. J.; Storey, R. F. *J. Appl. Polym. Sci.* **2008**, *109*, 3101-3107.
131. Thomson, M. A.; Melling, P. J. *In Situ Spectroscopy of Monomer and Polymer Systems*; Kluwer Academic/Plenum Publishers: New York, 2003.
132. Xu, L.; Li, C.; Simon Ng, K. Y. *J. Phys. Chem. A* **2000**, *104*, 3952-3957.
133. Yilgor, I.; Mather, B. D.; Unal, S.; Yilgor, E.; Long, T. E. *Polymer* **2004**, *45*, 5829-5836.
134. Aubrecht, K. B.; Hillmyer, M. A.; Tolman, W. B. *Macromolecules* **2002**, *35*, 644.
135. Messman, J. M.; Storey, R. F. *ACS Dic. Poly. Chem., Polym. Preprs.* **2002**, *43(2)*, 948.
136. Messman, J. M.; Storey, R. F. *J. Polym. Sci. Part A: Polym. Chem.* **2004**, *42*, 6238-6274.
137. Pasquale, A. J.; Long, T. E. *Macromolecules* **1999**, *32*, 7954-7957.
138. Lizotte, J. R.; Long, T. E. *Macromol. Chem. Phys.* **2004**, *204*, 692.
139. Bialas, N.; Hocker, H. *Makromol. Chem.* **1990**, *191*, 1843-1852.
140. Majumdar, K. K.; Kundu, A.; Das, I.; Roy, S. *Appl. Organometal. Chem.* **2000**, *14*, 79-85.
141. Rand, L.; Thir, B.; Reegen, S. L.; Frisch, K. F. *J. Appl. Polym. Sci.* **1965**, *9*, 1787-1795.
142. Schwetlick, K.; Noack, R.; Stebner, F. *J. Chem. Soc. Perkin Trans. 2* **1994**, 599.
143. Seneker, S. D.; Potter, T. A. *J. Coatings Technology* **1991**, *63*, 19-23.
144. Yilgor, I.; McGrath, J. E. *J. Appl. Polym. Sci.* **1985**, *30*, 1733-1739.
145. Yilgor, I.; Orhan, E. H.; Baysal, B. M. *Makromol. Chem.* **1978**, *179*, 109-112.
146. Mei, Y.; Kumar, A.; Gross, R. A. *Macromolecules* **2002**, *35*, 5444.
147. Save, M.; Schappacher, M.; Soum, A. *Macromol. Chem. Phys.* **2002**, *203*, 889.
148. Jacobson, S.; Fritz, H.; Degee, P.; Dubois, P.; Jerome, R. *Macromol. Symp.* **2000**, *153*, 261.
149. Schulz, V. R. C.; Schwab, J. *Die Makromol. Chem.* **1965**, *87*, 90.
150. Messman, J. M.; Scheuer, A. D.; Storey, R. F. *Polymer* **2005**, *46*, 3628-3638.
151. Yilgor, E.; Atilla, G. E.; Ekin, A.; Kurt, P.; Yilgor, I. *Polymer* **2003**, *44*, 7787.
152. Ueda, H.; Tabata, Y. *Adv. Drug Deliv. Rev.* **2003**, *55*, 501.
153. Tamber, H.; Johansen, P.; Merkle, H. P.; Gander, B. **2005**, *57*, 357.
154. Kylma, J.; Seppala, J. V. *Macromolecules* **1997**, *30*, 2876.
155. Vert, M. Polyglycolide and Copolyesters with Lactide. In *Biopolymers*; Steinbuchel, A., Doi, Y., Eds.; Wiley-VCH: Weinheim, 2002; Vol. 4, p 179-202.
156. Cooper, T. C.; Moravek, S. J.; Drake, D. J.; Storey, R. F. *Polymer* **2008**, Submitted.

157. Guelcher, S. A.; Gallagher, K. M.; Didier, J. E.; Klinedinst, D. B.; Doctor, J. S.; Goldstein, A. S.; Wilkes, G. L.; Beckman, E. J.; Hollinger, J. O. *Acta Biomaterialia* **2005**, 471-484.
158. Hassan, M. K.; Mauritz, K. A.; Storey, R. F.; Wiggins, J. S. *J. Polym. Sci., Part A: Polym. Chem.* **2006**, 44, 2990-3000.
159. Skarja, G. A.; Woodhouse, K. A. *J. Appl. Polym. Sci.* **2000**, 75, 1522-1534.
160. Braun, B.; Dorgan, J. R.; Dec, S. F. *Macromolecules* **2006**, 39, 9302-9310.
161. Bero, M.; Kasperczyk, J. *Macromol. Chem. Phys.* **1996**, 197, 3251-3258.
162. Kricheldorf, H. R.; Bornhorst, K.; Hachmann-Thiessen, H. *Macromolecules* **2005**, 38, 5017-5024.
163. Biodegradation of Materials Supplied by the University of Southern Mississippi in the Marine Environment Through Respirometry Experimentation According to ASTM D6691, U.S. Army Natick Soldier Research, Development and Engineering Center (NSRDEC) and the United States Navy, 2007, Unpublished data.
164. ASTM D6691-01 Standard Test Method for Determining Aerobic Biodegradation of Plastic Materials in the Marine Environment by a Defined Microbial Consortium, Book of Standards Volume 08.03, 2003.